AD-A037 154 ARMY ENGINEER WATERWAYS EXPERIMENT STATION VICKSBURG MISS F/G 20/4
LOS ANGELES AND LONG BEACH HARBORS MODEL STUDY. REPORT 4. MODEL--ETC(U)
FEB 77 D G OUTLAW, D L DURHAM, C E CHATHAM

UNCLASSIFIED WES-TR-H-75-4-4 NL

1 OF 3
AD
A037154

TECHNICAL REPORT H-75-4

LOS ANGELES AND LONG BEACH HARBORS MODEL STUDY

Report 4

MODEL DESIGN

by

Douglas G. Outlaw, Donald L. Durham
Claude E. Chatham, Robert W. Whalin

Hydraulics Laboratory
U. S. Army Engineer Waterways Experiment Station
P. O. Box 631, Vicksburg, Miss. 39180

February 1977

Report 4 of a Series

Prepared for U. S. Army Engineer District, Los Angeles
Los Angeles, Calif. 90053

Destroy this report when no longer needed. Do not return
it to the originator.

Unclassified

SECURITY CLASSIFICATION OF THIS PAGE (When Data Entered)

REPORT DOCUMENTATION PAGE

READ INSTRUCTIONS BEFORE COMPLETING FORM

1. REPORT NUMBER: Technical Report H-75-4
2. GOVT ACCESSION NO.
3. RECIPIENT'S CATALOG NUMBER: WES-TR-H-75-4-4
4. TITLE (and Subtitle): LOS ANGELES AND LONG BEACH HARBORS MODEL STUDY. Report 4, MODEL DESIGN.
5. TYPE OF REPORT & PERIOD COVERED: Report 4 of a series
6. PERFORMING ORG. REPORT NUMBER
7. AUTHOR(s): Douglas G. Outlaw, Donald L. Durham, Claude E. Chatham, Robert W. Whalin
8. CONTRACT OR GRANT NUMBER(s)
9. PERFORMING ORGANIZATION NAME AND ADDRESS: U. S. Army Engineer Waterways Experiment Station, Hydraulics Laboratory, P. O. Box 631, Vicksburg, Mississippi 39180
10. PROGRAM ELEMENT, PROJECT, TASK AREA & WORK UNIT NUMBERS
11. CONTROLLING OFFICE NAME AND ADDRESS: U. S. Army Engineer District, Los Angeles, P. O. Box 2711, Los Angeles, California 90053
12. REPORT DATE: February 1977
13. NUMBER OF PAGES: 109 (112 p.)
14. MONITORING AGENCY NAME & ADDRESS (if different from Controlling Office)
15. SECURITY CLASS. (of this report): Unclassified
15a. DECLASSIFICATION/DOWNGRADING SCHEDULE
16. DISTRIBUTION STATEMENT (of this Report): Approved for public release; distribution unlimited.

A016 904

17. DISTRIBUTION STATEMENT (of the abstract entered in Block 20, if different from Report)
18. SUPPLEMENTARY NOTES
19. KEY WORDS (Continue on reverse side if necessary and identify by block number)

Harbor oscillations	Los Angeles Harbor
Harbors	Prototype data
Hydraulic models	Water waves
Long Beach Harbor	Wave generation

038 100

20. ABSTRACT (Continue on reverse side if necessary and identify by block number)

This report describes the design of the Los Angeles and Long Beach Harbors hydraulic model for investigation of harbor oscillation characteristics of the existing harbor and for evaluation of various proposed harbor modifications. The effects of wave refraction, diffraction, viscous friction, wave reflection, wave transmission through the harbor breakwaters, wave filters, and wave absorbers were considered. Wave generator design, automated model data acquisition and control, and model data analyses are also

(Continued)

DD FORM 1 JAN 73 1473 EDITION OF 1 NOV 65 IS OBSOLETE

Unclassified

SECURITY CLASSIFICATION OF THIS PAGE (When Data Entered)

20. ABSTRACT (Continued).

described. This report is the fourth in series Technical Report H-75-4 published under the general title "Los Angeles and Long Beach Harbors Model Study." A model distortion ratio of 1:4 and a vertical scale ratio of 1:100 (1:400 horizontal scale ratio) were selected to minimize the model area and to provide a vertical scale ratio where accurate model wave measurements could be assured. The model reproduces approximately 253 square miles of prototype area. Model limits were selected to enclose a strong convergence zone seaward of the harbor breakwater. Adjustment of the initial generated wave-front position in the model was necessary to compensate for model distortion and the maximum model depth of -300 ft mllw.

The electrohydraulic wave generator used in the model study is composed of 14 separate 15-ft units for a total wave generator length of 210 ft and is capable of (a) generating waves with a prototype period ranging from 15 to 600 sec, (b) generating a wave with small variation in period and height between units, (c) defining resonant response over a narrow period band, (d) generating a variable wave height along the wave front, and (e) generating a curved wave front. Performance requirements for the wave generator include: (a) the amplitude error of the wave-paddle stroke for each unit must be less than 1 percent and (b) the phase lag of the wave-paddle response from the electronic command signal between each of the 14 units must be less than 4 degrees.

The four subsystems of the automated model data acquisition and control system include: (a) digital data recording and controls, (b) analog recorders and channel selection circuits, (c) wave sensors and interfacing equipment, and (d) wave generator units and control equipment.

Model wave record analyses include the capacity for determination of: (a) average, root mean square, and significant wave height and (b) average period. Procedures for Fourier analysis and least-squares harmonic analysis of the wave record are also available.

The hydraulic model can be used in a predictive mode to evaluate various proposed modifications to optimize the modifications from both a cost and functional standpoint. Potential future uses of the model include studies of (a) dispersion of effluent from specific outfalls in the harbor complex, (b) tsunami waves, (c) effects of various coastal structures from Point Fermin to Huntington Beach, (d) effects of artificial offshore islands or landfill seaward of the existing harbor breakwater on tidal circulation and wave conditions, (e) tidal circulation in areas such as Huntington Beach, Bolsa Chica Wildlife Reserve, Alamitos Bay, etc., (f) effect of various future harbor modifications on tidal circulation and wave conditions, (g) studies of the physical environment in the harbor and surrounding areas, and (h) wave and tidal circulation studies of the proposed Downtown and Queensway Marinas.

PREFACE

The Los Angeles and Long Beach Port Authorities plan to construct additional harbor basins and dredge deeper channels and harbor areas to meet growing future demands for expansion of ship mooring facilities. The Los Angeles and Long Beach Harbors model study was undertaken to investigate (a) incidence of harbor oscillations adverse to ship mooring, (b) tidal circulation characteristics of the existing harbor and proposed expansions, (c) optimum plan for future expansions, and (d) effects of future expansions on existing harbor conditions. This report, the fourth in a series to be published under the general title "Los Angeles and Long Beach Harbors Model Study," considers design criteria, wave generator design and control, and data acquisition for the hydraulic model.

Project administration and funding were provided by the U. S. Army Engineer District, Los Angeles (SPL), under project management of Messrs. J. Chapman, H. Converse, and T. Nizinski and under the general direction of Messrs. G. Fuquay, former Chief of the Engineering Division, T. Nishihara, Chief of the Engineering Division, and C. H. Fisher, Chief of the Coastal Resources Branch. COL R. J. Malley, CE, COL J. V. Foley, CE, and COL H. G. Robinson, CE, were District Engineers of SPL during the course of this study. General project administration for the U. S. Army Engineer Division, South Pacific, was provided by Messrs. O. F. Weymouth, O. T. Magoon, J. W. Gerhart, and A. E. Wanket.

The data analyses were conducted in the Hydraulics Laboratory of the U. S. Army Engineer Waterways Experiment Station (WES), under the general supervision of Messrs. H. B. Simmons and F. A. Herrmann, Chief and Assistant Chief, respectively, of the Hydraulics Laboratory. This report was prepared by Mr. D. G. Outlaw, Harbor Wave Action Branch (HWAB), Dr. D. L. Durham, HWAB, Mr. C. E. Chatham, Chief of HWAB, and Dr. R. W. Whalin, Chief of the Wave Dynamics Division.

Model construction was supervised by Mr. C. W. Brasfeild with the assistance of Mr. R. R. Bottin. Two-dimensional breakwater and harbor side-slope wave tests were conducted by Messrs. Chatham and L. A. Barnes,

Civil Engineering Technician. The prototype wave refraction analysis was conducted by Mr. Chatham and the model refraction analysis by Mr. Outlaw.

Directors of WES during the model design and the preparation and publication of this report were BG E. D. Peixotto, CE, COL G. H. Hilt, CE, and COL John L. Cannon, CE. Technical Director was Mr. F. R. Brown.

CONTENTS

CONVERSION FACTORS, U. S. CUSTOMARY TO METRIC (SI)
UNITS OF MEASUREMENT

U. S. customary units of measurement used in this report can be converted to metric (SI) units as follows:

Multiply	By	To Obtain
inches	25.4	millimetres
feet	0.3048	metres
miles (U. S. statute)	1.609344	kilometres
miles (U. S. nautical)	1.852	kilometres
fathoms	1.8288	metres
square feet	0.09290304	square metres
square miles (U. S. statute)	2.589988	square kilometres
acres	4046.856	square metres
cubic yards	0.7645549	cubic metres
gallons per day	3.785412	cubic decimetres per day
pounds (force)	4.448222	newtons
feet per second	0.3048	metres per second
feet per second per second	0.3048	metres per second per second
degrees (angle)	0.01745329	radians
Fahrenheit degrees	5/9	Celsius degrees or Kelvins*

* To obtain Celsius (C) temperature readings from Fahrenheit (F) readings, use the following formula: $C = (5/9)(F - 32)$. To obtain Kelvin (K) readings, use: $K = (5/9)(F - 32) + 273.15$.

LOS ANGELES AND LONG BEACH HARBORS MODEL STUDY

MODEL DESIGN

PART I: INTRODUCTION

Background and Model Study Objectives

1. The ports of Los Angeles and Long Beach are located on San Pedro Bay along the southern coast of California. A location map and the harbor configuration are shown in Figure 1. Development of the harbors and historical surge activity are reviewed in detail as a portion of a study completed by Science Engineering Associates (SEA)[1] for the U. S. Army Engineer District, Los Angeles (SPL), in July 1968. The four major objectives of the Los Angeles and Long Beach Harbors study conducted by the U. S. Army Engineer Waterways Experiment Station (WES) are to:

a. Determine incidence and severity of troublesome oscillations in the present harbor complex.

b. Investigate tidal circulation characteristics of the present and proposed harbors.

c. Determine the optimum plan for future expansions to provide safe and economical berthing areas.

d. Analyze the effect proposed expansions will have on existing harbors.

The study results are being published in a series of reports under the general title "Los Angeles and Long Beach Harbors Model Study." This report is the fourth in the series and covers model scale and size, wave generator design, and model data acquisition and analysis procedures, primarily for wave-induced harbor oscillations. Model operation and appurtenant equipment for tidal circulation studies are discussed in Report 5.[2]

2. To achieve the first objective and acquire prototype tidal data for the second objective, the WES approach was to:

a. Acquire prototype wave data over a 1-yr period.

b. Record observations of ship motion.

c. Catalog ships using Los Angeles and Long Beach Harbors.

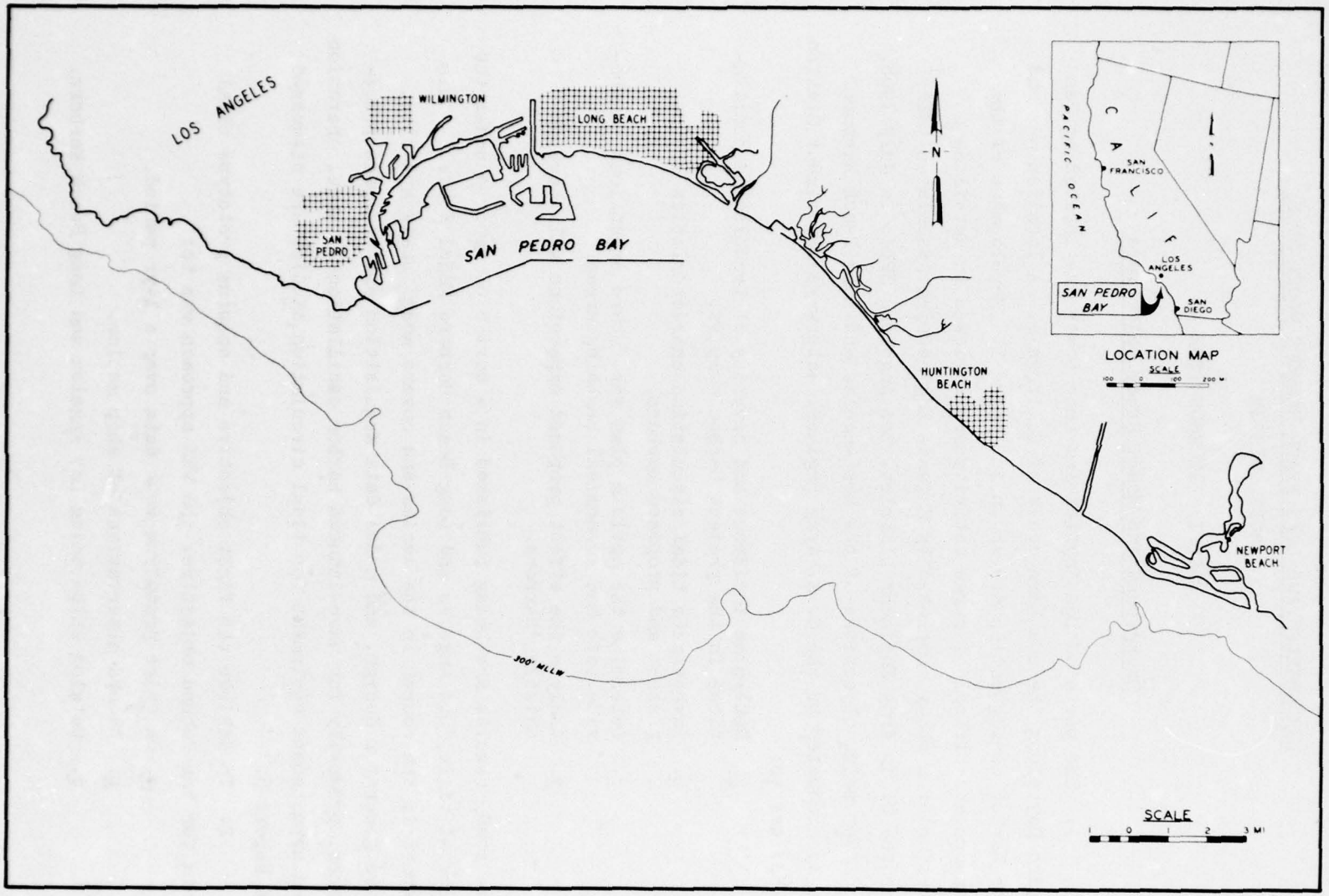

Figure 1. Site map

d. Conduct analytical investigations of moored ship response.

e. Perform extensive analyses of prototype wave data.

f. Attempt to correlate ship motion with wave height and frequency.

g. Collect prototype tidal height and current data to verify model tests of tidal circulation within the harbor complex.

The prototype data collection program for waves, ship motion, and tides is described in Report 1[3] and results of the wave data analyses are described in Report 3[4] of this series. Ship motion data were published in Report 2[5] and tidal data in Report 5.[2]

3. The purposes of the physical model study were to investigate harbor oscillation characteristics and tidal circulation for the existing harbor and to optimize design of the proposed harbor modifications to provide safe and economical berthing conditions while maintaining or improving circulation in the harbors.

4. Several previous model studies of San Pedro Bay have been conducted. The first model,[1] built in 1927, was of a relatively small section of Los Angeles Harbor and was used primarily to study the effect of various proposed modifications on surge conditions in East Channel. Other model studies[1,6,7,8,9] at WES and at the California Institute of Technology were conducted to study proposed plans for construction of a model for the Naval Base on Terminal Island, a proposed naval supply depot to be located near Point Fermin, and the Southeast Basin in Long Beach Harbor. In recent years, plans have been developed for additional expansion of the harbors (described in paragraphs 13-18) that would significantly modify the shape of the outer harbors and increase the depth in some areas to accommodate deep-draft vessels. As indicated in Reference 2, proposed plans are so extensive that a careful examination of their effects on existing harbor and expanded harbor facilities is required to ensure that the optimal cost effective expansion plan is developed in order to minimize the potential for undesirable effects which could prove either irreversible or extremely costly to correct. Wave-induced harbor oscillations can be of sufficient magnitude to create navigation, berthing, and mooring problems

due to their effect on ship motion. Should existing tidal circulation be impaired, the potential exists for insufficient pollutant dissemination and undesirable water quality. A physical hydraulic model is an excellent method for quantitatively investigating harbor oscillations and tidal circulation. Advantages of the physical model are that hydrodynamic phenomena can be scaled directly from model to prototype[1] (provided it is designed properly) and modifications to proposed harbor plans can readily be evaluated. Improper model design can result in the introduction[1] of spurious boundary effects and unnatural wave heights and mode shapes in the model.

5. In the SEA study, a physical model covering an area of approximately 9- by 16-nautical miles* with a 1:4-scale distortion was recommended for wave periods greater than 2 min and less than 1 hr. A second model of approximately 6- by 11-nautical miles with a 1:2-scale distortion at a larger scale was suggested for wave periods between 15 sec and 2 min. In the second model, the effect of model distortion on the time scale ratio at lower wave periods would be reduced. General model laws and scales for modal shapes and frequencies of oscillations, refraction, shoaling, and diffraction also were discussed in the SEA study for distorted physical models.

6. After review of the preceding physical model recommendations, the feasibility of using one model with a larger horizontal scale was considered at WES and a single model (Figure 2) was found to be feasible for investigation of both harbor oscillation phenomena and tidal circulation. In Part II of this report, the effects of wave refraction, diffraction, viscous friction, wave reflection, wave transmission through the harbor breakwaters, wave filters, and wave absorbers are considered in order to determine model scales and limits. In the remaining sections of the report, wave generator design and model data acquisition and analyses are described.

---

* A table of factors for converting U. S. customary units of measurement to metric (SI) units is presented on page 4.

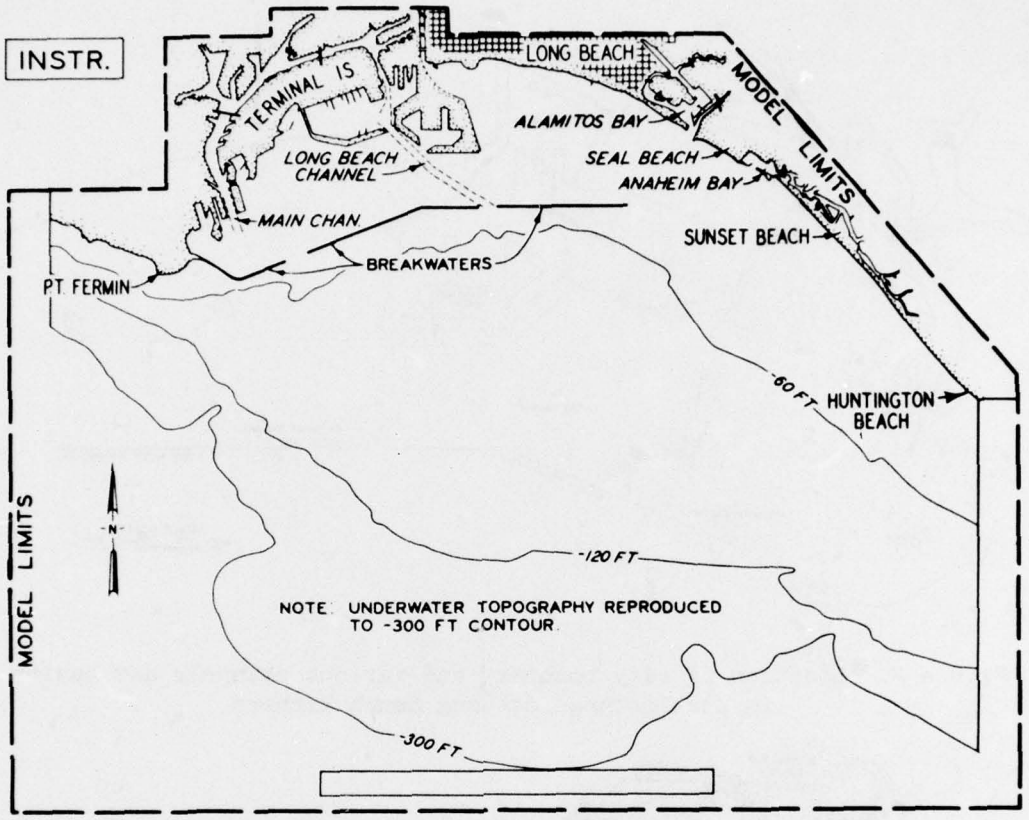

Figure 2. Los Angeles-Long Beach Harbors model

Description of Los Angeles and Long Beach Harbors

7. Los Angeles and Long Beach Harbors occupy a major part of San Pedro Bay and are separated by the city boundaries as shown in Figure 3. The harbor is 370 nautical miles southeast of San Francisco Bay and is 95 nautical miles northwest of San Diego Bay. San Pedro Bay is protected on the west by the Palos Verdes San Pedro Hills and Point Fermin but is exposed on the south and southeast. Santa Catalina Island and San Clemente Island partially shelter the harbor from the southwest. The offshore topography of the ocean bottom near San Pedro Bay is shown in Figure 4. As indicated on the figure, the continental shelf extends outward in a convex shape. Near the 100-fathom contour line, the shelf drops off sharply toward the San Pedro Channel, reaching

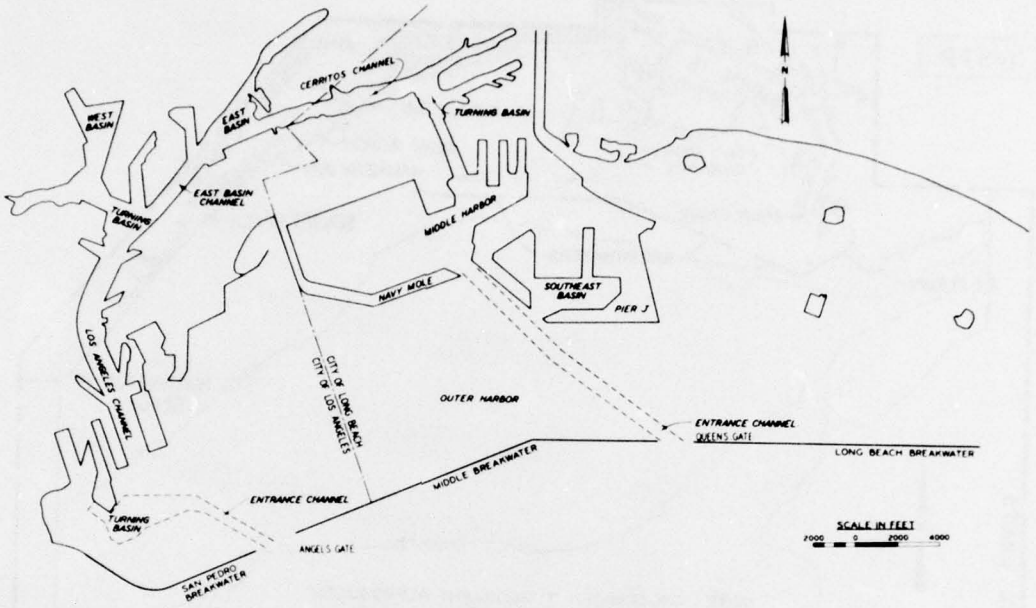

Figure 3. Location of city boundary and various channels and basins in the Los Angeles-Long Beach Harbors

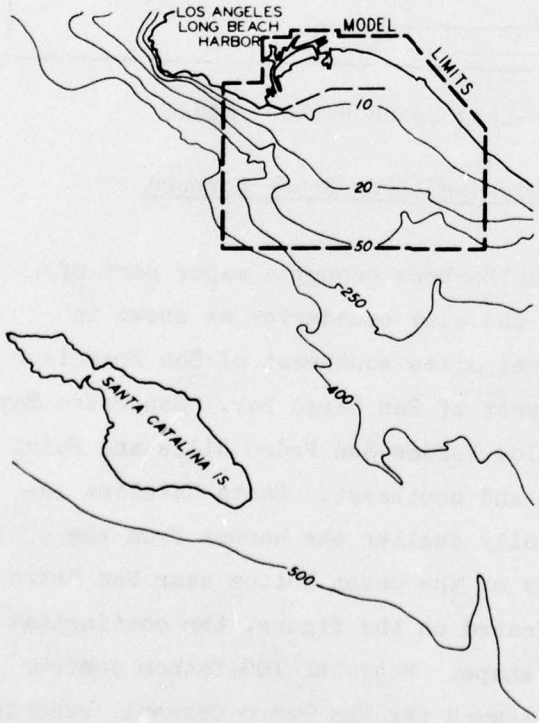

Figure 4. Underwater contours seaward of Los Angeles-Long Beach Harbors (contours in fathoms)

depths in excess of 500 fathoms. A submarine canyon also intersects the continental shelf on each side of the bay, and the canyons extend within the model limits as shown in Figure 4.

8. The harbor is protected on the seaward side by an 8-mile-long stone breakwater extending from Point Fermin eastward past the Long Beach Harbor (Figure 3). The breakwater[2] consists of three sections originally built approximately along the 50-ft contour line. The first to be constructed was the San Pedro breakwater from Point Fermin to Angels Gate, the Los Angeles Harbor entrance channel; the second was the Middle breakwater extending from Angels Gate to Queens Gate, entrance channel to Long Beach Harbor; and the third was the Long Beach breakwater.

9. The 11,152-ft-long San Pedro breakwater is of stone-mound construction with a cap course of granite blocks to an elevation of 14 ft above mean lower low water (mllw). The Middle and Long Beach breakwaters also are of stone-mound construction but have a sand core capped with a relatively impervious clay; the crown elevation of these two breakwaters also is +14 ft mllw. The impervious core in the Middle breakwater extends approximately 24 ft above the harbor bottom (-26 ft mllw) and the core of the Long Beach breakwater is 26 ft above the bottom (-24 ft mllw). Typical cross sections through the three breakwaters are shown in Figure 5.

10. Depths[10] in Los Angeles Harbor vary from 16 to 50 ft. Controlling depths for various channels and basins are:

Channel/Basin	Controlling Depth, ft mllw
Entrance channel	40
Midsection of entrance channel	51*
Turning basin (outer harbor)	51*
Los Angeles channel	35
Turning basin (inner harbor)	35
East Basin channel and Cerritos Channel	35
West Basin	35
East Basin	35

* Federal project depth of 40 ft; dredged to 51 ft by Port of Los Angeles.

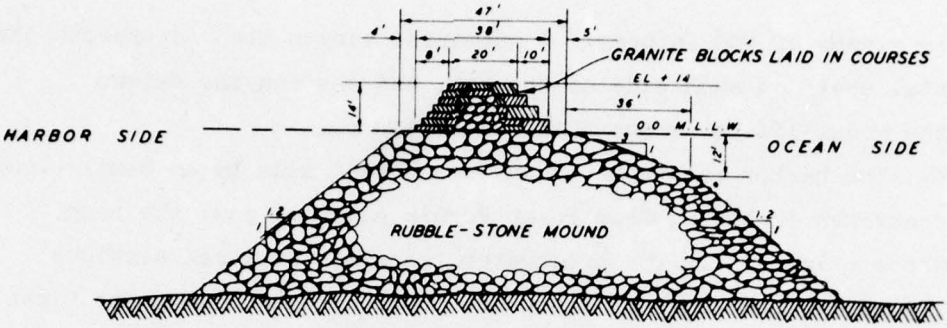

SAN PEDRO BREAKWATER

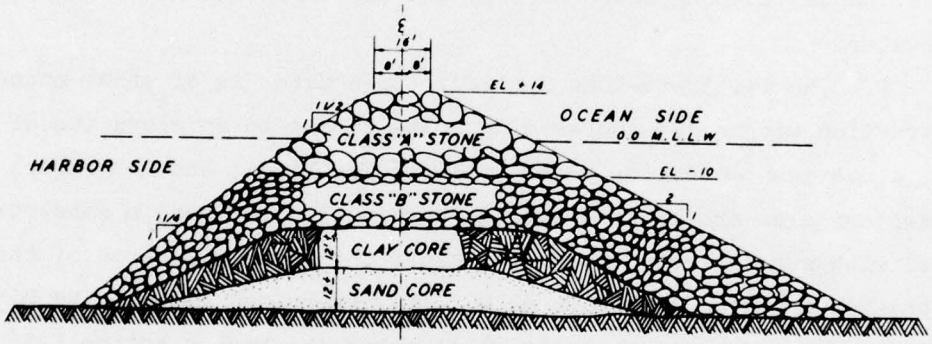

MIDDLE BREAKWATER

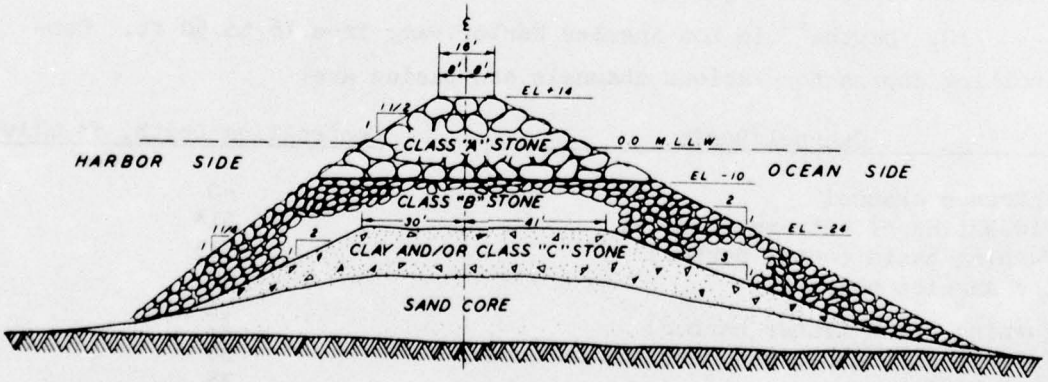

LONG BEACH BREAKWATER

Figure 5. Typical cross sections of the Los Angeles-Long Beach Harbors breakwater

In Long Beach Harbor, depths vary from 18 to 70 ft. Controlling depths for various channels and basins are:

Channel/Basin	Controlling Depth, ft mllw
Entrance channel	62
Cerritos Channel	50
Turning basin	55

The Federal project depth for the Long Beach turning basin and channels is 35 ft mllw, but the depths have been increased by the Port of Long Beach to accommodate deep-draft vessels. Considerable subsidence also has occurred in years past due to extraction of oil from the area.

11. Tidal circulation, freshwater discharge, salinity, and thermal stratification conditions in the existing harbors are discussed in Reference 2. A brief summary of the data from Reference 2 pertinent to model design is as follows:

a. Tides in San Pedro Bay are of a mixed type (two unequal tides per day) with a mean tidal range of 3.8 ft and a diurnal (mean higher high to mean lower low) range of 5.4 ft. Tidal datum is mllw which is 2.8 ft below mean sea level.

b. Tidal currents in the bay are rather weak with a normal maximum current velocity of approximately 1 fps. Wind-generated currents can be of the same order of magnitude.

c. Freshwater discharges are limited to intermittent storm runoff primarily through the Dominguez Channel and the Los Angeles River and a few other effluent discharges.

d. Salinity of the harbor is essentially uniform and very close to that of the surrounding coastal waters, approximately 33 to 34 ppt total salts. A surface layer of low salinity may form in individual basins due to storm runoff from rains, but these conditions are relatively rare and do not persist.

e. Low-salinity effluents include cannery wastes in the vicinity of Fish Harbor and discharge from the Terminal Island Sewage Treatment Plant. The effect of numerous other small effluent discharges in the harbor is not significant.

f. Cooling water discharges in Los Angeles Harbor are principally due to the Union Oil refinery which averages about 26 mgd with a maximum flow of about 30 mgd, and

the City of Los Angeles' harbor steam plant located adjacent to West Basin. The plant withdraws water from Los Angeles Harbor slip 5 and discharges into the northeast corner of West Basin with an average flow rate of 78 mgd. The plant operates at intervals dictated by peak electrical demand and has a capacity flow rate of 397 mgd with a 12-15°F temperature rise.

g. Thermal stratification in San Pedro Bay ranges from mild seasonal temperature gradients to strong local gradients near cooling water discharges. Ambient surface temperatures average about 50°F during the winter and 68°F during the summer.

An additional cooling water discharge is anticipated from a return to partial service of the Southern California Edison Company Generating Station on Terminal Island with a maximum flow rate of about 80 mgd. A second standby plant may increase the maximum flow rate by about 123 mgd at times. The cooling water intake and discharge are in the Long Beach back channel.

12. The average depth[2] of the entire harbor is approximately 36 ft below mllw; neglecting the inner harbor area, the average depth is approximately 38 to 39 ft. Navigation channels and ship berthing areas usually exceed the average depth, as discussed in paragraph 10. Average depths for various sections of the harbor are given in Reference 2.

Los Angeles and Long Beach Harbors
Proposed Development Plans

13. The proposed Federal project[11] includes dredging ship channels and turning basins in Los Angeles Harbor and deposition of the dredged material in parts of the harbor where new land areas are planned. The proposed Federal project will require dredging of approximately 10,000,000 cu yd and will provide about 187 acres of landfill. The dredged channel, shown in Figure 6, is needed in the Los Angeles Harbor to permit use of the port by larger general cargo bulk and container vessels. Diking for the landfill would be provided by local interests.

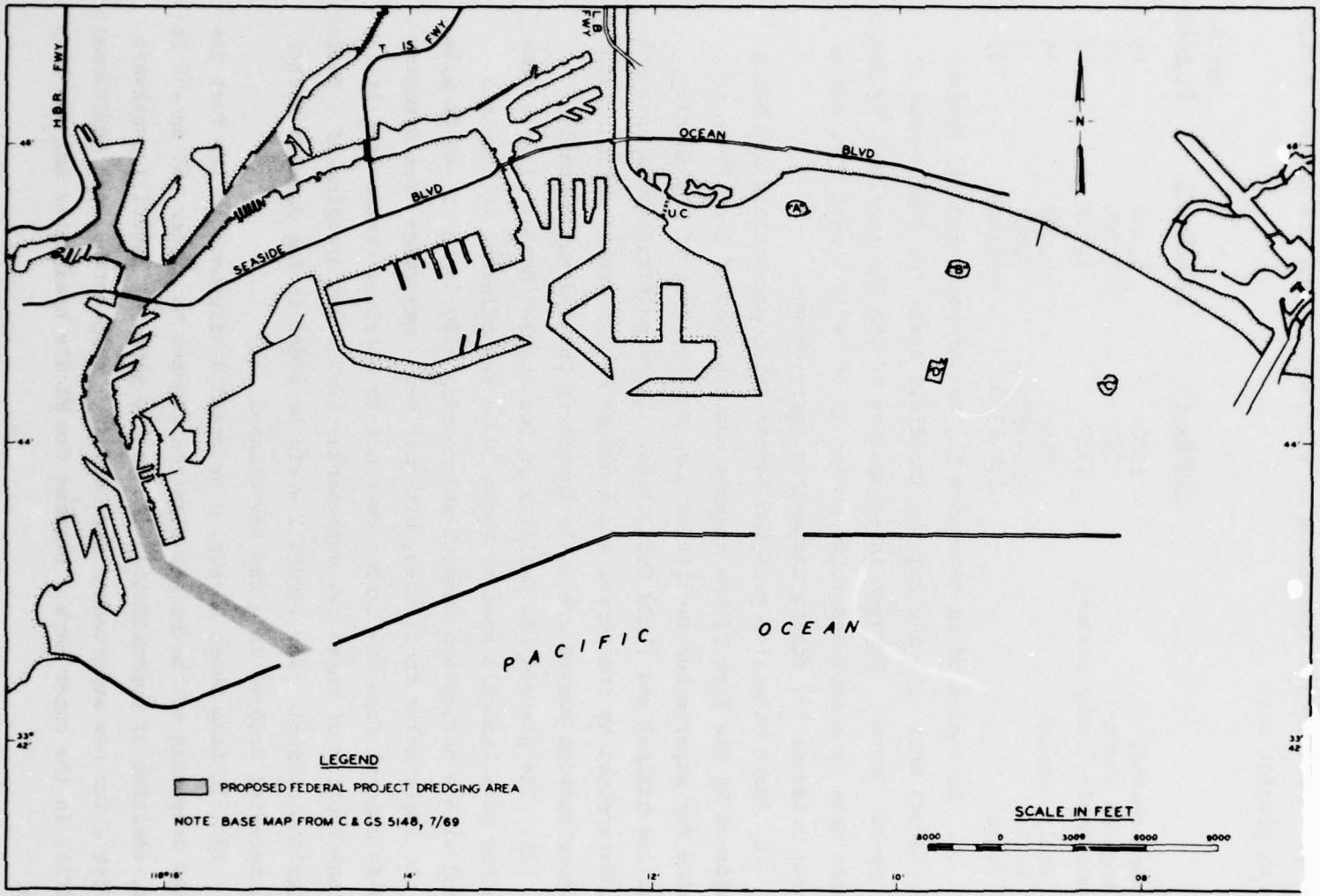

Figure 6. Dredging areas in the Los Angeles-Long Beach Harbors for the proposed Federal project

14. Recommended dimensions of waterways in the Los Angeles Harbor Federal project are:

	Width, ft	Length, ft	Depth, ft mllw
Entrance channel	1000	5,500	45
Los Angeles channel	750	12,500	45
Turning basin (inner harbor)	1350	1,650	45
East Basin channel	350	6,000	45
West Basin	350-1350	',800	45
East Basin	350-1350	variable	4

15. As indicated in Reference 11, the propo Federal project is concerned only with meeting the immediate needs for improvement of Los Angeles Harbor. Further investigation of the Los Angeles-Long Beach Harbors area is authorized to determine if there is a need for, and a Federal interest in, future navigation improvements.

16. More extensive proposed harbor development plans are being considered by the Port of Los Angeles and the Port of Long Beach to provide for supertanker facilities and, for the Port of Los Angeles, liquified natural gas (LNG) facilities. Exact configurations have not been determined by the ports, and a number of different configurations and construction phases are to be tested in the hydraulic model.

17. The planned LNG facility in Los Angeles Harbor will be constructed on a landfill area of about 300 acres adjacent to Terminal Island with a navigation channel and mooring slip depth of -45 ft mllw. For the supertanker facilities, alternatives[12] may range from dredging a 65-ft channel from the harbor entrance to existing tanker facilities to construction of three new supertanker berths and dredging of a deeper navigation channel. New landfill would be added in Los Angeles Harbor with material dredged from the new channel.

18. In Long Beach Harbor, a proposed development by the Port includes deepening of the main navigation channel to either -65 or -82 ft mllw, addition of approximately 120 to 130 acres of landfill southward of Pier J for new supertanker and container ship berths, and additional landfill in the outer harbor between the Middle breakwater and the Navy Mole.

19. An example of an early proposed development plan which included a marine development by the City of Long Beach east of the Southeast Basin is shown in Figure 7. The development plan is preliminary but provides an indication of planned harbor improvements. In Long Beach Harbor several revisions including reduction in the size of the landfill and addition of a breakwater have been proposed adjacent to Pier J. Future development of the harbor will undoubtedly be constructed in phases.

Model Description

20. The Los Angeles-Long Beach Harbors hydraulic model (Figure 2) was molded in cement mortar and reproduced to scale San Pedro Bay and a portion of the Pacific Ocean surrounding the harbor area. The model shoreline extended from approximately 2 miles northwest of Point Fermin to Huntington Beach. Underwater contours were reproduced out to the

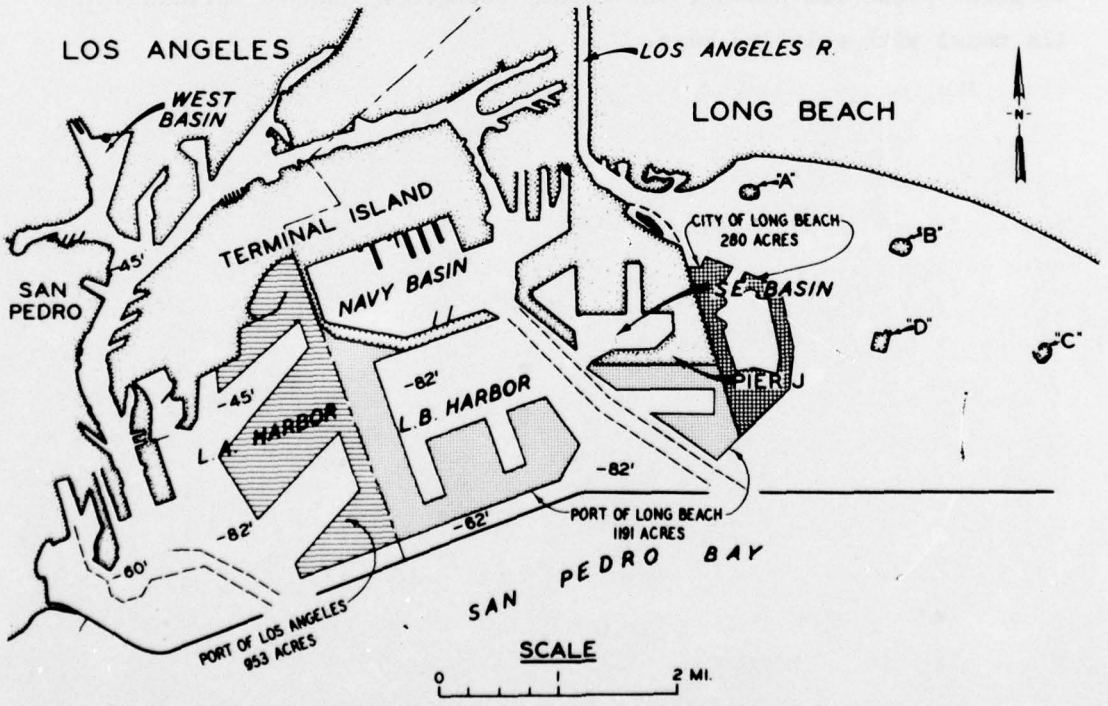

Figure 7. Example of a proposed development plan for the Los Angeles-Long Beach harbors

-300 ft mllw contour, and sufficient additional offshore area was included to provide room for wave generators and the tide generator. A general view of the model is shown in Figure 8. Operation of the tide generator system is discussed in Reference 2.

21. The model scales were 1:100 vertically and 1:400 horizontally. The model area was approximately 44,000 sq ft, representing about 253 square miles of prototype area. Depth data for model contours were obtained from the U. S. Coast and Geodetic Survey (now National Ocean Survey) Charts 5101 and 5147, and from harbor soundings provided by the Ports. Major piers and wharves were reproduced in the model with 1/16- and 1/32-in.-diam brass rods used to simulate pier piling. The bays east of the harbor such as Alamitos Bay and Anaheim Bay were correctly reproduced in plan but depths were averaged in the model in order to expedite construction and, at the same time, permit proper reproduction of approximate tidal volumes. If future studies in these areas are needed, the actual topography can be installed in the model with relative ease.

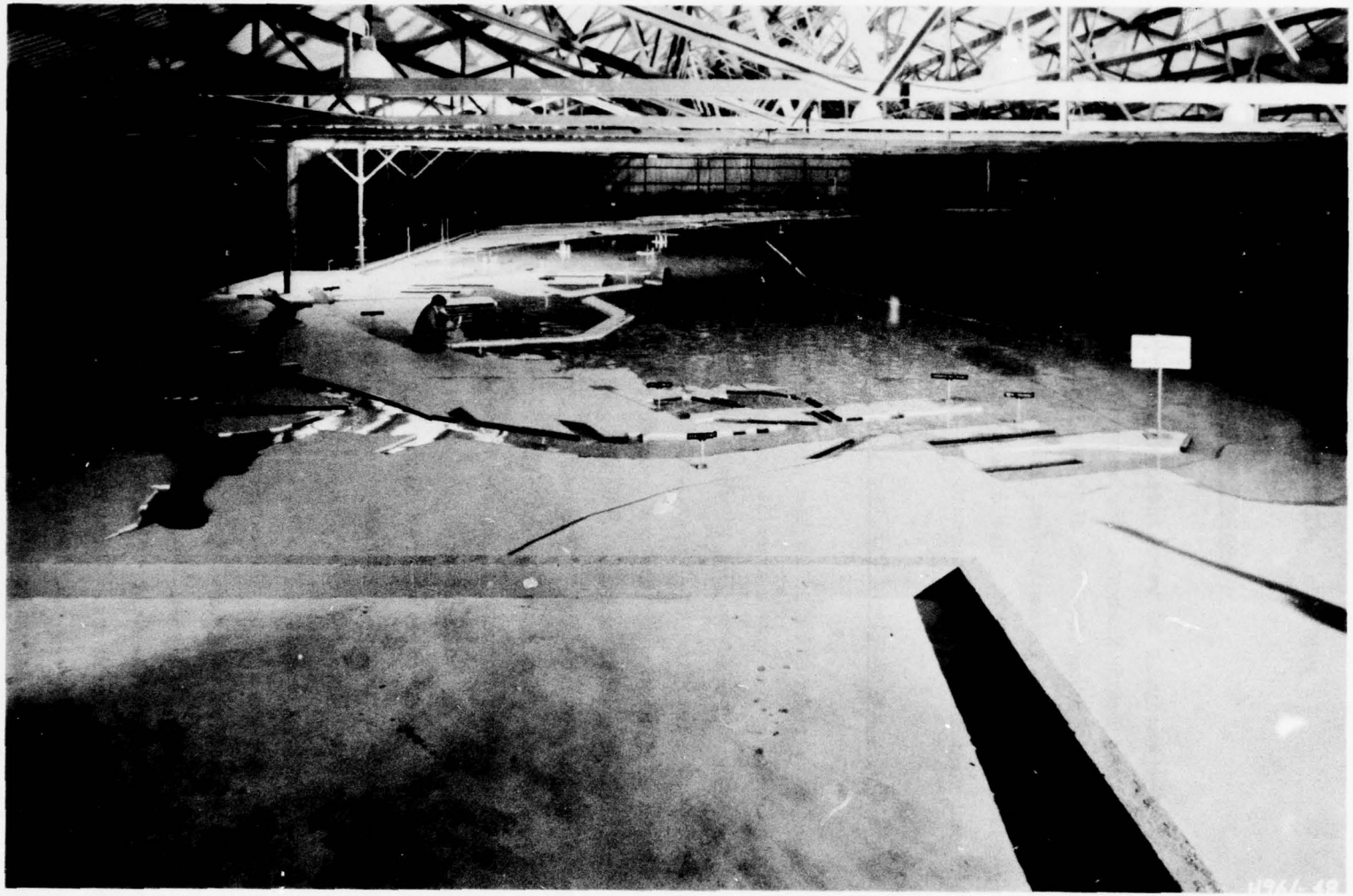

Figure 8. General view of the Los Angeles-Long Beach Harbors model

PART II: MODEL DESIGN ANALYSIS

Design of Model

22. For analysis of wave-induced harbor oscillations in the Los Angeles-Long Beach Harbors, the parameters considered during model design were wave refraction and diffraction, viscous friction effects, wave reflection, wave transmission, and wave filters and wave absorbers. Also considered were the absolute dimensions of model wave heights and periods and cost of model construction.

Wave Refraction, Diffraction, and Harbor Response

23. Wave refraction[13] is the process by which the direction of waves approaching a coastal area at an angle to the contours is changed. The part of the wave advancing in shallower water moves more slowly than that part advancing in deeper water, causing the wave crest to bend toward alignment with the underwater contours. Dependent upon the shape of the underwater contours, bending of the wave front may increase or decrease the wave height. The protection provided San Pedro Bay by the offshore islands and the broad sill west of San Pedro Bay connecting San Nicolas and Santa Rosa Islands varies with wave direction and period. However, previous refraction studies[1] have shown that the bay is relatively well protected from long-period wave attack except for directions between south-southeast and south-southwest. Wave refraction analysis[1] by SEA indicates that short-period waves (near 15 sec) from the south are focused along the breakwater near the Long Beach Harbor navigation entrance due to the convex shape of the underwater contours. SEA wave refraction diagrams[1] from the south for longer period waves (30 sec or larger) indicate that these waves can propagate into the harbor area through the Gulf of Santa Catalina without encountering any effective natural barriers. Wave heights seaward of the harbor area also would be relatively unaffected. The refraction analysis by SEA also included other directions for 15-, 30-, 60-, and 120-sec waves, and

the results[1] support the conclusion that San Pedro Bay is relatively well protected except from the south-southeast through the south-southwest.

24. Diffraction[13] is the phenomenon by which energy is transmitted laterally along a wave crest. Near an island or breakwater, the waves propagate into the sheltered area in the lee of the structure. In a distorted-scale model, refraction and diffraction cannot both be properly scaled simultaneously. Refractive effects depend on wave celerity and are a function of h/L (the ratio of water depth h to wavelength L). Diffraction is a function of x/L or y/L (the ratio of horizontal distance to wavelength). If wavelength is scaled according to the vertical length scale in a distorted-scale model, the ratio h/L will be in exact similitude and consequently refraction similitude will be achieved. If wavelength is scaled according to the horizontal length scale in a distorted-scale model, the ratio x/L or y/L will be in exact similitude and diffraction similitude will be achieved. In the Los Angeles-Long Beach model study, the most important design constraint is that similitude of mode shapes and resonant frequencies of oscillation be precisely achieved. The governing Helmholtz equation[1] for harbor oscillations is

$$\frac{\partial}{\partial x}\left(h\,\frac{\partial \eta}{\partial x}\right)+\frac{\partial}{\partial y}\left(h\,\frac{\partial \eta}{\partial y}\right)+\frac{\sigma^2}{g}\,\eta=0 \qquad (1)$$

where

x,y,z = axes of a rectangular coordinate system fixed at the mean water surface

η = local surface elevation

σ = angular frequency

g = acceleration due to gravity

Since the same equation applies in model and prototype, Equation 1 may be written as

$$\left(\frac{h_r \eta_r}{x_r^2}\right) \frac{\partial}{\partial x_p}\left(h_p \frac{\partial \eta_p}{\partial x_p}\right) + \left(\frac{h_r \eta_r}{y_r^2}\right) \frac{\partial}{\partial y_p}\left(h_p \frac{\partial \eta_p}{\partial y_p}\right)$$

$$+ \eta_r \sigma_r^2 \left(\frac{\sigma_p^2}{g}\right) \eta_p = 0 \qquad (2)$$

where the subscript p represents the prototype and r, the scale ratio of model to prototype. From inspectional analysis, the coefficients of Equation 2 must be equal, or

$$\frac{h_r}{x_r^2} = \frac{h_r}{y_r^2} = \sigma_r^2 \qquad (3)$$

after dividing through by η_r. Equation 3 indicates that a hydraulic model may be distorted for proper simulation of harbor resonant oscillation frequencies. The angular frequency may be written in terms of wavelength and water depth and Equation 2 indicates that the wavelength must be scaled by the horizontal scale ratio. Wave height, however, may be scaled by the vertical scale ratio.

25. Therefore, using the horizontal scale ratio L_r for wavelength, diffraction and harbor oscillation frequencies will be in similitude but refraction will have a scale effect due to model distortion. For shallow-water waves where the wave celerity is governed by the local depth, model distortion will have little effect on refraction. The equation for wave celerity C from small amplitude wave theory is

$$C = \left(\frac{g}{k} \tanh kh\right)^{1/2} \qquad (4)$$

where k is the wave number, $2\pi/L$. As the wave period increases, $\tanh kh$ approaches kh and, for shallow-water waves, the celerity becomes

$$C = (gh)^{1/2} \qquad (5)$$

Consequently, for shallow-water waves, model distortion has a negligible effect on wave refraction. The ratio of celerity calculated from Equation 4 to the shallow-water approximation of Equation 5 is shown in Figure 9 as a function of wave period for water depths of 39, 50, 100, and 300 ft (for both the prototype and the distorted-scale model). As indicated by Figure 9, the distortion scale effect on wave celerity is negligible (<1.3% at 300 ft) for $T \geq 120$ sec. At depths less than 300 ft, the wave period above which the wave celerity remains relatively constant (i.e. $C \rightarrow \sqrt{gh}$) decreases. The shape of the offshore topography also influences wave refraction patterns, and if the wave front propagates approximately normal to the offshore contours, refraction patterns may be similar at periods much less than the lower limit indicated for 1.3 percent accuracy by the shallow-water celerity approximation.

26. Due to the model distortion, the time scale ratio T_r is affected by the choice of vertical or horizontal scale for wavelength. The angular wave frequency is

$$\sigma = \frac{2\pi}{T} = (gk \tanh kh)^{1/2} \tag{6}$$

Using the horizontal scale for wavelength, the time scale ratio can then be written as

$$T_r = \left[L_r \frac{\tanh\left(\frac{2\pi}{L_p} h_p\right)}{\tanh\left(\frac{2\pi}{L_m} h_m\right)} \right]^{1/2} \tag{7}$$

where the subscript m refers to model quantities. The equation can also be written as

$$T_r = \left[L_r \frac{\tanh\left(\frac{2\pi}{L_p} h_p\right)}{\tanh\left(\frac{2\pi n}{L_p} h_p\right)} \right]^{1/2} \tag{7a}$$

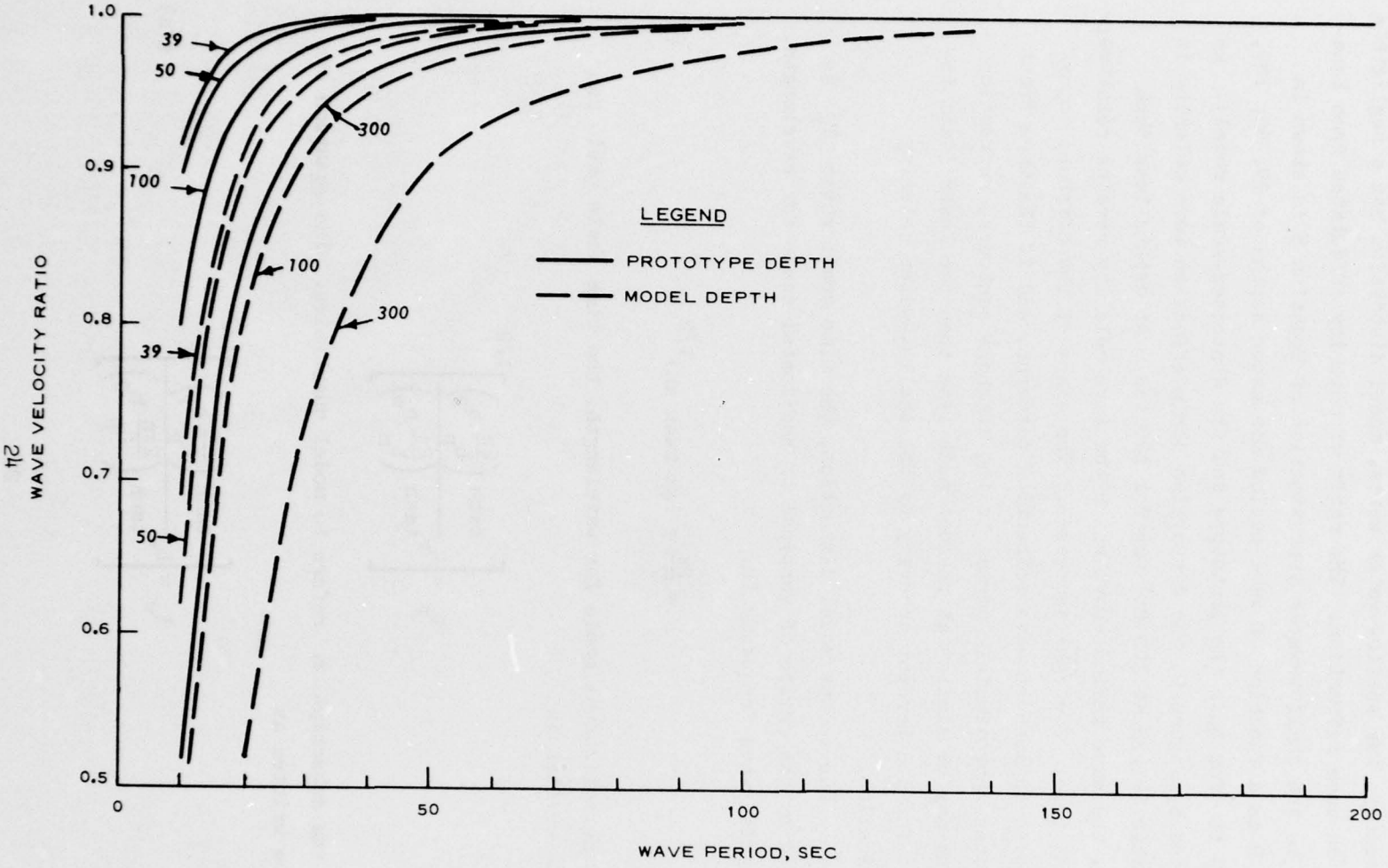

Figure 9. Ratio of wave celerity calculated from the shallow-water approximation for depths of 39, 50, 100, and 300 ft

where n is the model distortion. As tanh kh approaches kh , the time scale ratio may be approximated by

$$T_r = \frac{L_r}{(h_r)^{1/2}} \tag{7b}$$

For an average depth of 39 ft, the prototype wave period calculated from Equation 7b is within 1 percent of the period calculated from Equation 7 for $T \geq 85$ sec . In a distorted-scale model where refraction is the most significant effect and wavelength is scaled by the vertical scale, the time scale ratio is:

$$T_r = (h_r)^{1/2} \tag{7c}$$

27. In summary, for analysis of wave-induced harbor oscillations, the preceding discussion of simulating refraction, diffraction, and resonant frequencies of oscillation in a distorted model indicates that:

a. Wavelengths in the model should be scaled by the horizontal scale ratio.

b. The time scale ratio from model to prototype is dependent on wave period and water depth and is given by Equation 7.

c. The harbor is relatively well protected from long-period wave attack except from the south-southeast through south-southwest.

d. Refraction in the distorted-scale model and prototype will be in similitude (to a very close approximation) for longer wave periods (say, greater than 75 sec). However, at shorter wave periods, there may be some refraction scale effects that require adjustment in either the wave generator position and/or wave height in order to ensure similitude of wave refraction.

Results of a detailed wave refraction analysis are given in the next sections for distorted- and undistorted-scale conditions.

Wave Refraction Analysis

28. A detailed wave refraction analysis was conducted for the

offshore area using an analysis procedure[14] that calculates wave orthogonals with the usual assumption that wave energy is not transmitted along the wave front perpendicular to the wave orthogonal. Wave height H is given by

$$H = K_r K_s H_i \tag{8}$$

where

K_r = refraction coefficient
K_s = shoaling coefficient
H_i = initial wave height

Bottom reflection is neglected since this effect is normally not significant for small slopes. Bottom friction and percolation also are neglected[15] since their effect is minor in the prototype for small amplitude, long-period waves. As a part of the procedure, a second-degree polynomial is fitted by a least-squares technique to 12 points in a rectangular grid with a square mesh surrounding the area through which the orthogonal is propagating.

29. The accuracy of the polynomial representation of complex offshore topography increases as the number of points in the rectangular grid increases. Two rectangular grids were used for prototype conditions in the wave refraction analysis: Grid 1 covers a large area with a wide grid spacing; Grid 2 covers a small area adjacent to the harbor with a more detailed grid; and the boundaries of the two grids are shown in Figure 10. The wave refraction data from Grid 1 are used for the initial wave orthogonal data in Grid 2. Grid point spacing and grid size were:

Grid No.	Point Spacing, ft	Grid Size, ft
1	9740	360,380 × 418,820
2	1675	110,550 × 187,600

Depth data at each grid point were obtained from the U. S. Coast and Geodetic Survey (now National Ocean Survey) Chart 5101 for Grid 1 and Chart 5142 for Grid 2. Grid 2 data also were used for the physical

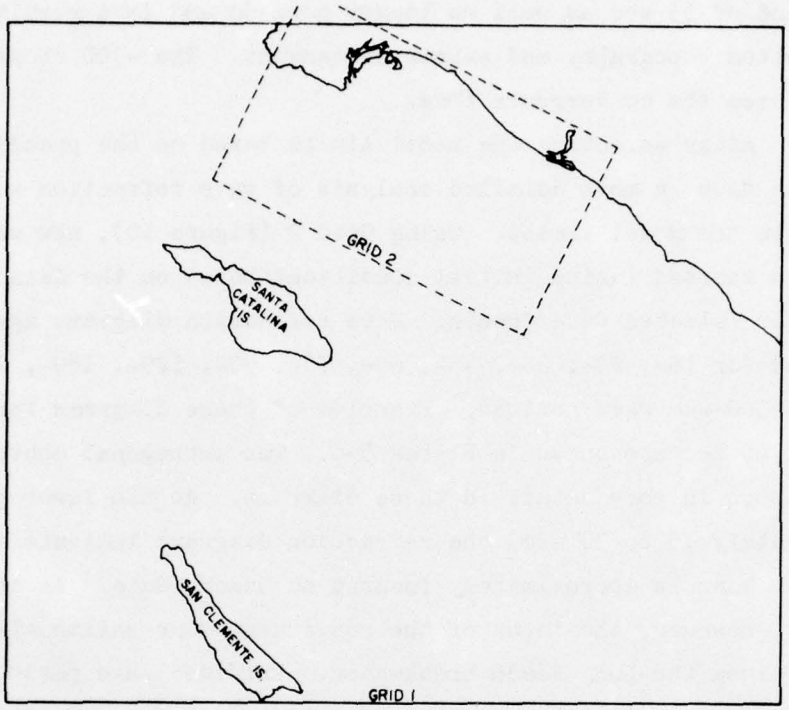

Figure 10. Location of wave refraction Grids 1 and 2

model wave refraction analysis with depths limited to a maximum of 300 ft mllw.

30. Wave refraction diagrams were calculated for 15, 20, 30, 45, 60, 75, 90, 120, 180, 240, 300, and 360 sec using Grid 1 for waves approaching from the south. Plates 1-4 show the refraction diagrams for wave periods of 15, 30, 60, and 300 sec. Refraction patterns for the remaining periods are similar. The diagrams show the effect of Santa Catalina Island on wave refraction at the longer wave periods. Strong convergence of wave energy seaward of the Queens Gate breakwater entrance is vividly illustrated. The model limits also are shown in Plates 1-4 and have been selected to ensure that the convergent zone is included within the model area. Within the strong convergent zone, diffraction effects not accounted for by normal wave refraction analyses become quite significant[16,17] and refraction coefficients are no longer valid. The convergent zone, although not as pronounced, exists for a

wave period of 15 sec as well as longer periods and is a result of the convex bottom topography and submarine canyons. The -300 ft mllw contour encloses the convergence zone.

31. After selecting the model limits based on the preceding wave refraction data, a more detailed analysis of wave refraction was necessary within the model limits. Using Grid 2 (Figure 10), new wave orthogonals were started (using initial conditions based on the data from Grid 1) for selected wave fronts. Wave refraction diagrams again were calculated for 15-, 20-, 30-, 45-, 60-, 75-, 90-, 120-, 180-, 240-, 300-, and 360-sec wave periods. Examples of these diagrams for 30, 60, 180, and 360 sec are shown in Plates 5-8. The orthogonal convergent zone is shown in more detail in these diagrams. At the lower periods (approximately 15 to 30 sec) the refraction diagrams indicate that the convergent zone is approximately focused on Queens Gate. As the period increases, however, the focus of the convergent zone shifts slightly eastward along the Long Beach breakwater. Provided wave periods are greater than approximately 75 sec, refraction patterns are similar near the convergent zone. The wave orthogonals do not directly overlay since the orthogonals were started from varying locations along the wave front selected for each wave period due to refraction occurring seaward of the initial wave front used for the detailed analysis. Similarity of refraction patterns (for $T \geq 75$ sec) is primarily due to the effect of depth on wave celerity discussed in paragraph 25.

32. The shape of the wave front for 15-, 20-, 30-, 45-, 60-, 75-, and 360-sec wave periods immediately after the wave front enters within the model limits and approaches the -300 ft mllw contour is shown in Plates 9-11. The 15- and 20-sec wave fronts are relatively straight but the 30- and 45-sec wave fronts are starting to curve as the refractive effects increase. For longer wave periods, shape of the wave fronts is similar near the -300 ft mllw contour. However, near the east and west model limits wave front shape varies with wave period. This variation is due to the effect of Santa Catalina Island, the two submerged canyons, and nearshore topography at the east and west model limits. The variation also can be seen in the large grid wave refraction diagrams shown

in Plates 1-4. In general, bathymetry near Santa Catalina Island causes the wave orthogonals passing the island to bend northwestward as the period increases. Nearshore, the orthogonals tend to bend perpendicular to the offshore topography as the period increases. The complexity of these effects precludes a consistent trend in wave front shape (as a function of period) near the model limits. It will be illustrated later that differences in wave front location at longer wave periods (in the prototype) seem to be balanced by the effects of model distortion and limitation of model depths to -300 ft mllw, and consequently, a single wave front position can be used in the model for longer periods.

33. The effect of model scale distortion on wave refraction was initially investigated using Grid 2 with the grid point distance scaled by the horizontal scale and depths by the vertical scale for the following conditions:

Condition No.	Distortion Ratio	Vertical Scale	Horizontal Scale
1	1:2	1:100	1:200
2	1:3	1:100	1:300
3	1:4	1:100	1:400

As indicated above, model distortion ratios of 1:2, 1:3, and 1:4 were considered. Change in model scale with the same distortion ratio produces identical refraction patterns and is not considered. The 1:100 vertical scale was near the minimum scale ratio necessary for measurement of small amplitude waves. Typical examples of distorted-scale wave refraction diagrams are shown in Plates 12-23 for conditions 1 to 3 at 30-, 60-, 180-, and 360-sec wave periods. The distorted-scale refraction analysis also included the 15-, 20-, 45-, 75-, 90-, 120-, 240-, and 300-sec periods. The initial data for orthogonal azimuth and wave front starting location were taken from the results of the undistorted-scale (prototype) Grid 2 wave refraction analysis. Comparison of the distorted-scale wave refraction diagrams indicates that wave refraction patterns for the 1:3 and 1:4 distortion ratios are similar for all wave periods. However, at 15 and 30 sec, the wave refraction pattern for the 1:2 distortion ratio varies significantly

from the two larger distortion ratios. At and above 60 sec, the refraction patterns are similar for all three distortion ratios. Also, comparison of the refraction diagrams for the prototype with the corresponding refraction diagrams for distorted-scale conditions at 15-, 30-, 45-, and 60-sec wave periods indicates that the prototype and distorted-scale refraction will be similar above approximately 60 sec; but near 60 sec and below, the location of the wave front for distorted-scale conditions is affected by the distortion and must be adjusted in order for model wave refraction tc simulate the prototype refraction.

34. Due to the results of the preceding analysis of distortion effects on wave refraction, a model distortion ratio of 1:4 was selected. The 1:4 distortion ratio minimizes the model area and does not significantly increase the period range over which adjustment of the initial model wave front is necessary for refraction similitude. It was clearly illustrated that there was a negligible difference in refraction scale effects when changing the distortion factor from 3 to 4; however, there was a difference for a distortion ratio of 2. Thus, the only question is whether to choose a distortion of 2 or 4. The cost reduction achieved by the large reduction in model area (a factor of 4) using a 4 distortion ratio greatly outweighs the relatively modest technical advantage of slightly smaller refraction scale effects. This is especially true when the refraction scale effect can be corrected (as is the case here) by a change in the model wave front position. Since the wave refraction convergent zone is inclosed within the -300 ft mllw contour, the underwater contours were reproduced out to this contour. The submerged canyons near the east and west model limits are not reproduced (below the -300 mllw contour) and adjustment of the initial model wave front to compensate for the decreased depths in the canyon areas is necessary.

35. Adjustment of the initial model wave front position was accomplished by an iterative procedure. A wave front location and wave orthogonal azimuth were selected, a refraction diagram calculated, a comparison made with the refraction diagram calculated using Grid 2 for the same period, and the process was repeated until approximate

similitude of wave fronts and orthogonal azimuths was achieved seaward of the breakwater and adjacent to the convergent zone. The initial prototype and adjusted wave front locations are shown in Plates 9-11 for 15-, 20-, 30-, 45-, 60-, 75-, and 360-sec wave periods. Also shown in Plates 9-11 are the comparisons of wave front positions for each of the wave periods seaward of the harbor breakwater after the convergent zone has formed.

36. In general, the prototype and model wave fronts near the breakwater compare closely at the lower wave periods and reasonably well as the period increases. For the longer periods shown in Plates 10 and 11, the model wave fronts tend to diverge slightly from the prototype near either end. While it may appear that minor shifting of the initial model wave front would result in more exact agreement, the prototype wave orthogonal azimuths along the wave front also must be simulated and the intial wave front shown represents a compromise between the requirements that both wave front position and orthogonal azimuth should be in similitude. Examples of the agreement between prototype and model orthogonals are given in Tables 1 and 2 for 20- and 75-sec wave periods. As indicated by the azimuth data, the maximum variation of the model azimuth from the prototype for the 20-sec wave period is 9.1 degrees with an average variation of 3.9 degrees. Four of the ten 20-sec orthogonals have a model azimuth less than the prototype. For the 75-sec period, the maximum azimuth variation is 8.1 degrees. The variation for the remaining 12 orthogonals is less than 5 degrees and the average variation is 2.8 degrees. Five of the thirteen 75-sec orthogonals have a model azimuth less than the prototype.

37. The adjusted wave front location shown in Plates 9-11 is composed of straight line segments corresponding to the length of each unit of the wave generator. The straight-line segments also affect the accuracy within which the wave front location and orthogonal azimuth can be matched.

38. As indicated in Plates 9-11, the initial model wave front locations for 15-, 20-, and 30-sec wave periods show little variation, especially in the central sections of the wave front near the -300 ft

contour; thus, in the 15- to 30-sec range, an average of the three initial wave front locations was selected for the initial model wave front location. Similarly, an average wave front was selected for the 45- to 60-sec range. These average initial wave fronts are shown in Plate 24 along with the initial model wave front for the 75-sec and above wave period range. As shown in Plate 24, the average of the initial model wave front for the 45- to 60-sec range is shifted significantly from the 15- to 30-sec average initial wave front along the western limit of the wave front. Additional model wave refraction analysis was necessary to determine the initial model wave front to be used in the transition from 30 to 45 sec. The wave front selected as a result of the additional analysis for 35 sec also is shown in Plate 24 and provides a smooth transition from the 15- to 30-sec range to the 45- to 60-sec range. The additional analysis indicated the average 45- to 60-sec model wave front was acceptable for a 40-sec period.

39. Wave heights at each of the wave generators also were calculated in the refraction analysis. The prototype wave height was calculated using Equation 8 at a location seaward of the convergent zone and within the -300 ft contour. Then, normalized wave heights along the wave front at the wave generator were calculated using model refraction coefficient data. The normalized wave heights for each of the 14 wave generator units at 15, 20, 30, 45, 60, 75, and 90 to 360 sec are shown in Table 3. The shoaling coefficient has not been used in developing Table 3. There is a shoaling coefficient scale effect in the model (due to the scale distortion and method of scaling) which will be accounted for in analyzing the model data; however, shoaling does not affect the normalized wave height at the wave generator.

40. Normalized wave heights tend to reach a maximum near wave generator units 10, 11, and 12 in the 15- to 30-sec period range; but at 45 sec and above, the maximum normalized value occurs near wave generator unit 12. Location of wave generator units in the 15- to 30-sec period range are shown in Figure 11. The shift in the maximum normalized wave height to wave generator unit 12 is probably due to the increased northwestward refraction near Santa Catalina Island discussed

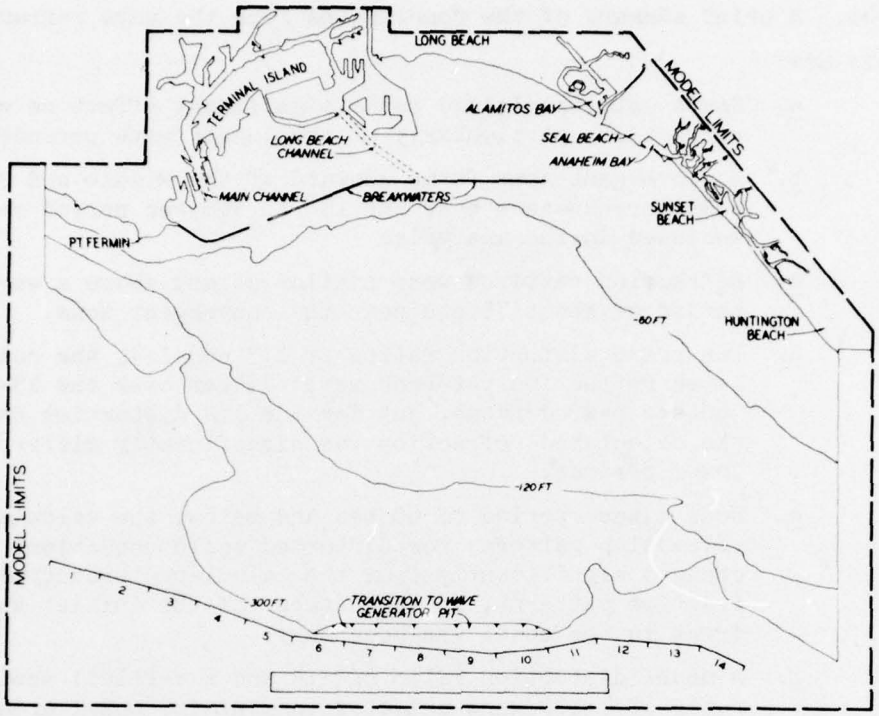

Figure 11. Location of wave generator units 1 to 14 in 15- to 30-sec period range

in paragraph 31. The minimum normalized wave height along the initial model wave front occurs at wave generator unit 2 and is probably due to the effect of the submerged canyon on the western side of the harbor area on wave refraction. The normalized wave height data also indicate that the height of the wave front propagating into the Los Angeles Harbor area is less than the height of the wave front propagating into the Long Beach Harbor area. For a 15-sec wave period, the refraction analysis indicates that for an initial wave front, the wave height at Angels Gate should be approximately 40 percent of the wave height at Queens Gate. If the variation in wave height along the wave front is not simulated, the resonant frequencies in the harbor area will not be affected but resonant response amplitudes and the wave energy distribution could be affected. Thus, it was planned to simulate the variable height along the wave front.

41. A brief summary of the conclusions from the wave refraction analysis are:

a. Santa Catalina Island has a significant effect on wave refraction, particularly at the longer wave periods.

b. A convergent zone forms seaward of the Middle and San Pedro breakwaters over the 15- to 360-sec period range included in the analysis.

c. Refraction patterns were similar at and above a wave period of about 75 sec near the convergent zone.

d. For scale distortion ratios of 1:3 and 1:4, the calculated refraction patterns were similar over the 15- to 360-sec period range, but for the 1:2 distortion ratio, the calculated refraction was significantly different at lower periods.

e. Near a wave period of 60 sec and below, the calculated refraction patterns for distorted scale conditions changed significantly from the calculated prototype refraction patterns, and adjustment of the initial wave front in the model was necessary.

f. A model distortion ratio of 1:4 and a vertical scale ratio of 1:100 were selected to minimize model area and to provide a vertical scale ratio where accurate model measurements could be assured.

g. The position of the initial model wave front must be adjusted to compensate for distortion scale effects and for refraction caused by bathymetry at depths greater than -300 ft mllw (limit of model bathymetry).

h. Normalized wave-height variation along the prototype wave front is significant and should be reproduced in the model wave tests.

Model Wave-Height Attenuation

42. Waves in a model may be attenuated by surface tension, internal friction, and friction in the bottom boundary layer. In the wave period range to be simulated in this study, surface tension effects increase as the wave period decreases; and for a model wave period of 0.5 sec, near the minimum to be generated in the model, the effect of surface tension on wave celerity is less than 0.1 percent.[18] Internal friction effects decrease as the wave period increases, and for the 0.5-sec model wave period, the wave-height attenuation from wave

generator unit 9 to the Long Beach breakwater is less than 3.2 percent. For a 1-sec wave period, the height attenuation is less than 0.2 percent. Using an average harbor depth of 39 ft, the 0.5- and 1-sec wave periods represent prototype periods of 14.4 sec and 37.0 sec, respectively. The wave-height attenuation due to internal friction was calculated[19] from

$$\frac{H_t}{H_i} = e^{-8\pi^2 \nu t / L^2} \tag{9}$$

where H_t is the wave height at time t and ν is the kinematic viscosity. The kinematic viscosity was assumed to be 1.059 (10^{-5}) for 70°F.

43. The attenuation of wave height for a progressive oscillatory wave with distance x due to friction in the bottom boundary layer may be calculated from Keulegan's equation[20]

$$\frac{H}{H_i} = e^{-\alpha x} \tag{10}$$

where

$$\alpha = \frac{5\pi^{3/2} \nu^{1/2} T^{1/2}}{L^2 \left(\sinh \frac{4\pi h}{L} + \frac{4\pi h}{L} \right)} \tag{11}$$

and T is the wave period. In developing Equation 11, the width of the wave crest is assumed to be many times greater than the depth in a rectangular channel of uniform cross section. The attenuation factor at various periods for two locations is tabulated below. The first attenuation factor column is for a wave traveling from wave generator unit 1 in the 45- to 60-sec position to the San Pedro breakwater which has a minimum wave travel distance. The second attenuation factor column is for a wave traveling from wave generator unit 9 to the Long Beach breakwater and is representative of the maximum wave travel distance before entering the harbor.

Period, sec	Attenuation Factor, $\frac{H}{H_i}$ San Pedro Breakwater	Long Beach Breakwater
15	0.99	0.99
20	0.99	0.97
30	0.98	0.94
45	0.97	0.92
60	0.97	0.93
75	0.97	0.93
90	0.98	0.94
120	0.98	0.95
180	0.99	0.97
240	0.99	0.98
300	0.99	0.98
360	0.99	0.99

44. The maximum variation in the attenuation factor for the two travel distances is 0.05, indicating that variation in travel distance for the present case has a relatively small effect on wave-height attenuation. The wave height may be varied along the generated wave front to correct for the small variation in wave-height attenuation or, when comparing model wave heights with prototype heights directly, the observed model wave heights can be increased to reflect attenuation in the model.

Wave Reflections

45. Wave reflections may occur from the underwater topography seaward of the harbor, from the breakwaters, and from the harbor side slopes. In the prototype, wave reflection from the underwater topography and the breakwater would propagate seaward; but in the model, waves reflected from these sources may also re-reflect from the model wave generator and possibly affect the incident waves. Reflections from the model side slopes within the harbor may affect[21] the amplitude of harbor oscillations and should be correctly simulated. The wave reflection coefficient C_r is the ratio of the reflected wave height H_r to the incident wave height H_i or

$$C_r = \frac{H_r}{H_i} \tag{12}$$

The reflection coefficient varies from 1.0 for total reflection to 0.0 for no reflection. In general, the magnitude of the reflection coefficient will depend on geometry, composition of a structure, and incident wave characteristics such as wave steepness η/L, (η is the local water-surface elevation) and relative depth h/L near the structure.

46. Reflection from the offshore contours was estimated using a theory developed by Rosseau[22] which provides an analytical solution for the reflection coefficient. The development of the theory also is described in Reference 16. Rosseau's theory requires no assumptions concerning wave form other than linear small amplitude progressive waves propagating from $+\infty$ in a canal of variable depth as shown in Figure 12, and that the bottom profile may be described by a specified function such that the depth approaches H_2 as y goes to $-\infty$ and h_1 as y goes to $+\infty$. The solution is not valid for a discontinuous change in slope; however, the Rosseau contour can approach the shape of a discontinuous sloped step in bottom contours. An incompressible nonviscous fluid is assumed and the solution is obtained using a conformal mapping technique.

47. In the bottom contour reflection analysis, the following three cases were considered for a typical model depth variation with a length of 50 ft and a change in depth of 1.5 ft:

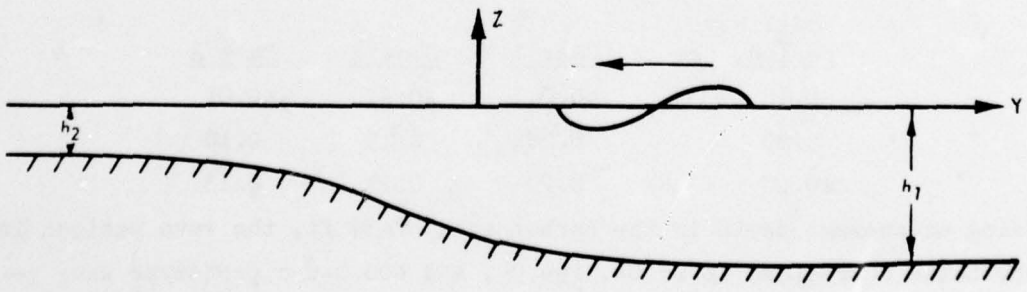

Figure 12. Rosseau canal

Case No.	Depth h_1, ft	Depth h_2, ft
1	2.0	0.5
2	2.5	1.0
3	3.5	2.0

These depths are representative of steep model-depth changes seaward of the harbor breakwater. In Figure 13, a comparison of the Rosseau contour with the bottom contour for Case 1 shows that the Rosseau contour closely fits the bottom slope. The comparisons for Cases 2 and 3 are similar.

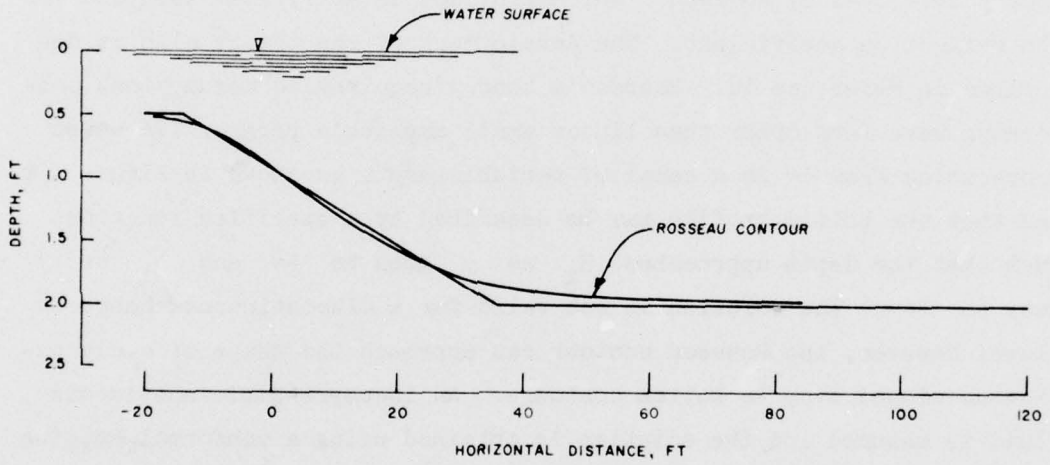

Figure 13. Rosseau contour for Case 1

48. Reflection coefficients for various model wave periods calculated for the three cases are given in the following tabulation:

Model Wave Period, sec	Case 1	Case 2	Case 3
0.75	<0.01	<0.01	<0.01
5.00	0.20	0.15	0.10
10.00	0.29	0.21	0.13

Using an average depth in the harbor area of 39 ft, the wave periods in the table correspond to 26.0-, 199.9-, and 400.0-sec prototype wave periods. The reflection coefficients range from essentially 0 in the lower wave period range to 0.29 for Case 1. The reflection coefficients

for all three cases, however, indicate that wave filters in front of the wave generator will be required at longer periods to attenuate the height of the reflected wave from changes in the offshore topography. The period range over which wave filters will be required is also affected by reflection from the harbor breakwaters and model sidewalls. Many sections of the steep model depth changes are oriented such that the wave is reflected toward the model's perimeter walls, and wave absorbers will be required along the walls to attenuate these reflections.

49. Wave reflections from the distorted-scale harbor breakwater also may require attenuation by the wave filters. Two-dimensional wave flume tests conducted in the 20- to 100-sec prototype wave period range (described in paragraph 56) to determine the reflection coefficient from the Middle and Long Beach model breakwaters indicate the reflection coefficient varies from approximately 0.4 to 0.6. Two-dimensional flume tests were not conducted above 100 sec due to flume length limitations. The model wave reflection coefficients determined from the two-dimensional tests are given in Table 4 for 20-, 30-, 40-, 50-, 60-, 79-, 80-, 90-, and 100-sec prototype wave periods. The reflection coefficients given in Table 4 are for prototype wave heights of approximately 1 ft and for approximately 3 to 4 ft. Design of the model breakwater is discussed in more detail in the following breakwater transmission section. Two-dimensional tests were not conducted for the San Pedro breakwater section; however, the reflection coefficient should decrease without an impervious core.

50. To evaluate the effect of side-slope distortion in the harbor area, two-dimensional tests in a 2-ft-wide flume with a flapper-type wave generator were conducted for a typical prototype side slope (Figure 14) with a vertical wall down to -5 ft and a 1-on-1.5 slope from -5 to -50 ft at a 1:25 scale. Still-water level during the tests was at +5 ft. Wave data from a moving wave gage were recorded on strip charts during the tests. Reflection coefficients were calculated from

$$C_r = \frac{H_a - H_n}{H_a + H_n} \tag{13}$$

where

H_a = wave height at the antinode of the wave envelope recorded by the moving wave gage

H_n = height at the node

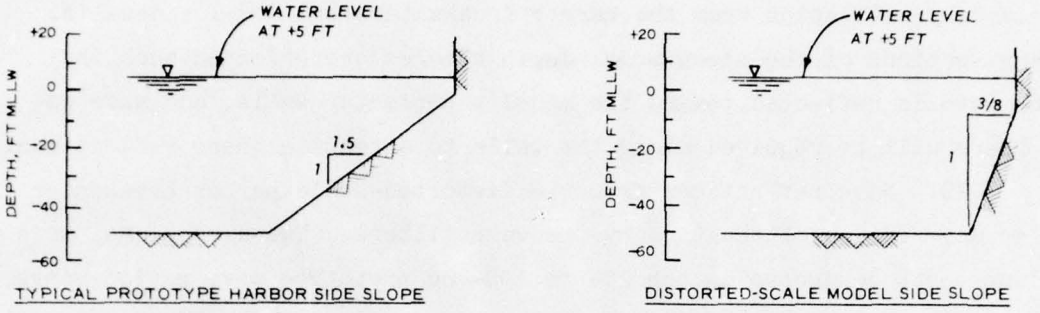

Figure 14. Typical prototype and model side-slope section

51. The reflection coefficients calculated using Equation 13 for various periods are as follows.

Prototype Wave Period, sec	Prototype Wave Height, ft	Reflection Coefficient
20	0.93	0.84
30	0.96	0.80
40	1.05	0.78
50	0.97	0.78
60	1.24	0.75

In some cases, harmonics observed on the strip chart wave record made determination of the wave height at the node H_n difficult. Generally, in the presence of harmonics at the node, the reflection coefficient[23] was actually higher than that calculated from Equation 13.

52. If the typical side-slope section is considered as a smooth slope with a 1-on-1.5 slope, the theoretical reflection coefficient, calculated from the Miche theory[21] for wave reflection from a plane sloping beach, is 1.0 for the periods of 20 sec or longer and wave steepness values H/L included in the experimental test series. For a flat side slope, the reflection coefficient is usually modified by an empirical coefficient (<1) which is constant for a given structure. For a flat

side slope, a value[24] of 0.9 can be used and the resulting theoretical reflection coefficient for small wave steepness (as in this case) is 0.9 at periods of 20 sec and longer. Allowing for experimental error, the calculated reflection data from the two-dimensional wave tests for the typical side slope and the theoretical reflection coefficient for a flat side slope are in good agreement and indicate that the typical side slope selected (vertical wall down to -5 ft and a 1-on-1.5 slope) may be considered as a plane 1-on-1.5 side slope for calculation of the reflection coefficient.

53. In the distorted-scale model, steepness of the typical side-slope section will be increased by a factor of 4 to a side slope of 1 on 3/8 as shown in Figure 14. Again considering the distorted-scale side slope as a plane slope, the theoretical reflection coefficient is 0.9 for small wave steepness in the 20-sec and longer wave period range. Thus, no modification in the shape of the distorted-scale side slope is necessary for simulation of prototype reflection in the distorted-scale model.

54. The surface of the typical side slope modeled in the two-dimensional wave tests was smooth. In the harbor, many side slopes are covered by a protective layer of rock. However, the size of the rock on the side slopes is small relative to the wavelength. Experimental data[25] with various relative roughness values indicate that the slope protection will have little effect on the reflection coefficient, and the slope protection was not reproduced in the model.

Wave Transmission

55. Long-period wave energy may enter a harbor either by penetration through rock-fill breakwaters or diffraction through harbor entrances. Wave penetration or transmission through the harbor breakwater is especially important in the case of Los Angeles and Long Beach Harbors due to the long extent of the breakwater. Energy transmission through the breakwater will affect harbor resonance and should be simulated in the model. Two-dimensional flume tests were conducted to

estimate the wave transmission coefficient of a typical section of the Long Beach breakwater (illustrated in Figure 5 with the top of the impermeable section at an elevation of -24 ft). Typical prototype dimensions (diameter D) of the Class A and Class B rock are 4.7 and 1.8 ft, respectively. The breakwater section was modeled at a 1:20 scale with a prototype water depth of 50 ft. Wave transmission tests were conducted in a 2-ft-wide flume approximately 150 ft long with a flapper-type wave generator. The wave transmission test series was conducted in the 20- to 100-sec wave period range. The wave period range was limited to 100 sec by the wave flume length. The wave transmission coefficient C_t was calculated from

$$C_t = \frac{H_{tm}}{H_i} \tag{14}$$

where H_{tm} is the transmitted wave height. The calculated transmission coefficient for the 20- to 100-sec period range is shown in Plate 25 as the curve for undistorted-scale conditions. The transmission coefficient varies from 0.17 for 20 sec to 0.24 for 100 sec.

56. A wave transmission test series also was conducted in the two-dimensional flume for three distorted-scale breakwater sections with a 1:100 vertical scale and a 1:400 horizontal scale as shown in Figure 15. The three breakwaters tested included a cross section composed entirely of the larger (Class A) rock scaled by the vertical scale ratio, a cross section composed entirely of the smaller (Class B) rock scaled by the vertical scale ratio, and a cross section with Class A and Class B rock scaled by the vertical scale ratio. The calculated wave transmission coefficient for each of these three cross sections is shown in Plate 25. As shown by the wave transmission data in Plate 25, the section composed only of the larger (Class A) rock has a higher transmission coefficient over the period range than the undistorted-scale cross section, and the section composed only of the smaller rock has a lower transmission coefficient. However, the wave transmission coefficient for this breakwater section composed of Class A and B rock agrees closely with the data for the undistorted-scale section. Therefore, this breakwater section was

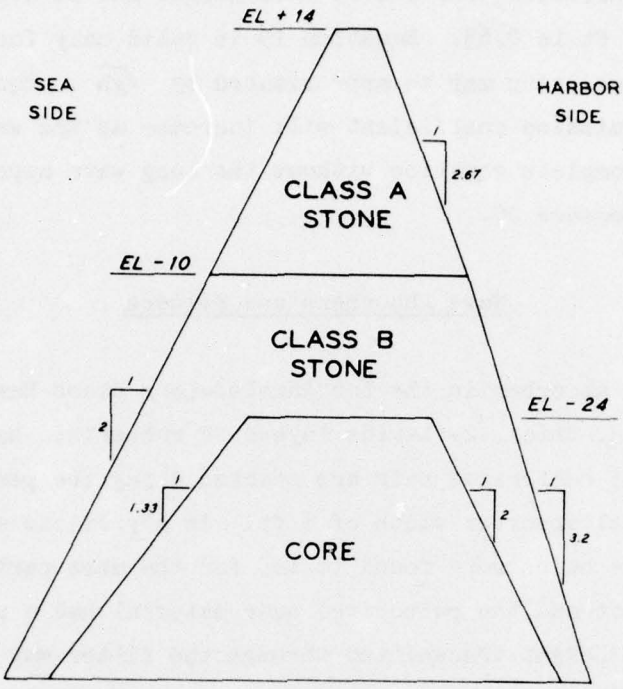

Figure 15. Typical section of model breakwater; distortion = 4; rock sizes scaled using vertical scale (1:100)

selected for installation in the model for the Middle and Long Beach breakwaters.

57. As shown in Figure 5, the San Pedro Breakwater has a solid granite cap but does not have an impervious core. The rock size is Class A or a typical dimension of 4.7 ft. The vertical scale ratio of 1:100 also was used for selecting rock in the San Pedro breakwater. Without the impervious core or the smaller (Class B) rock, the San Pedro breakwater should have a larger transmission coefficient than the other two breakwaters. Using the following equation[26] developed by Dr. G. H. Keulegan for wave transmission in the prototype

$$\frac{H_i}{H_{tm}} = 1 + \frac{2.11}{D}\left(\frac{H_i}{2h}\right)\Delta L \qquad (15)$$

where ΔL is the length through the breakwater structure; the wave

transmission coefficient for a 1-ft wave height and an average length at middepth of 128 ft is 0.63. Equation 15 is valid only for long waves where the wave celerity may be approximated by $\sqrt{gh}$. Equation 15 indicates the transmission coefficient will increase as the wave height decreases. The complete equation without the long wave approximation can be found in Reference 26.

Wave Absorbers and Filters

58. Wave absorber in the Los Angeles-Long Beach Harbors model is composed of 2-in.-thick, 2-ft-wide layers of rubberized hair. Three adjacent rows of rubberized hair are stacked along the perimeter of the model for a total absorber width of 6 ft. In a previous study,[27] the diameters of the hairs were found to be, for the most part, approximately 0.00051 ft and the rubberized hair material had a porosity of 0.96. The wave height transmitted through the filter may be calculated from the following equations developed by Dr. G. H. Keulegan:[27]

$$\left(\frac{H_0}{H_1}\right)^{1/2} = 1 + \beta \left(\frac{H_0}{2h}\right)^{1/2} \frac{\Delta L}{L} \tag{16}$$

where

H_0 = initial wave height in the filter
H_1 = final wave height before leaving the filter
ΔL = length of the filter

$$\beta = 5.4 \, (LT)^{1/2} \tag{17}$$

for a kinematic viscosity of 0.9 (10^{-5}).

59. From Equations 16 and 17 and assuming a reflection coefficient of 1.0 for the model wall, the ratio of the incident wave height to the final wave height for a 0.05-ft model wave height transmitted through the rubberized hair to the model wall and reflected back through the hair again in model depths of 0.5 and 3.0 ft is:

Model Wave Period, sec	H_1/H_0	
	0.5-ft Depth	3.0-ft Depth
0.64	0.01	0.06
1.09	0.01	0.09
1.56	0.02	0.10
2.03	0.02	0.11
2.52	0.02	0.11
3.74	0.02	0.12
5.01	0.02	0.12
10.0	0.02	0.12

Equation 16 has been confirmed with experimental data in the 0.77- to 1.91-sec wave period range but has not been confirmed with experimental data in the longer period range. The preceding reflection data indicate that 6 ft of wave absorber along the model perimeter will be sufficient. Provision has been made in the model for an additional 4-ft thickness of wave absorber if required for future wave tests. The wave will also be partially reflected from the front surface of the rubberized hair as the wave first impinges on the hair, but WES experience with rubberized hair wave absorber in a previous hydraulic model investigation[28] of oscillation in Port Hueneme Harbor, California, indicates that surface reflections will not adversely affect the generated wave heights.

60. In the tidal headbay area of the model, the width of the wave absorber has been decreased to 4 ft. The decrease in width will allow for tidal inflow during circulation studies without modification of the absorber. The remaining wave absorber will not adversely affect normal tidal circulation.

61. Two-dimensional wave flume tests also were conducted for design of wave filters to be placed in front of the wave generator for attenuation of waves reflected from offshore topography and the harbor breakwater. The wave filter test series was conducted in the 2-ft flume with a flapper-type wave generator. The filters were made using sections of 2-in.-thick rubberized hair retained in metal frames and suspended on edge in the flume. The frames were made from angle iron with a 6-in.-square wire mesh holding the hair in place. The frames were 1 ft apart in the flume and tests were run with 2, 4, and 6 filter

frame sections placed in series. The wave-height transmission coefficients for the test configuration are shown in Figure 16 for the 0.5- to 10-sec model period range. The data show the transmission coefficients are small at 0.5 sec but rise rapidly to approximately 3 to 4 sec and then continue with a gradual increase in the remaining period range. The data for two filter sections in series are shown only in the 0.5- to 4-sec range.

62. Arrangement and choice of the number of filter sections to be used will be based somewhat on experience gained during model operation. Initially, it is anticipated that in the shorter period range (up to approximately 45- to 60-sec prototype), the wave travel time between the generator and the breakwater will be sufficient to allow time for any resonant oscillations to form in the harbor and for measurements to be taken prior to arrival of any re-reflected waves from the wave generator. Therefore, wave filters may not be needed in this period range. Above this period range, however, various combinations of the filter sections will be required.

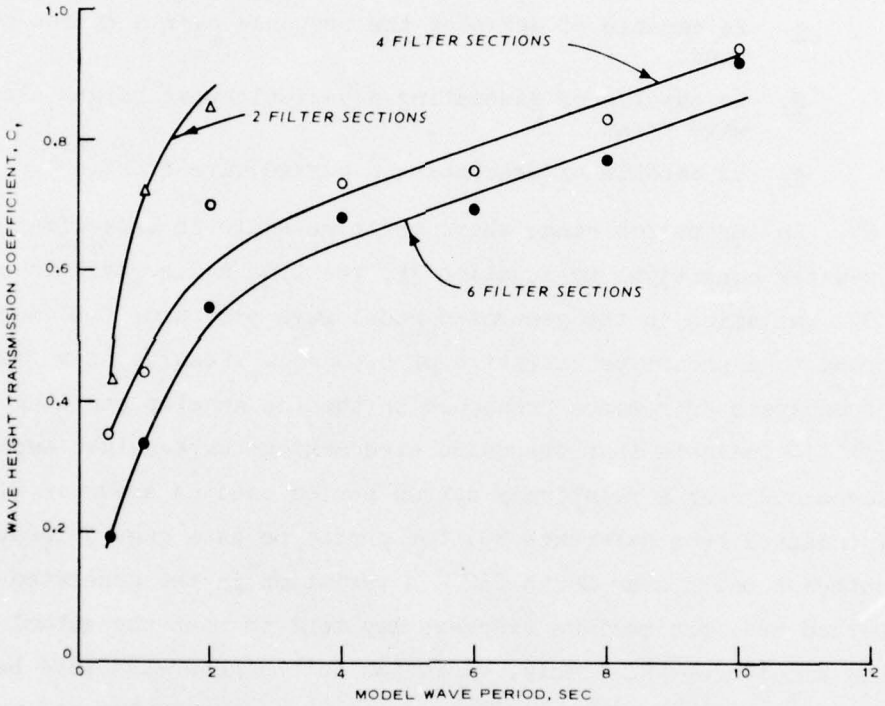

Figure 16. Wave transmission coefficient for rubberized hair filter sections

PART III: MODEL WAVE GENERATOR OPERATION AND PERFORMANCE REQUIREMENTS

63. In a physical model study of resonant response in Los Angeles and Long Beach Harbors, the wave generator should:

a. Be capable of generating waves with a prototype period ranging from approximately 15 to 600 sec.

b. Have a small variation in the generated wave period and height between wave generator unit to unit.

c. Be capable of defining the response over a narrow period band.

d. Be capable of generating a variable wave height along the wave front.

e. Be capable of generating a curved wave front.

64. In the period range where the time scale is approximated for shallow-water conditions by Equation 7b, the time scale ratio is constant at 1:40. Variation in the generated model wave period of 0.01 sec would correspond to a prototype variation of 0.40 sec. Results of a finite element analysis of resonant response in the Los Angeles and Long Beach Harbors[29,30] indicate that the calculated maximum wave-height amplification may occur over a relatively narrow period band as shown in Figure 17 (adapted from Reference 30) for prototype data gage 5 located in the southeast basin near Berth 232. A variation in the generated model wave period near the maximum response may tend to mask the actual maximum response amplitude. Similarly, variation in the generated wave height will affect the level of incident wave energy in the harbor and could affect the maximum resonant amplitude. Generally, past WES studies such as the hydraulic model investigation[28] of Port Hueneme, California, indicate that the physical model tends to respond over a broader period band and at a lower amplitude where a sharply peaked maximum resonant response is calculated numerically. The wave generator should, however, have a sufficiently small generated wave period variation to adequately define the response within a relatively narrow period band.

65. The necessity for variation of the generated wave height along the wave front and a curved wave front has been discussed in the

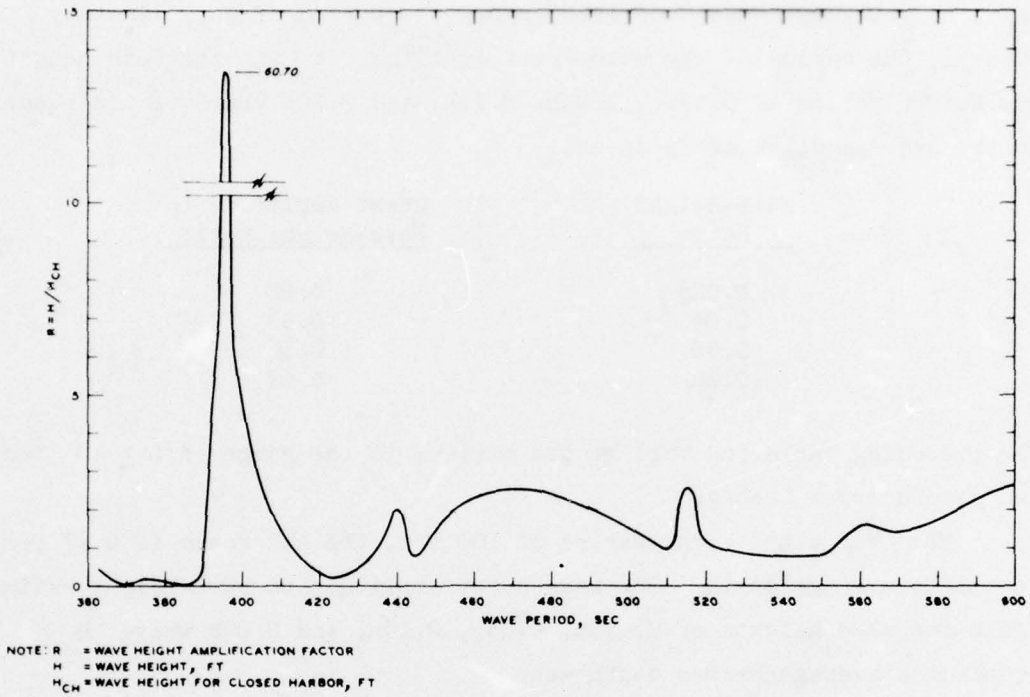

Figure 17. Calculated wave-height amplification at prototype wave gage location 5 from numerical harbor oscillation analysis (adapted from Reference 30)

wave refraction analysis section of Part II. Prototype wave heights over the low frequency portion of the 15- to 600-sec period range are quite small and could not be measured accurately in the model; therefore, increased wave heights will be used during the model test series and the wave response data will be normalized. The increase in wave height should be limited to the wave-height range in which the increased height will have little effect on the wave form.

66. In evaluating the effect of an artificial increase in wave height, the second order Stokes wave theory,[31] where the ratio of water depth to wavelength is 1/10 or larger, may be used; and for a depth to wavelength ratio of less than 1/10, cnoidal theory may be used. The second order Stokes theory predicts[31] that for a finite amplitude wave, the amplitude of the crest is larger than the trough amplitude and the form of the wave crest is more peaked and shorter than the trough. At a

depth to wavelength ratio of 1:10 (prototype period of approximately 44 sec), the ratios of the wave crest amplitude a_c to the wave height for height ratios of 0.025h, 0.05h, 0.10h, and 0.20h where h is equal to the average depth of 39 ft are:

Wave-Height Ratio	Crest Amplitude to Wave-Height Ratio
0.025	0.52
0.05	0.53
0.10	0.56
0.20	0.62

The preceding variation will be the maximum in the range $h/L \geq 10$ for the second order theory.

67. For a prototype period of 100 sec, the h/L ratio is 0.17 for the 39-ft average depth. The wave crest amplitude to wave-height ratios, again for wave heights of 0.025h, 0.05h, 0.10h, and 0.20h where h equals the average harbor depth are:

Wave-Height Ratio	Crest Amplitude to Wave-Height Ratio
0.025	0.56
0.05	0.62
0.10	0.70
0.20	0.78

At longer periods, the wave crest is more sharply peaked (smaller wave trough amplitude) for each wave-height ratio.

68. The effects of finite amplitude on wave celerity may be approximated[19] by

$$C = (gh)^{1/2} \left(1 + \frac{3}{2}\frac{a}{h}\right)^{1/2} \tag{18}$$

for waves of long length where the curvature of the profile is small. For the depth to wave-height ratio of 1:10, the ratios of the wave celerity to the shallow-water approximation of wave celerity (Equation 5) for wave heights of 0.025h, 0.05h, 0.10h, and 0.20h where h equals the average harbor depth are:

Wave-Height Ratio	Celerity Ratio
0.025	1.01
0.05	1.02
0.10	1.04
0.20	1.07

The effect of the finite amplitude increases as the wave amplitude increases and has more effect on the surface wave form than on wave celerity. In order to minimize the effects of finite amplitude, the maximum wave heights for long-period waves in the harbor area should be limited to 0.20h and, where possible, less than 0.10h. For the 1:100 vertical and average depth of 39 ft, the maximum wave height in the model thus should be limited to 0.078 ft.

69. As a result of the preceding operational criteria, an electrohydraulic wave generator was selected for the model study. The wave generator is composed of 14 units with 15-ft wave paddles. The sections may be positioned to approximate a curved wave front, as indicated in Plates 9-11, and the wave height may be varied for each wave generator. A 15-ft unit of the wave generator with the frame, wave paddle, and hydraulic power supply is shown in Figure 18.

70. A mechanical wave generator with an electric motor and mechanical linkage similar to those presently in use at WES was considered; however, the necessity for small variations in the generated wave period, difficulty in setting an extremely exact wave paddle stroke, and the requirement for model wave periods near 0.5 sec precluded their use. Also, a curved wave front with wave-height variation along the wave front would be difficult to obtain with a mechanical wave generator. A pneumatic wave generator was considered for use in the model study and several modifications of a pilot pneumatic wave generator were constructed and evaluated in a two-dimensional wave flume (10 ft wide with a 3-ft water depth). During the evaluation, oscillations of the pneumatic chamber produced a secondary wave of approximately 0.8 sec on the primary wave form above approximately 2 sec. The height of the secondary wave was of the same order of magnitude as the wave height to be used in the model study. Several methods (principally additional

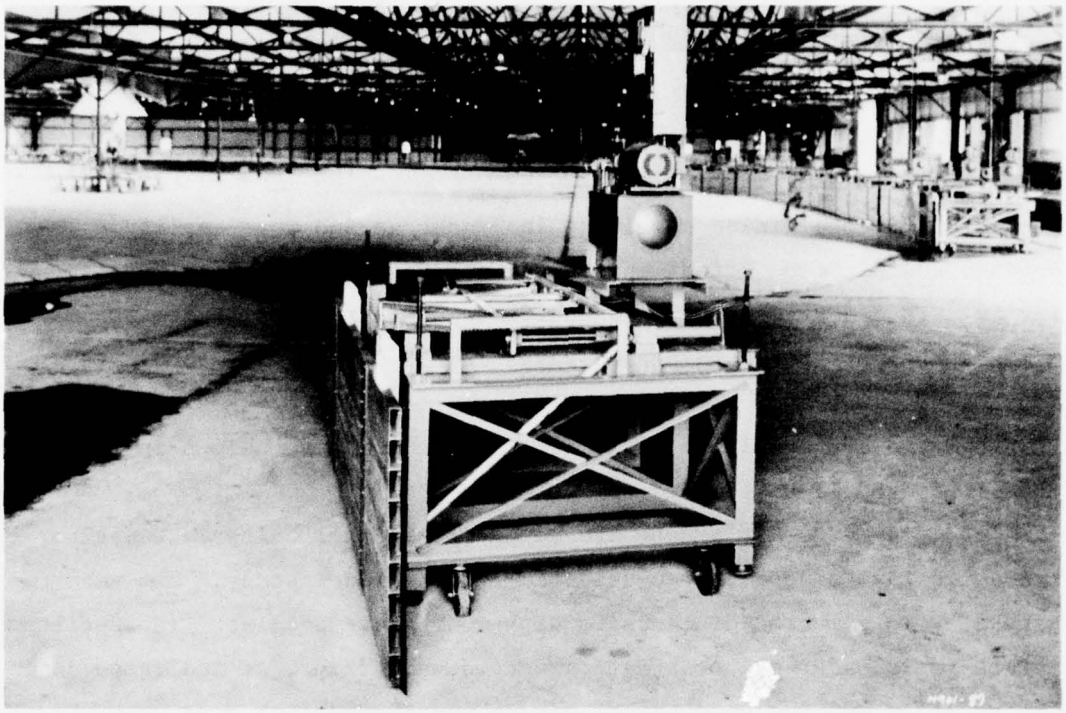

Figure 18. Electrohydraulic wave generator section with frame, wave paddle, and hydraulic supply

frame-bracing, baffles, and filters) were tried in an effort to eliminate the secondary wave but were not successful. It became apparent that a substantial research and development effort was required to overcome these problems. Consequently, the pneumatic generator approach was abandoned for this project model investigation. The preceding evaluation is valid only for the pilot pneumatic generator configuration considered by WES and for the rather large operating range required and should not be considered as generally applicable to pneumatic wave generators.

71. As a result of the preceding pneumatic wave generator analysis, and considering the advances made in electrohydraulic systems in recent years, the electrohydraulic wave generator concept was selected for evaluation. Initially, a pilot electrohydraulic wave generator was designed and constructed at WES using a digitally controlled actuator (hydraulic cylinder used to move the wave paddle) with a position feedback control system. An evaluation of the pilot generator

with a digitally controlled actuator indicated that the electrohydraulic wave generator was feasible but the digitally controlled actuator did not provide sufficient velocity response in the high-frequency range. To improve the actuator response, the final wave generator design included an electrohydraulic actuator with an analog servocontroller as shown in Figure 19. The main components in each drive system are the

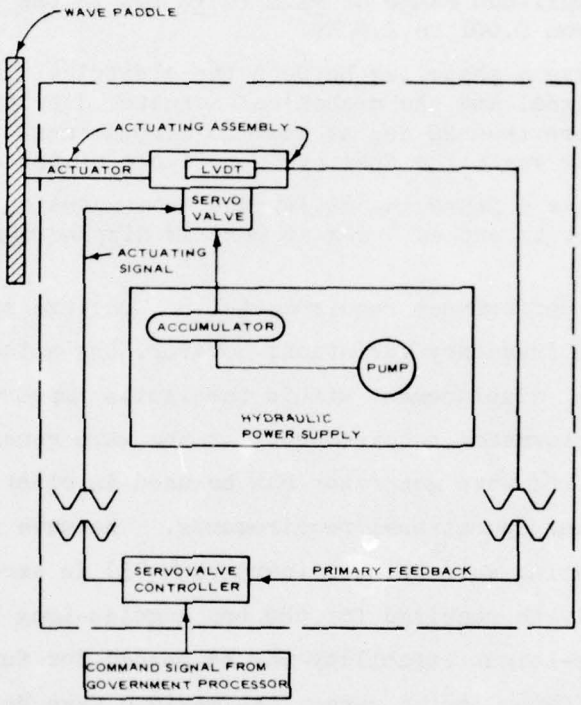

Figure 19. Schematic diagram of electrohydraulic actuator system

actuator with servovalve and linear voltage differential transformer (LVDT), servocontroller, hydraulic power supply, and interconnecting electrical cables and hoses. The electrohydraulic actuator systems were supplied by a private contractor and the wave generator frames and wave paddles were designed and built at WES. Performance requirements for each of the 14 actuator systems, including the controllers, were that each actuator system should:

a. Respond over a frequency range from 0.001 to 2 Hz.

b. Have a displacement of ±6 in. at 0.001 Hz and ±1.3 in. at 2 Hz in response to a sinusoidal command input signal.

c. Be capable of responding to any command signal frequency and amplitude which does not exceed the ±6 in. displacement limit or the velocity limit corresponding to ±1.35 in. at 2 Hz.

d. Maintain a static actuator position error of less than ±0.06 in.

e. Maintain a peak-to-peak displacement error within 1% relative to the command signal amplitude over the amplitude range of ±1.2 to ±6 in. in the frequency range from 0.001 to 2.0 Hz.

f. Have a phase lag between the electrical input control signal and the mechanical actuator displacement of not more than 20 deg at maximum displacement with a phase lag variation from cycle to cycle of not more than ±1 deg.

g. Have a phase lag difference from actuator to actuator not to exceed 4 deg at maximum displacement.

In the preceding performance requirements, no specific requirement is given for maximum frequency variation; however, the actuator must follow the command signal displacement within the limits imposed by requirements e and f. The performance requirements for the wave generator were selected so that the wave generator can be used in other models or wave flumes with similar operational requirements. The wave generator is capable of generating wave heights (paragraph 73) in excess of those that will probably be required for the Los Angeles-Long Beach model; however, the wave-height capability may be needed for future studies. In the 0.5- to 1.0-sec period range, the maximum wave height will probably be steepness limited.

72. The wave height and force required to generate a particular wave for the 3-ft water depth in the Los Angeles-Long Beach Harbors model can be estimated using small amplitude theory and neglecting the effects of viscosity, turbulence, and leakage around the wave paddle. The development of the theory is described in Reference 32 and is summarized briefly in the following section. The velocity potential ϕ for waves propagating in the $+x$ direction is given by

$$\phi = \frac{hs\sigma}{\alpha}\left[-b_o \cosh (m_o z)e^{im_o x} + i \sum_{n=1}^{\infty} b_n \cos (m_n z)e^{-m_n z}\right]e^{-i\sigma t} \qquad (19)$$

where the center of the coordinate system is at the base of the wave paddle, y is the positive upward, b_o and b_n are coefficients, s is the amplitude of the displacement of the wave paddle, and

$$\alpha = \frac{\sigma^2 h}{g} \tag{19a}$$

The coefficient m_o is defined by

$$m_o g \tanh m_o h = \sigma^2 \tag{20}$$

and m_n is defined by

$$m_n g \tanh m_n h = -\sigma^2 \tag{20a}$$

The velocity potential satisfies the boundary conditions that the free surface is at a constant pressure, the velocity of the wave paddle and the water adjacent to the wave paddle are the same, and the vertical velocity across the x-axis is zero. The velocity potential and its first derivatives are finite in the region

$$0 \leq x$$

and

$$0 \leq z \leq h$$

and the coefficients b_o and b_n are evaluated through the boundary condition that the horizontal wave paddle and water velocities be the same.

73. The generated wave height is given by

$$H = \frac{2\sigma}{g} |\phi| , \qquad \begin{matrix} z = h \\ x \to \infty \end{matrix} \tag{21}$$

or, having evaluated b_o ,

$$\frac{H}{s} = 2b_o \cosh m_o h \tag{21a}$$

The pressure fluctuation per unit width along the face of the wave paddle may be evaluated from

$$p = \rho \left[- \frac{\partial \phi}{\partial t} + g(h - z) \right] \tag{22}$$

or

$$p = -\left[\rho g s i b_o \cosh m_o z + \rho g s \sum_{n=1}^{\infty} b_n \cos (m_n z) \right] e^{-i\sigma t} + \rho g (h - z) \tag{23}$$

The first term in Equation 23 represents the dynamic pressure on the wave paddle and is composed of a resistive part in phase with the wave paddle velocity and an inertial part in phase with the wave paddle acceleration. The second term in Equation 23 represents the hydrostatic pressure on the wave paddle, and, in the Los Angeles-Long Beach Harbors model, is canceled by the water pressure on the rear of the wave paddle.

74. The force F per unit width is given by

$$F = \int_o^h p\,dz \tag{24}$$

Substituting from Equation 23, Equation 24 may be rewritten as

$$F = -(iF_R + F_I)e^{-i\sigma t} \tag{25}$$

where F_R is the resistive force and F_I is the inertial force defined as

$$F_R = \frac{\rho g s b_o}{m_o} \sinh m_o h \tag{26}$$

$$F_I = \rho g s \sum_{n=1}^{\infty} b_n \sin \frac{m_n h}{m_n} \tag{27}$$

The maximum force F_m during a cycle is

$$F_m = (F_R^2 + F_I^2)^{1/2} \qquad (27)$$

The wave generator can be operated in either a piston or flapper mode as shown in Figure 20. The solutions for b_o and b_n are dependent

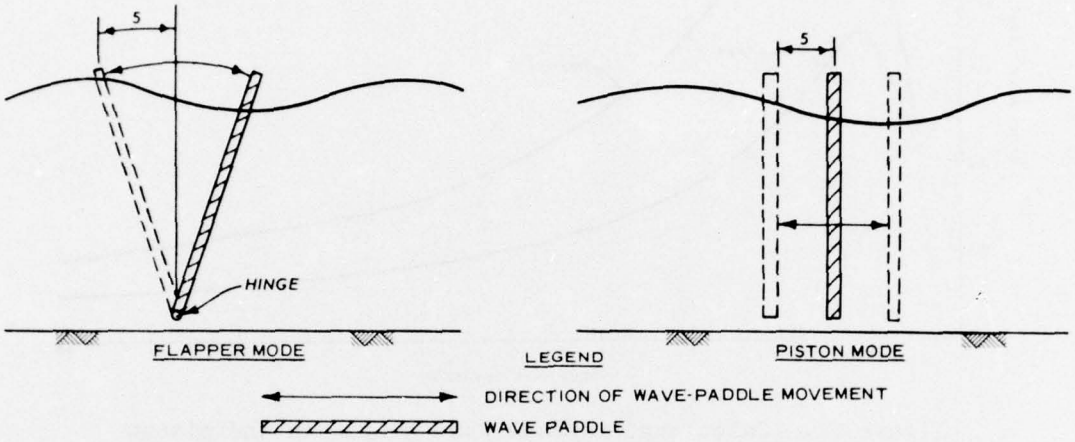

Figure 20. Wave generator piston and flapper modes of wave generation

on the mode of operation; therefore, the wave height and maximum force will vary with the mode of operation. The maximum calculated wave height that can be generated and maximum force on the wavepaddle are shown in Figures 21 and 22 over the 0.5- to 10.0-sec period range. The maximum wave height occurs near 1.25 sec for the flapper mode and near 1.75 sec for the piston mode. The decrease in amplitude below these periods is due to the decreased length of the maximum stroke as the period decreases. As indicated by Figure 21, the maximum calculated height for the larger wave periods in the flapper mode is approximately one-half the height in the piston mode. Near 0.5 sec in the short-period range, the wave heights approach the same value.

75. Selection of the wave generator mode of operation, either flapper or piston, is somewhat at the discretion of the model operator, provided a sufficient wave height can be obtained in the flapper mode. However, the calculated vertical profile over depth of horizontal velocity for a wave is more nearly matched by the velocity regime generated by the piston mode at wave periods larger than approximately

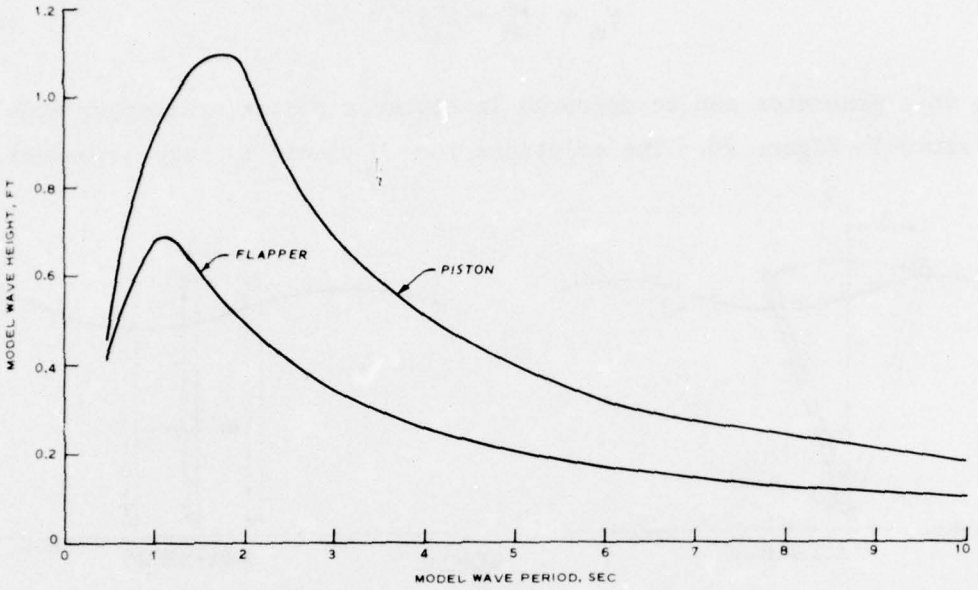

Figure 21. Calculated maximum wave height in the piston and flapper modes

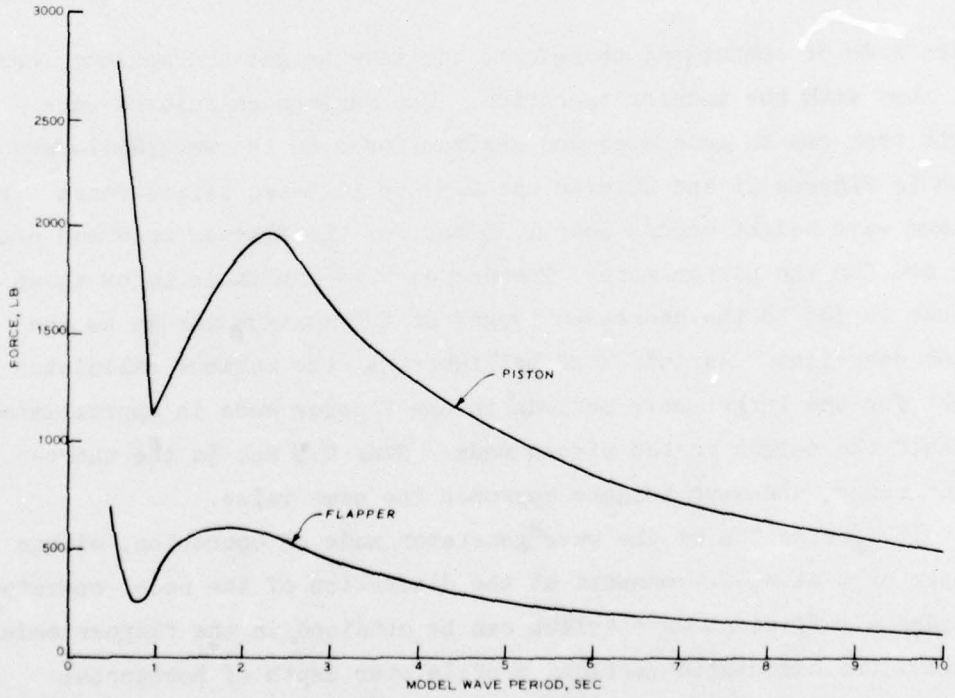

Figure 22. Calculated maximum force for each wave generator section in the piston and flapper modes

1.75 sec in the model. A transition region near 1.75 sec is suggested for the change from flapper to piston mode. The theoretical wave velocity profile calculated from small amplitude wave theory for 1.75 sec is shown in Figure 23 for a 3-ft water depth. The wave velocity is normalized by the surface velocity. Also shown in Figure 23 are the velocity profiles for the flapper and piston modes. At lower periods, the wave velocity profile tends to approach the flapper velocity profile and at longer periods, the piston velocity profile. Without a transition point from the flapper to piston mode, a calibration of the wave generator for wave height versus stroke would be necessary for those wave periods used with both modes.

76. Equations 21 and 27 for the wave height (except over a limited range) and wave force have not been verified[32] experimentally. Available data[32] do indicate that leakage around the wave generator may significantly affect the generated wave height, and the wave generator must be calibrated experimentally for wave height versus stroke. Also, initial data from test runs with the wave generator indicate performance requirement e of paragraph 71 for a 1 percent peak-to-peak displacement

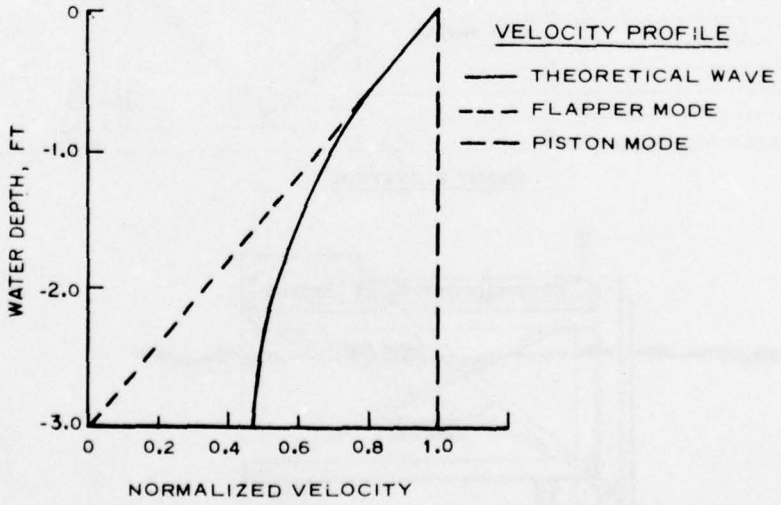

Figure 23. Normalized theoretical, flapper mode, and piston mode vertical wave velocity profiles for a 1.75-sec model wave in a 3-ft depth

error relative to the command signal amplitude may be difficult to maintain consistently, and this requirement may have to be relaxed slightly during model operation.

Wave Generator Frame Design

77. The wave generator support frame for each unit is constructed of structural grade steel with welded joints. The frame is 10 ft long by 6 ft wide by 3.7 ft high. Front and end elevations of the frame with the wave paddle are shown in Figure 24. The frame is mounted on swivel casters and, when in position, can be leveled using screw-type adjustable legs. The frame includes a drip pan to prevent contamination of water in the model in the event of a hydraulic fluid leak.

78. The wave paddle is driven by two 2-in. drive rods at points 4.5 ft from the ends of the wave paddle. The drive rods are chrome-coated stainless steel and each rod is supported by two bronze bushings

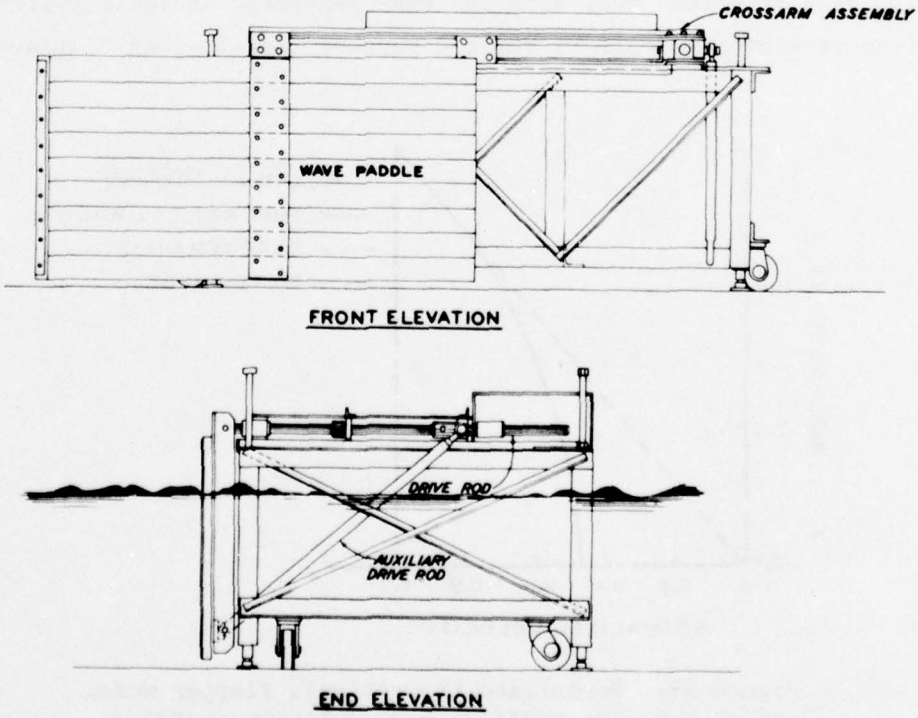

Figure 24. Sectional views of the wave generator frame

mounted on an 8-in. channel section. The bottom of the wave paddle is supported by two auxiliary drive rods at points 4.04 ft from the ends of the wave paddle. The force from the actuator is transmitted to the drive rods by an aluminum crossarm assembly shown in Figure 24. In the piston mode, the auxiliary drive rod is connected to the crossarm assembly. In the flapper mode, the auxiliary drive rod is connected to the support frame and the wave paddle rotates about the auxiliary drive rod pinned connection at the wave paddle.

79. The wave paddle is 15 ft long and 3.75 ft high, and is made up of 2- by 5-in. rectangular aluminum tubes. The tubes are open on either end to reduce the buoyant uplift force on the wave paddle. The actuator pushes against a reaction block welded to the support frame and the aluminum crossarm assembly to drive the wave paddle.

80. The wave generator frames were initially painted with a lead primer coat and a latex enamel surface coat; however, they have recently been repainted with a coal tar epoxy on the basis of recommendation* from the U. S. Army Construction Engineering Research Laboratory (CERL) to provide additional corrosion protection.

---

* Telephone communication between Dr. R. W. Whalin of WES and Mr. Bob Quatroon of CERL.

PART IV: MODEL DATA ACQUISITION AND CONTROL SYSTEM

System Requirements

81. The extreme complexity and large size of the Los Angeles-Long Beach Harbors model as well as the anticipated volume of model data to be collected have forced abandonment of conventional techniques of model data acquisition and control and model data analyses. For example, manual procedures for collecting and analyzing this model's wave data would require approximately seven man-years to reduce and analyze the anticipated volume of data without considering the efforts to manually collect these data. To meet the demands of this model, an automated data acquisition and control system (ADACS) with supporting software for model control, data acquisition, and analyses has been designed, implemented, and checked out.

82. In the model, the variables to be monitored during harbor oscillation studies are water-surface elevation changes and water velocity. Based on past experience, prototype wave data, and this model's scaling relations, the range of model wave periods is expected to be 0.50 to 10 sec with the minimum period of 0.50 sec posing the most stringent constraints on ADACS design. The expected maximum wave height to be monitored in the model is about 4.0 in. (0.333 ft). Wave period resolution of 0.01 sec and wave-height accuracy of ±0.001 ft are desired capabilities of ADACS with ±0.001 ft accuracy being the most restrictive requirement for system design. For design purposes, the upper limit of the velocity variable is less critical than the lower or threshold value. Model velocities as low as 0.05 fps may be of interest in this model. The desired threshold velocity is 0.01 fps which is a stringent requirement for existing model velocity sensors and is very restrictive in system design. In addition to meeting the requirements of the above variables, automated controls for electrohydraulic actuators (wave generator units) and calibration of the wave gages are required capabilities of ADACS.

83. The following characteristics and requirements were put

forth as design criteria which must be met by an ADACS for use in the Los Angeles-Long Beach hydraulic model study.

a. Model wave characteristics.

(1) Wave frequencies as high as 2 Hz (wave period range of 0.50 to 25.00 sec).

(2) Wave heights in operating range of 0.01 to 0.5 ft.

(3) Wave-height accuracy of ±0.001 ft.

b. Wave Gages.

(1) Variable number of wave gages not to exceed 50.

(2) Water-surface-piercing, parallel wire, resistance-type gages.

c. Sampling techniques.

(1) Data collected over at least 20 wave periods.

(2) Sampling frequency variable and high enough to define the first three harmonics of the 2-Hz wave frequency (minimum sampling rate of 60 samples/cycle).

(3) Minimum time delay (not to exceed 6 msec between sampling digitally the first and fiftieth wave gage during any one scan of the 50 gages, and this time delay should be constant and independent of the sampling frequency.

(4) Time interval between scans of all gages should be controlled to within a few microseconds.

d. Recording modes.

(1) Digital recording of data from all 50 channels in binary code with provisions for BCD recording of specific information regarding test identification and data analysis.

(2) Digital data recorded on 9-track magnetic tape with IBM compatible record format.

(3) Continuous analog recording of 50 channels.

(4) Time correlation of digital and analog recording modes.

e. Calibration of wave gages.

(1) Efficient and accurate means of calibrating the wave gages before a series of wave tests.

(2) Recording of calibration data in digital and analog modes.

f. Wave generator controls.

(1) Provide a sinusoidal analog voltage whose amplitude can vary within ±10 volts full scale (F.S.) at 0.05 percent F.S. increments and whose period (frequency) can change over 0.50 to 25.00 sec at 0.01-sec increments.

(2) Capable of varying the number of cycles or total time of control signal for generator units.

g. Mobility of system.

(1) Entire data acquisition system to be sufficiently mobile to service various hydraulic models from different locations with a minimum effort and cost in moving and installing the system.

(2) Compact interfacing and panels for wires to wave gages in model, thus allowing efficient mobility of wave gages for expedient relocation within the model.

h. Environment for system.

(1) ADACS is housed in a controlled environment whose temperature ranges from 65 to 75°F and humidity ranges from 40 to 55 percent.

(2) Emergency notification of appropriate personnel if temperature and humidity change beyond specified range.

System Configuration

84. The system configuration (Figure 25) of ADACS consists of the following subsystems:

a. Digital data recording and controls.

b. Analog recorders and channel selection circuits.

c. Wave sensors and interfacing equipment.

d. Wave generator units and control equipment.

85. The digital data recording and control subsystem is basically a minicomputer (1 μsec memory cycle time) with the following characteristics and peripheral devices:

a. 32K, 16 bit words of core memory.

b. Analog to digital pack featuring 64 analog inputs (±10 volts F.S.), 45 kHz multiplexer, and 12 bit (including sign) analog to digital (A/D) converter.

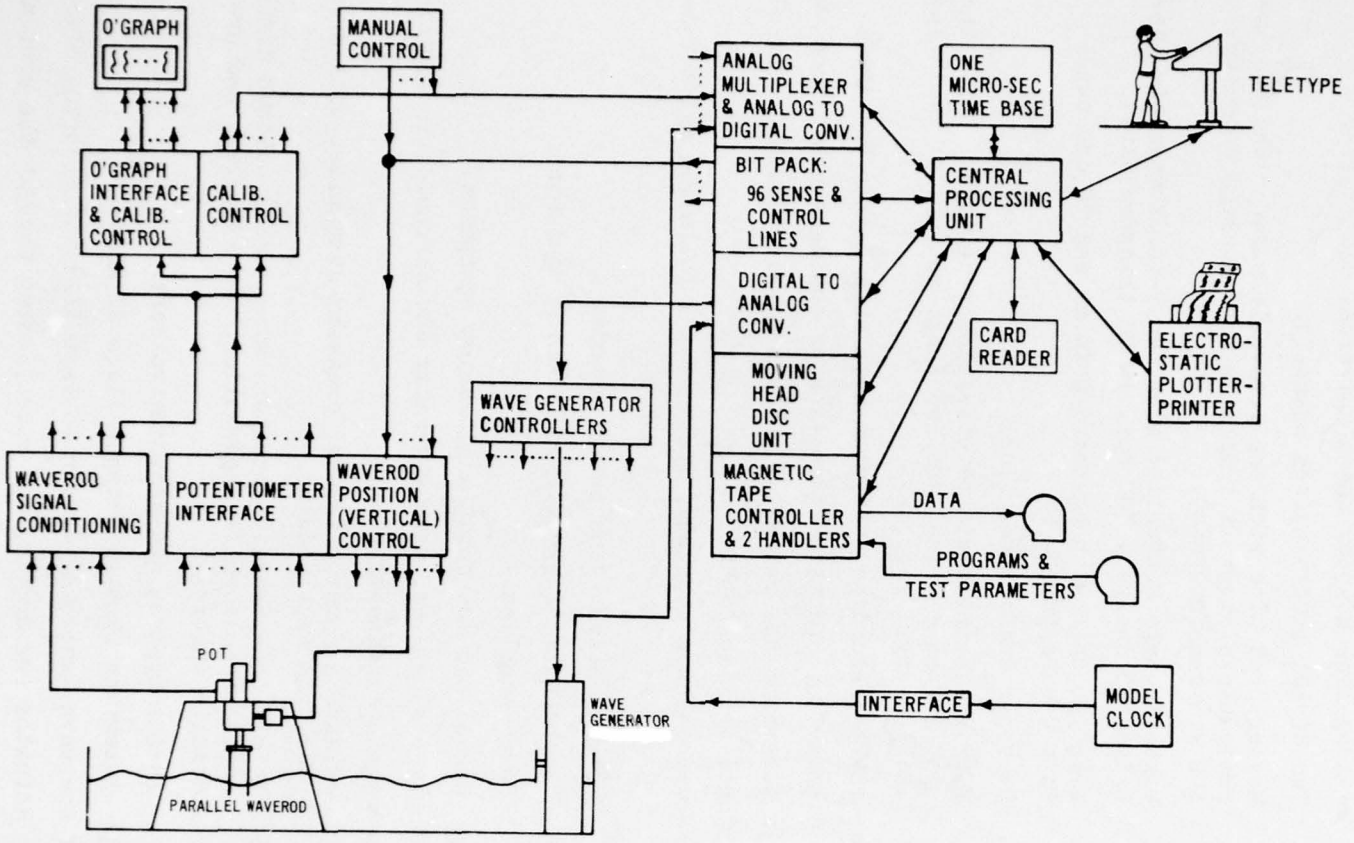

Figure 25. Automated data acquisition and control system (ADACS) for hydraulic wave models

c. Interval timer with a 1 μsec counter.

d. A long line adapter and a universal controller.

e. Two direct memory access channels.

f. Moving head disc with one removable platter and one non-removable platter (1.1 million word storage capacity, 100 kc transfer rate).

g. Magnetic tape controller with two 9-track magnetic tape units (25 in./sec, 800 bpi, 10 kc transfer rate).

h. Teletype unit with keyboard/printer and 10 cps paper tape reader/punch.

i. 96 sense and control lines.

j. Matrix electrostatic printer/plotter (print: 1620 lines/min, 132 char./line, and 128 char. set; plot: 4 in./sec and 100 styli/in.).

86. The analog recording subsystem acts as a backup for ADACS and a visual display for operator inspection of analog signals from wave sensors. This subsystem has manual or automated selection and control of five 12-channel oscillographs.

87. The wave sensor subsystem includes the following major components:

a. 50 wave-height sensors and stands.

b. 50 channels of signal conditioning equipment.

c. Power supplies.

d. Manual and automatic calibration equipment.

88. The last subsystem, wave generator and controls, is composed of the following major components.

a. 14 wave generator frames, crossarm assemblies with drive rods, and wave paddles.

b. 14 electrohydraulic actuators with linear voltage differential transformers, hydraulic power supplies, and hydraulic controls.

c. 14 servovalves and servocontrollers.

d. Interface from servocontrollers to ADACS.

Each unit of the wave generator (refer to Part III) utilizes the electrohydraulic actuator for driving the wave paddles through the crossarm assembly and drive rods. The electrohydraulic actuator is controlled by the servovalve and servocontroller which accepts ADACS command

signals controlling wave heights and periods (refer to paragraphs 93-95). Except for the wave sensors and the wave generator units, all components of ADACS are compactly housed in a trailer (Figure 26) to provide easy control of the environment of the system.

Figure 26. Automated data acquisition and control system

Wave Sensors

89. The data acquired from wave models are the water-surface variations about a reference water level. This information is collected at selected geographic locations within the model for specified wave conditions at the wave generator. Wave sensors are used to obtain this information at selected locations in the model. Water-surface-piercing, parallel-rod wave gages (Figure 27) are the wave sensors used in the Los Angeles-Long Beach Harbors model. This type of sensor has been used on past wave models with much success. However, for the present case, this sensor required some modifications to the electronics (to

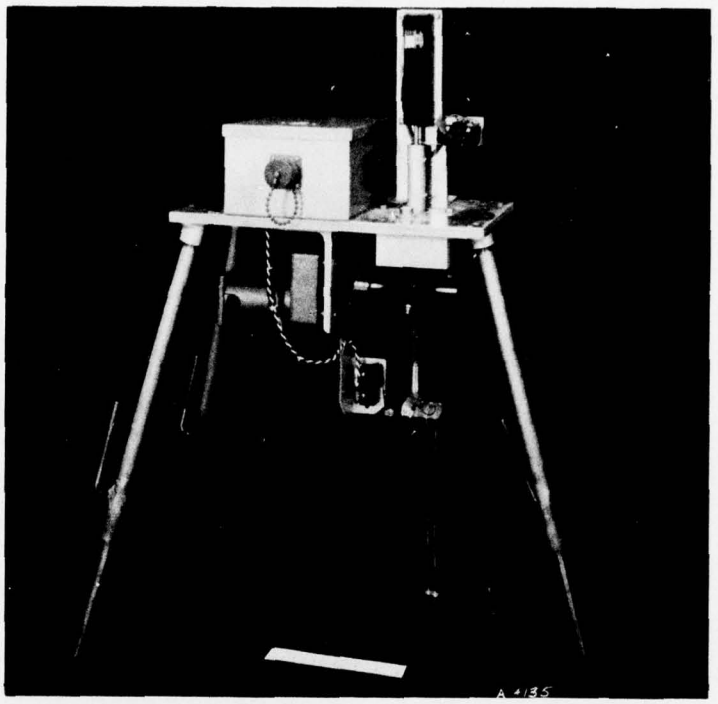

Figure 27. Parallel-rod wave sensor

increase accuracy and stability) and to the physical configuration (for automated calibration).

90. Each water-surface-piercing, parallel-rod wave sensor is connected to a Wheatstone bridge (Figure 28). The transducer measures the conductance of the water between two parallel rods mounted vertically. The conductance is directly proportional to the depth of submergence of the two rods in the water. The output of each wave sensor is routed through shielded cables to its signal conditioning equipment where it is processed for recording. The output of the signal conditioning equipment is connected through shielded cables to analog oscillographs where an analog time history is recorded and to the analog multiplexer of the digital recording subsystem where it is digitized and recorded in a binary format on magnetic tape and/or disc. The signal conditioning equipment (Figure 29) consists of a carrier amplifier and various power supplies. This system can detect changes in water-surface elevations to an accuracy of ±0.001 ft. To obtain this accuracy,

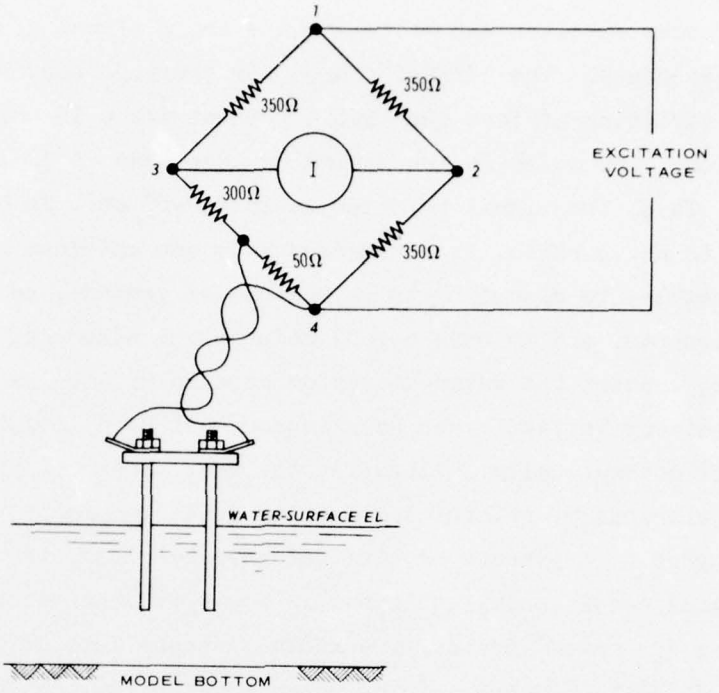

Figure 28. Schematic of parallel-rod bridge transducer

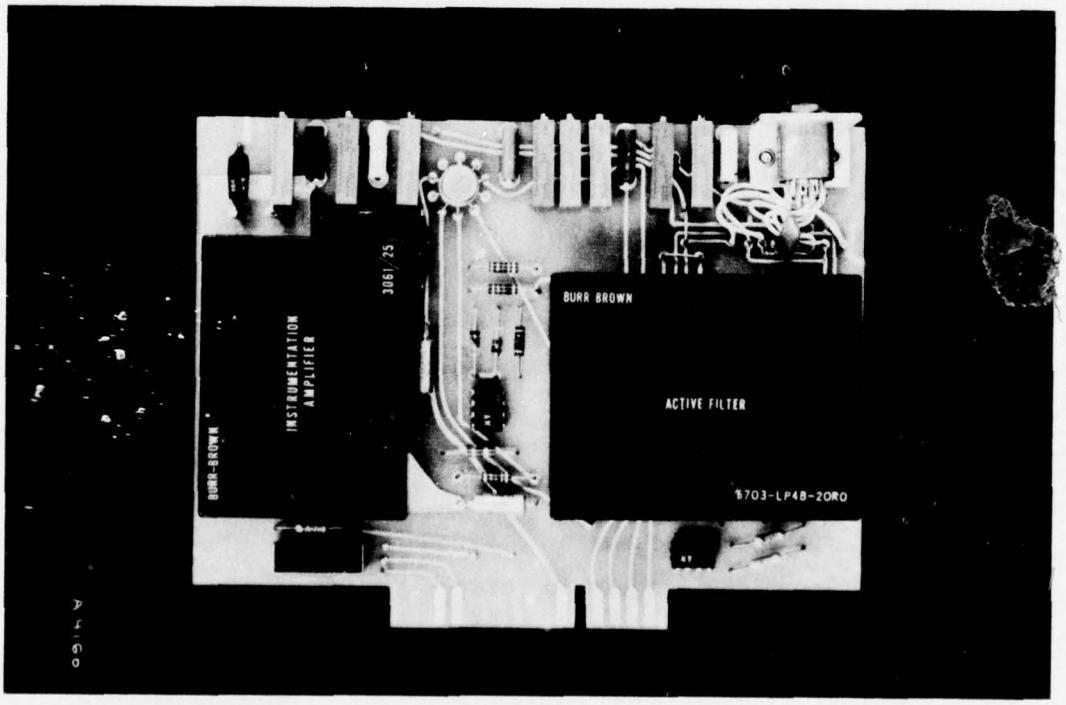

Figure 29. Signal conditioning equipment for wave rod amplifiers

ultrastable power supplies and better-than-average signal to noise ratios are necessary. The carrier source for the wave sensor bridge maintains a variation of less than 0.025 percent for a 10 percent power-line variation. The noise in the system is less than ±5 mv for ±10 v full range. Thus, the signal to noise ratio is -66 db. To maintain this signal to noise ratio, it is necessary to use shielded cables wherever possible, to discriminate selections of grounds, to use high-quality components, and to have a good maintenance schedule.

91. To convert the water-elevation data in millivolts to water-surface elevations in feet, each wave sensor must be calibrated. The capability of automatically calibrating the wave sensors (maximum of 25 rods simultaneously) prior to collecting data also is provided by ADACS. In order to calibrate each set of parallel rods, the voltage from the signal conditioning equipment is monitored and recorded as the parallel rods are moved vertically a known distance into or out of the water. A precision, linear-position potentiometer is located on the wave sensor stand and is coupled directly to the parallel rods by a gear-train driven electric motor. By moving the coupled wave sensor and potentiometer wiper vertically with the electric motor and by monitoring the output voltage from the potentiometer, the wave sensor can be moved a precise distance. The electric motor for each wave sensor is controlled by a control/sense line and a relay contact. The minicomputer controls the vertical movement of each wave sensor by actuating its associated control/sense line. The central processing unit (cpu) acts as a voltage comparator by monitoring the potentiometer voltage and comparing it with a reference voltage which is determined from desired displacement and potentiometer calibration. When the voltage comparison is satisfied, the control/sense line is reactivated, the electric motor stops, and voltage samples from the rods and potentiometers are acquired.

92. By systematically moving each wave sensor through 11 quasi-equally spaced locations (Figure 30) over the range of the rod length used, voltage versus known displacements are obtained from which a calibration curve for each sensor can be calculated and recorded on

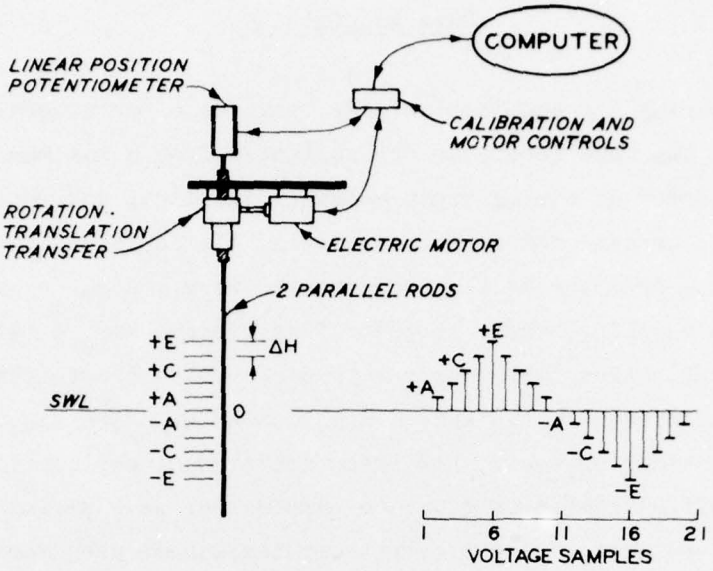

Figure 30. Schematic of wave rod calibration procedure

magnetic tape or disc. After collecting the calibration data, the minicomputer analyzes these data by least-squares fitting a set of curves (linear, quadratic, or spline) to the data, determining the best order of fit, and comparing the maximum deviation of the best fit with a previously acceptable value for this maximum deviation. If the fitted curves are not acceptable, the minicomputer flags that channel in the calibration record on the magnetic tape or disc for further analyses. Any malfunctioning sensors are listed on the teletype for the operator to determine the required action (i.e., accept present calibration, clean bad rods, recalibrate, etc.). Having completed the calibration mode, the original calibration data for each set of parallel rods and potentiometer as well as the calibration coefficients are written into a file on magnetic tape or disc. Analytical considerations of calibration curve fitting, accuracy of reference potentiometers, and repeatability test of calibration procedures have demonstrated that an accuracy of ±0.001 ft in wave height is obtainable.

Data Acquisition

93. During the acquisition mode, wave data for a specified wave condition at the wave generator are collected from a maximum of 50 wave sensors, recorded on analog strip charts, digitized, and recorded on magnetic tape or disc for further analyses. In addition, actuator displacement data from the 14 electrohydraulic wave generator units are acquired. The sampling scheme is quite flexible and can be tailored for different applications with maximum thru-put rates theoretically limited by the multiplexer rate (45 kHz) and allocatable buffer size. However, for specific types of tests, the execution time of applications software and the specified number of discrete samples per wave period reduce the maximum thru-put rate. The present sampling scheme used for each wave sensor is 60 discrete voltage samples equally spaced over each wave period for a predetermined number of periods. The minicomputer calculates from input parameters the required timing interval between multiplexer scans to provide the correct sampling rate and initializes counters for determining completion of wave tests. In addition, it controls the starting of the wave generator units, generates and updates the control signal to the wave generator units, lags the beginning of data acquisition by a specified number of wave periods after starting the generator, and provides timing pulses for synchronizing and controlling the analog recorders. At completion of the acquisition mode, the calibration data, wave data, and actuator displacement data (paragraph 95) have been recorded in both analog and digital form. These data with a header for test identification and pertinent parameters are available in binary form from disc for direct analyses by the minicomputer or on magnetic tape in a format suitable for backup analyses on the WES Honeywell G-635 computer.

Wave Generator Controls

94. Through the digital to analog converter, ADACS provides to the wave generator an electrical command signal that drives the electrohydraulic actuator at a given frequency and amplitude of

displacement. The actuator drives the wave paddle which generates a water wave that has the same frequency as the actuator and a wave height proportional to the actuator's displacement. The control signal is a d-c analog voltage that can vary between ±10 v. The functional form of the control signal can be varied to generate the required wave regime such as monochromatic, spectral, or any time-dependent wave form. The only restriction on the form of the control signal is the maximum velocity limitation of the electrohydraulic actuator system. For initial wave tests, a sinusoidal or monochromatic wave form will be used, and within the desired range of wave frequencies and heights, no limitations on actuator response exist.

95. The desired analog command signal from ADACS is applied to the wave generator control unit (Figure 31) which provides 14 parallel

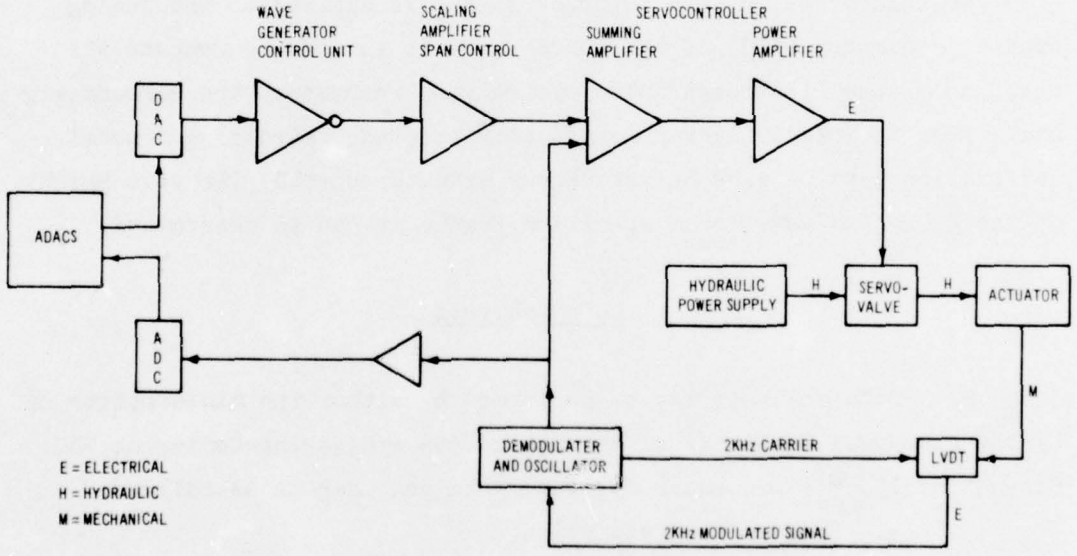

Figure 31. Schematic of wave generator controls

inverted output signals. These output signals are adjusted for selected quiescent and amplification levels and then are applied to the input of their respective scaling amplifier of the servocontroller. It is in this section of the servocontroller with the span control potentiometer that the system is calibrated for a ±6.000-in. stroke for a ±10.000-v command signal. This calibrated command signal along with the actuator

position feedback signal is applied to the summing junction of the servo-controller. The algebraic sum of these two signals is then applied to a power amplifier which is suitable for driving the coil of the servovalve. The servovalve controls the flow of hydraulic fluid to the cylinders in the actuator; thus, the displacement of the piston is proportional to the electrical command signal. The actuator position feedback transducer, a linear variable differential transformer (LVDT), provides a modulated 2-kHz output which is proportional to the actuator position. This feedback signal is demodulated and then calibrated for a scale factor of approximately 1.66 v/in. Therefore, the feedback signal along with the loop gain is used to stabilize the closed loop electrohydraulic system, thus ensuring that the actuator tracks the command input within the desired accuracy.

96. In addition, the feedback signal is applied to the analog digital converter (ADC) of the ADACS where it is used to compute the response of the electrohydraulic system with respect to the command signal. From the electrohydraulic actuator response (stroke) and model calibration data of wave height versus actuator stroke, the wave height of the generated wave for a specified frequency can be determined.

Data Analysis

97. Data analysis may be performed by either the minicomputer or by the Honeywell G-635 of the Automatic Data Processing Center at WES. Schematically, the procedure for wave data analyses is as follows:

a. Program initialization.
   (1) Input test parameters and option flags.
   (2) Read and decode data files on magnetic tape or disc.
   (3) Demultiplex data files and scale data.

b. Wave record analyses.
   (1) $\overline{H} \pm \sigma_H$ and $\overline{T} \pm \sigma_T$.
   (2) H_{RMS} .
   (3) H_x where x is a specified percent of the highest wave heights, normally $x = 0.333$; thus, $H_{1/3}$ is significant wave height.

(4) Option to plot wave heights versus time.

c. Fourier analyses.

(1) Autospectrum.

(a) Amplitude-frequency.

(b) Energy.

(c) Spectral smoothing.

(d) Plots of above parameters.

(2) Cross spectrum.

(a) Energy.

(b) Coherency.

(c) Phase.

(d) Plots of above parameters.

d. Least-squares harmonic analysis.

(1) Amplitude and phase for specified wave period.

(2) Relative phases and amplification factors between gages.

(3) Analysis of residual variance.

(4) Graphic output of above results.

98. The analysis of actuator displacement data is basically the above least-squares harmonic analysis from which can be determined the actuator response. The results of the data analyses can be plotted by electrostatic printer/plotter on minicomputer or by pen plotter or CRT plotter (microfilm and hard copy) on the Honeywell G-635 system. For each model test, original data and analyzed results of all tests are permanently stored on magnetic tape and disc files for future reference and data table generation for reports, etc.

99. With the analyses of wave records from various harbor locations, amplification factors or harbor responses for various input wave conditions are estimated. These results provide the hydraulic engineers with the basic data whereby the effects of various proposed expansions and modifications to existing harbors can be evaluated.

PART V: CONCLUSIONS

100. Based upon the design considerations discussed in this report, it is concluded that a 1:100-vertical-, 1:400-horizontal-scale hydraulic model of Los Angeles and Long Beach Harbors will accurately simulate prototype wave conditions so that effects of proposed harbor modifications may be accurately evaluated. All predominant parameters (refraction, shoaling, diffraction, viscous friction, reflection, transmission, harbor oscillation, incident waves, etc.) have been adequately reproduced (either naturally or artificially by adjustment of the model and its appurtenances). Tests of existing conditions should be conducted initially to obtain a base for comparison. The model can then be used in a predictive mode to evaluate various proposed modifications, thereby optimizing the harbors design from both a cost and a functional standpoint.

101. Potential future uses of the model not previously discussed, include studies of:

a. Dispersion of effluent from specific outfalls in the harbor complex.

b. Tsunami waves.

c. Effects of various coastal structures from Point Fermin to Huntington Beach.

d. Effects of artificial offshore islands or landfill seaward of the existing harbor breakwater on tidal circulation and wave conditions.

e. Tidal circulation in areas such as Huntington Beach, Bolsa Chica Wildlife Reserve, Alamitos Bay, etc.

f. Effect of various future harbor modifications on tidal and wave phenomena.

g. The physical environment in the harbor and surrounding area.

h. Wave and tidal circulation in the proposed Downtown Marina and Queensway Marina.

REFERENCES

1. Wilson, B. W. et al., "Wave and Surge-Action Study for Los Angeles-Long Beach Harbors," Final Report No. 1, Jul 1968, U. S. Army Engineer District, Los Angeles, Los Angeles, Calif.; prepared under Contract No. DACW09-67-C-0065.

2. McAnally, W. J., Jr., "Los Angeles and Long Beach Harbors Model Study; Tidal Verification and Base Circulation Tests," Technical Report H-75-4, Report 5, Sep 1975, U. S. Army Engineer Waterways Experiment Station, CE, Vicksburg, Miss.

3. Pickett, E. B., Durham, D. L., and McAnally, W. H., Jr., "Los Angeles and Long Beach Harbors Model Study; Prototype Data Acquisition and Observations," Technical Report H-75-4, Report 1, Jun 1975, U. S. Army Engineer Waterways Experiment Station, CE, Vicksburg, Miss.

4. Durham, D. L. et al., "Los Angeles and Long Beach Harbors Model Study; Analyses of Wave and Ship Motion Data," Technical Report H-75-4, Report 3, Jul 1976, U. S. Army Engineer Waterways Experiment Station, CE, Vicksburg, Miss.

5. Crosby, L. G. and Durham, D. L., "Los Angeles and Long Beach Harbors Model Study; Observations of Ship Mooring and Movements," Technical Report H-75-4, Report 2, Jan 1975, U. S. Army Engineer Waterways Experiment Station, CE, Vicksburg, Miss.

6. Hudson, R. Y., "Model Study of Wave and Surge Action, Naval Operating Base, Terminal Island, San Pedro, California," Technical Memorandum No. 2-237, Sep 1947, U. S. Army Engineer Waterways Experiment Station, CE, Vicksburg, Miss.

7. _____, "Wave and Surge Action, Point Fermin Naval Supply Depot, San Pedro, California; Model Investigation," Technical Memorandum No. 2-238, Nov 1947, U. S. Army Engineer Waterways Experiment Station, CE, Vicksburg, Miss.

8. U. S. Army Engineer Waterways Experiment Station, CE, "Wave and Surge Action, Long Beach Harbor, Long Beach, California; Model Investigation," Technical Memorandum No. 2-265, Sep 1949, Vicksburg, Miss.

9. Knapp, R. T. and Vanoni, V. A., "Wave and Surge Study for the Naval Operating Base, Terminal Island, California," Jan 1945, Hydraulic Structures Laboratory, California Institute of Technology, Los Angeles, Calif.

10. U. S. Army Engineer District, Los Angeles, "Los Angeles-Long Beach Harbors, Interim Review Report," Jun 1971, Los Angeles, Calif.

11. Office, Chief of Engineers, Department of the Army, "Final Environmental Statement, Los Angeles-Long Beach Harbors, Los Angeles County, California," 1974, Washington, D. C.

12. Port of Los Angeles, "Comprehensive Master Plan 1990," Apr 1976, Los Angeles, Calif.

13. U. S. Army Coastal Engineering Research Center, CE, "Shore Protection Manual," 1973, Fort Belvoir, Va.

14. Dobson, R. S., Some Applications of a Digital Computer to Engineering Problems, M.S. Thesis, Stanford University, Stanford, Calif., 1947.

15. Bretschneider, C. L. and Reid, R. O., "Modifications of Wave Height due to Bottom Friction, Percolation, and Wave Refraction," Technical Memorandum No. 45, Oct 1954, Beach Erosion Board, CE, Washington, D. C.

16. Whalin, R. W., "The Limit of Applicability of Linear Wave Refraction Theory in a Convergence Zone," Research Report H-71-3, Dec 1971, U. S. Army Engineer Waterways Experiment Station, CE, Vicksburg, Miss.

17. _____, "Wave Refraction Theory in a Convergence Zone," Proceedings, Thirteenth Coastal Engineering Conference, Jul 1972.

18. Whalin, R. W. and Butler, H. L., "Criteria for Use of Ripple Tanks: Refraction Scale Effects," Research Report H-74-1, Sep 1974, U. S. Army Engineer Waterways Experiment Station, CE, Vicksburg, Miss.

19. Rouse, H., ed., Engineering Hydraulics, Wiley, New York, 1950.

20. Keulegan, G. H., "The Gradual Damping of a Progressive Oscillatory Wave with Distance in a Prismatic Rectangular Channel" (unpublished), May 1950, U. S. Bureau of Standards, Washington, D. C.

21. Lee, J.-J. and Raichlen, F., "Wave Induced Oscillations in Harbors with Connected Basins," Contract Report H-71-2, Aug 1971, U. S. Army Engineer Waterways Experiment Station, CE, Vicksburg, Miss.

22. Rosseau, M., "Contribution a la theorie des ondes liquides de gravite en pro fondeur variable," Publ. Sci. et Tech. du Ministere de l'Air, No. 275, pp 1-73.

23. Madson, O. S. and White, S. M., "Reflection and Transmission Characteristics of Porous Rubble Mound Breakwaters," Report No. 27, Dec 1975, Ralph M. Parsons Laboratory for Water Resources and Hydrodynamics, Massachusetts Institute of Technology, Cambridge, Mass.

24. LeMehaute, B., "Wave Absorbers in Harbors," Contract Report No. 2-122, Jun 1965, U. S. Army Engineer Waterways Experiment Station, CE, Vicksburg, Miss.

25. Moraes, C. C., "Experiments of Wave Reflection on Impermeable Slopes," Proceedings, Twelfth Coastal Engineering Conference, Vol I, Sep 1970.

26. Keulegan, G. H., "Wave Transmission Through Rock Structures; Hydraulic Model Investigation," Research Report H-73-1, Feb 1973, U. S. Army Engineer Waterways Experiment Station, CE, Vicksburg, Miss.

27. _____, "Wave Damping Effects of Fibrous Screens; Hydraulic Model Investigation," Research Report H-72-2, Sep 1972, U. S. Army Engineer Waterways Experiment Station, CE, Vicksburg, Miss.

28. Crosby, L. G., Durham, D. L., and Chatham, C. E., Jr., "Expansion of Port Hueneme, California; Hydraulic Model Investigation," Technical Report H-75-8, Apr 1975, U. S. Army Engineer Waterways Experiment Station CE, Vicksburg, Miss.

29. Houston, J. R., "Los Angeles Harbor Numerical Analysis of Harbor Oscillations" (in preparation), U. S. Army Engineer Waterways Experiment station, CE, Vicksburg, Miss.

30. _____, "Long Beach Harbor Numerical Analysis of Harbor Oscillations" (in preparation), U. S. Army Engineer Waterways Experiment Station, CE, Vicksburg, Miss.

31. Ippen, A. T., Estuary and Coastline Hydrodynamics, McGraw-Hill, New York, 1966.

32. Gilbert, G., Thompson, D. M., and Brewer, A. J., "Design Curves for Regular and Random Wave Generators," Report No. INT 91, Jun 1970, Hydraulics Research Station, Wallingford, Berkshire, England.

Table 1

Comparison of Ten Model and Prototype Orthogonal Azimuths for a Wave Period of 20 sec

Prototype Azimuth, degrees	Model Azimuth, degrees
214.7	208.0
199.4	193.0
197.1	192.7
187.5	188.7
182.8	184.2
178.4	179.8
166.8	167.8
188.7	191.3
191.4	185.2
216.0	225.1

Table 2

Comparison of Thirteen Model and Prototype Orthogonal Azimuths for a Wave Period of 75 sec

Prototype Azimuth, degrees	Model Azimuth, degrees
227.3	229.7
225.9	226.8
217.4	222.3
209.0	209.7
191.2	194.3
186.7	184.1
178.2	180.9
174.6	175.7
155.9	153.3
151.5	146.9
144.0	152.1
184.5	182.3
183.5	183.1

Table 3

Normalized Wave-Height Variation Along the Generated Model Wave Front

Wave Period sec	Wave Generator Unit No.													
	1	2	3	4	5	6	7	8	9	10	11	12	13	14
15	0.41	0.31	0.59	0.60	0.60*	0.60*	0.58	0.63*	0.69	1.00	1.00*	1.00	0.85*	0.63
20	0.27*	0.17	0.24*	0.49*	0.80	0.86	0.91*	0.98*	1.00	1.00*	0.89*	0.67	0.74	0.72
30	0.36*	0.17*	0.36*	0.36*	0.30*	0.40*	0.42	0.50*	0.58	1.00*	1.00	0.80	0.76	0.72
45	0.27	0.17	0.29	0.31*	0.36*	0.45	0.53	0.50*	0.50*	0.49	0.58	1.00	0.67*	0.49
60	0.25*	0.16	0.25*	0.25	0.26*	0.28	0.38	0.45*	0.50*	0.50*	0.54	1.00	0.72*	0.58
75	0.45	0.24	0.38	0.38	0.37	0.40	0.40	0.40	0.50	0.60	0.69	0.99	1.00	0.94
90-360	0.21	0.18	0.38	0.38	0.32	0.43	0.49	0.44	0.50	0.54	0.69	1.00	0.85	0.90

* Averaged value.

Table 4

Wave Reflection Coefficients for the Distorted-Scale Middle and Long Beach Breakwaters

Prototype Wave Period, sec	Prototype Wave Height, ft	Reflection Coefficient
20	0.91	0.64
	2.15	0.50
30	1.26	0.44
	3.04	0.41
40	1.15	0.43
	3.89	0.45
50	1.00	0.48
	4.14	0.51
60	1.02	0.52
	3.75	0.49
70	1.03	0.39
	3.93	0.46
80	1.31	0.46
	3.46	0.52
90	1.24	0.48
	4.61	0.38
100	1.55	0.39
	3.81	0.42

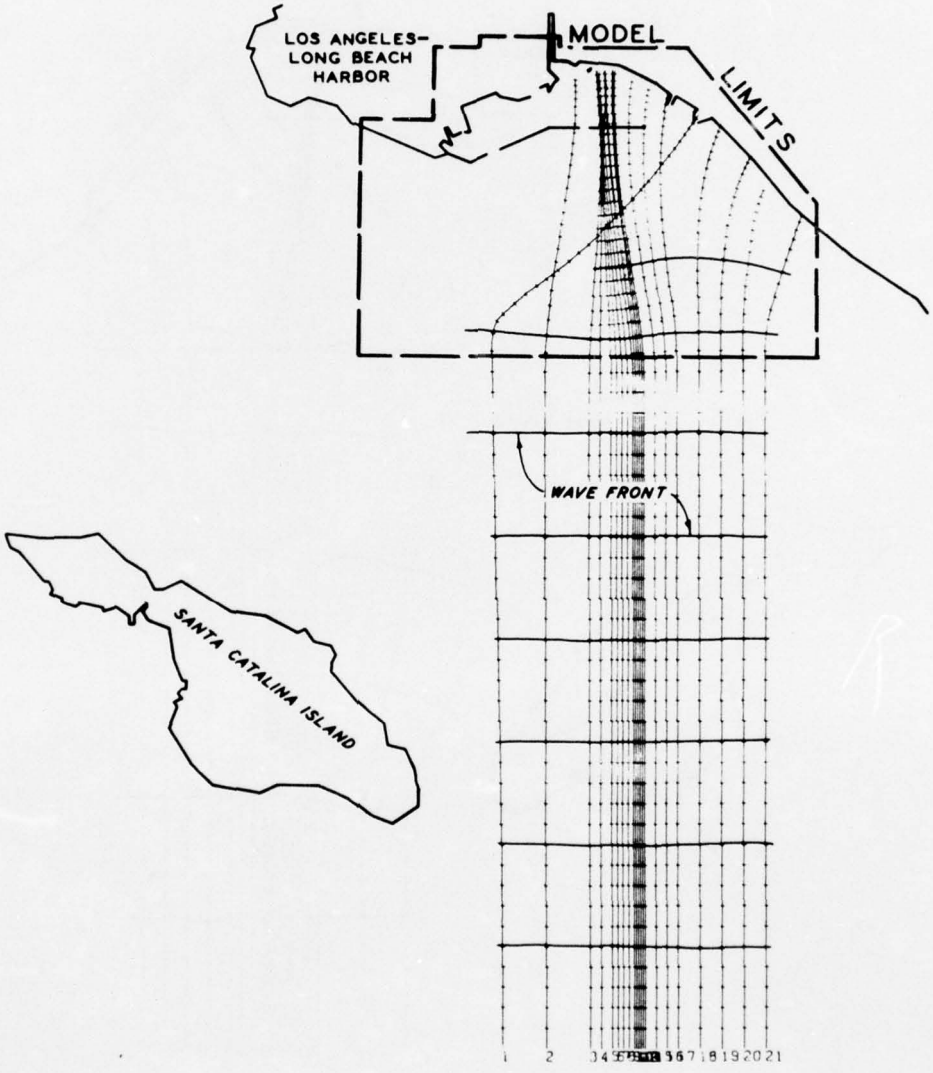

REFRACTION DIAGRAM FOR 15-SECOND WAVE FROM SOUTH

GRID 1

PLATE 1

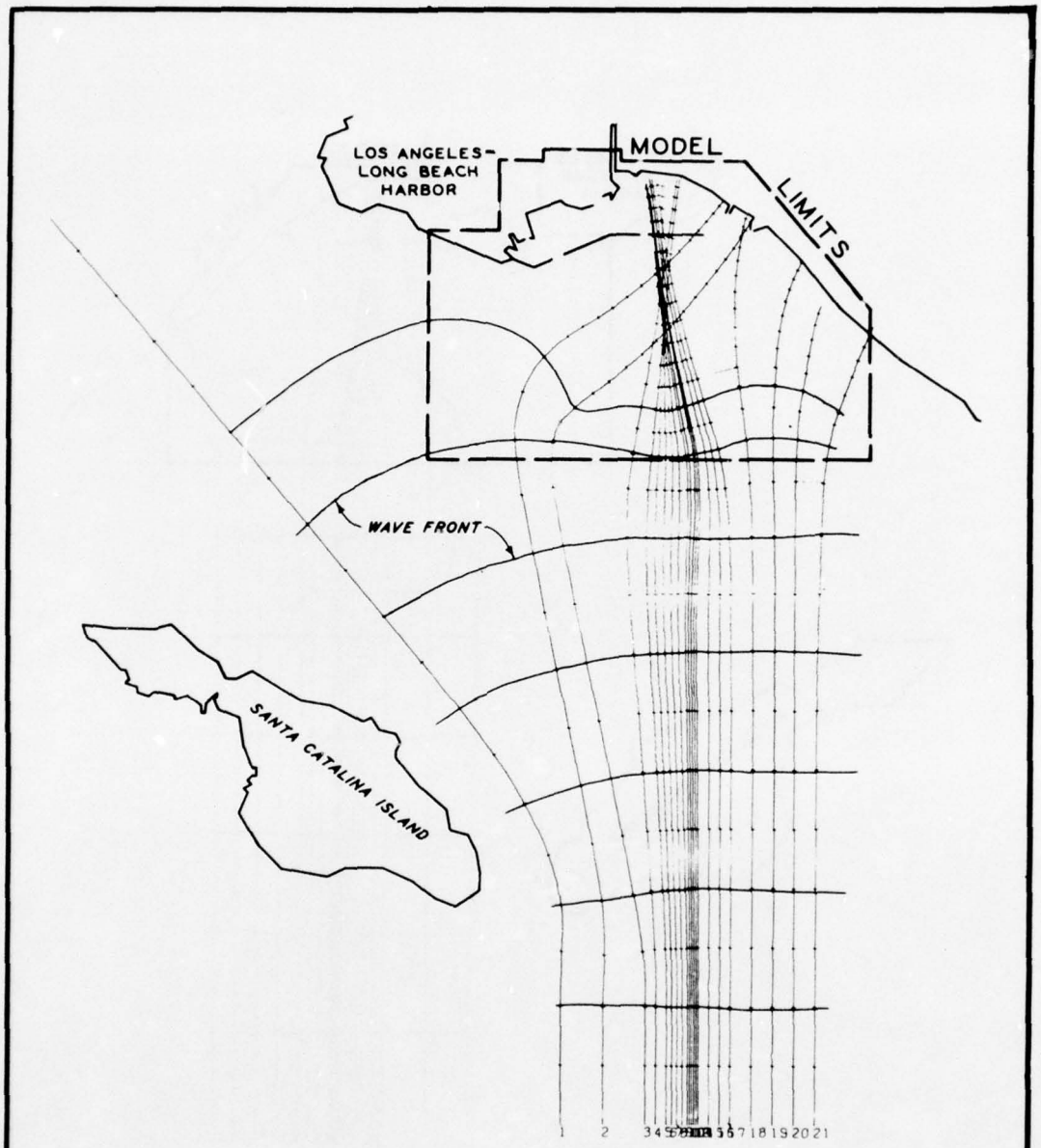

REFRACTION DIAGRAM FOR 30-SECOND WAVE FROM SOUTH

GRID 1

PLATE 2

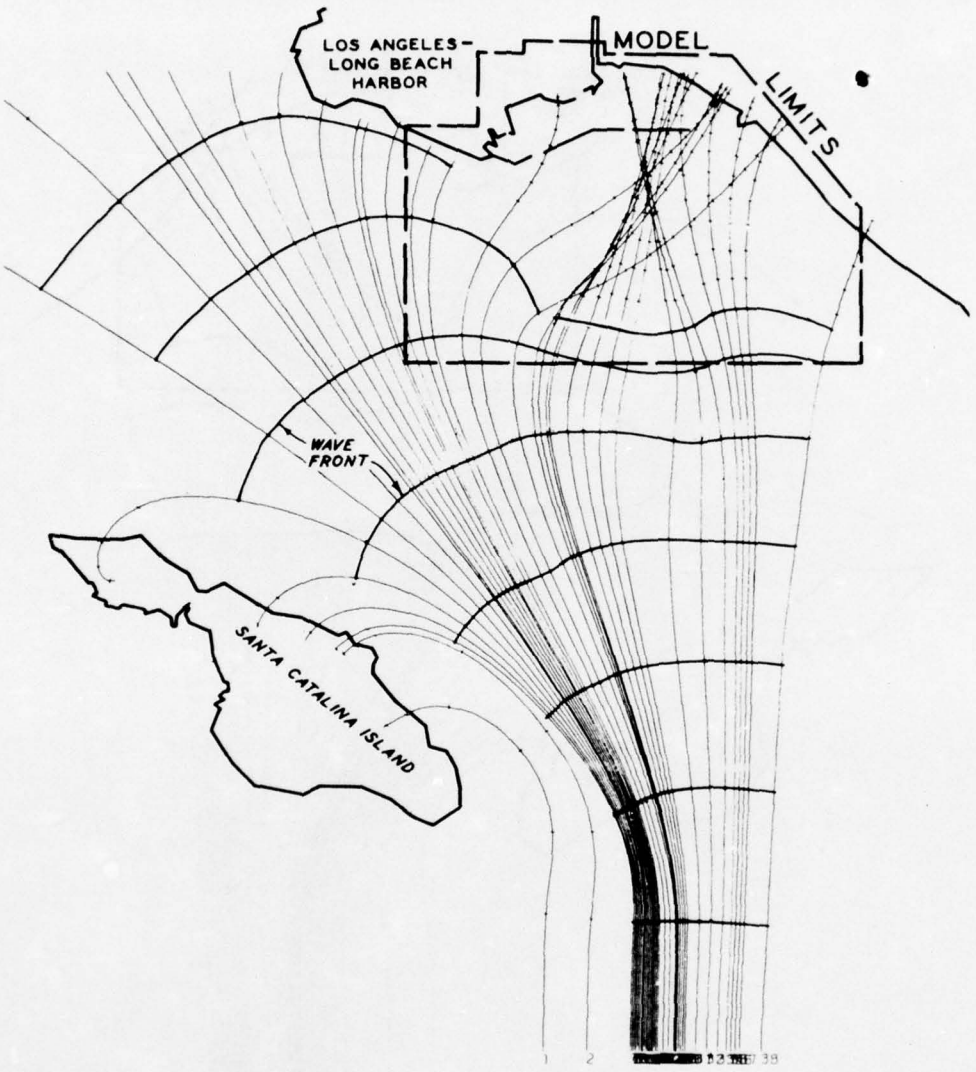

REFRACTION DIAGRAM FOR
60-SECOND WAVE
FROM SOUTH
GRID 1

PLATE 3

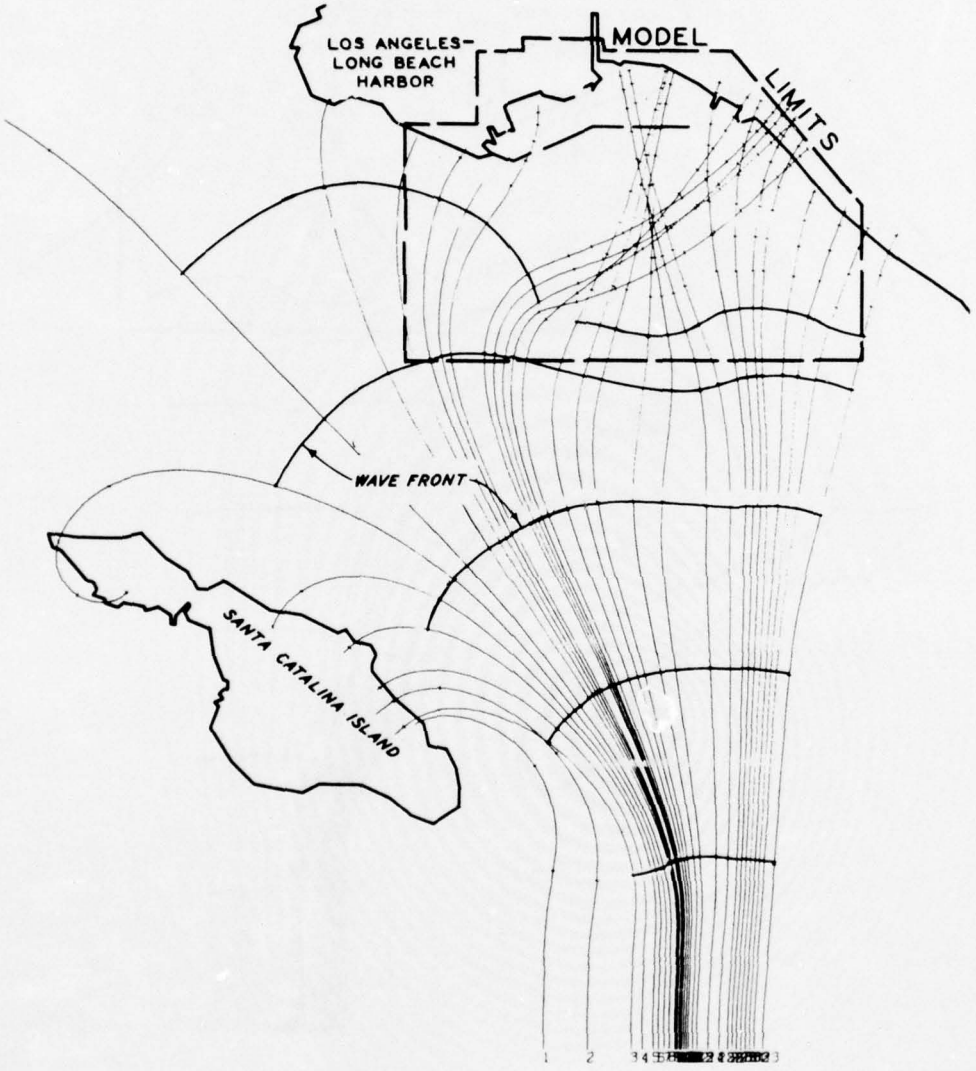

REFRACTION DIAGRAM FOR
300-SECOND WAVE
FROM SOUTH
GRID 1

PLATE 4

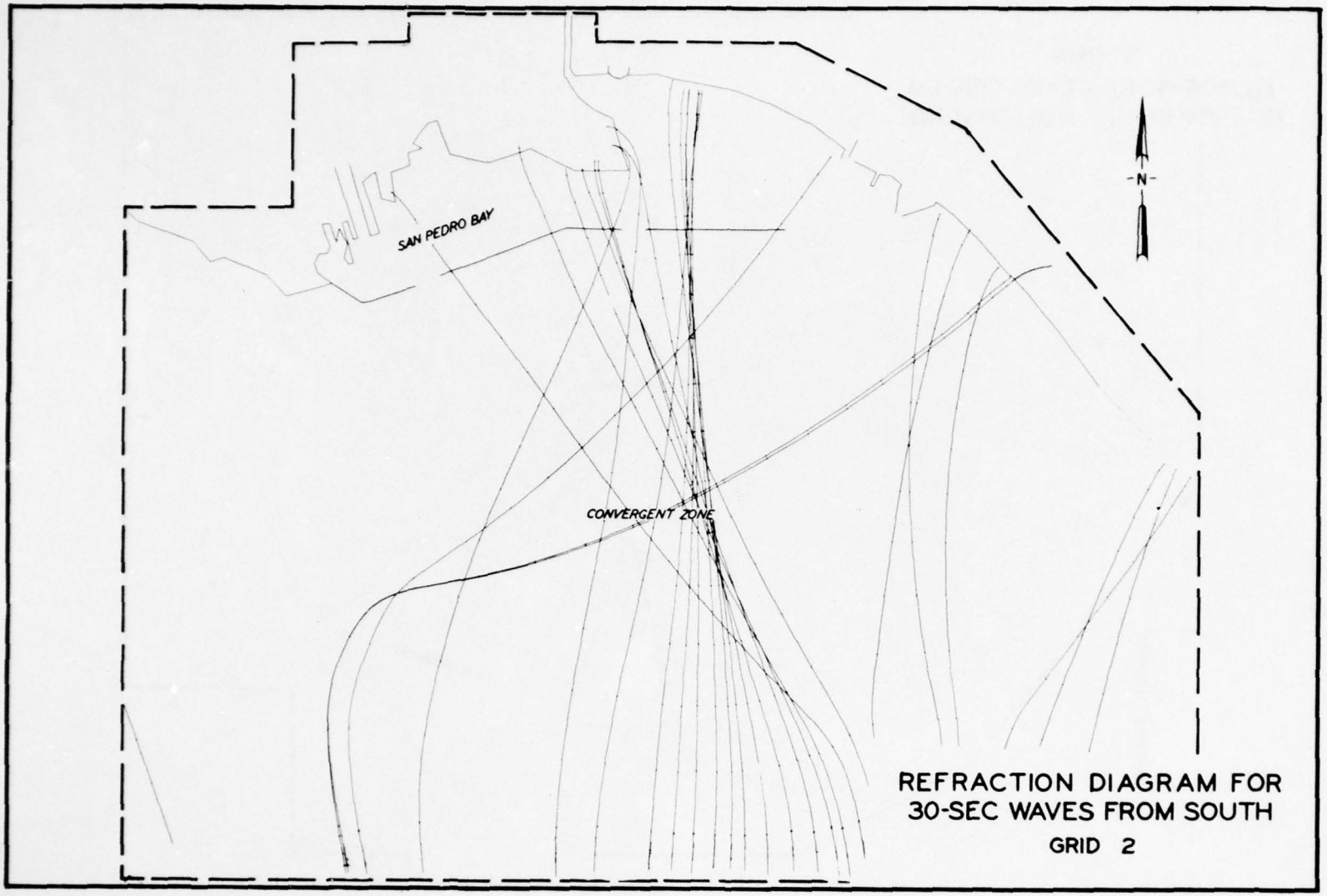

REFRACTION DIAGRAM FOR
30-SEC WAVES FROM SOUTH
GRID 2

PLATE 5

PLATE 6

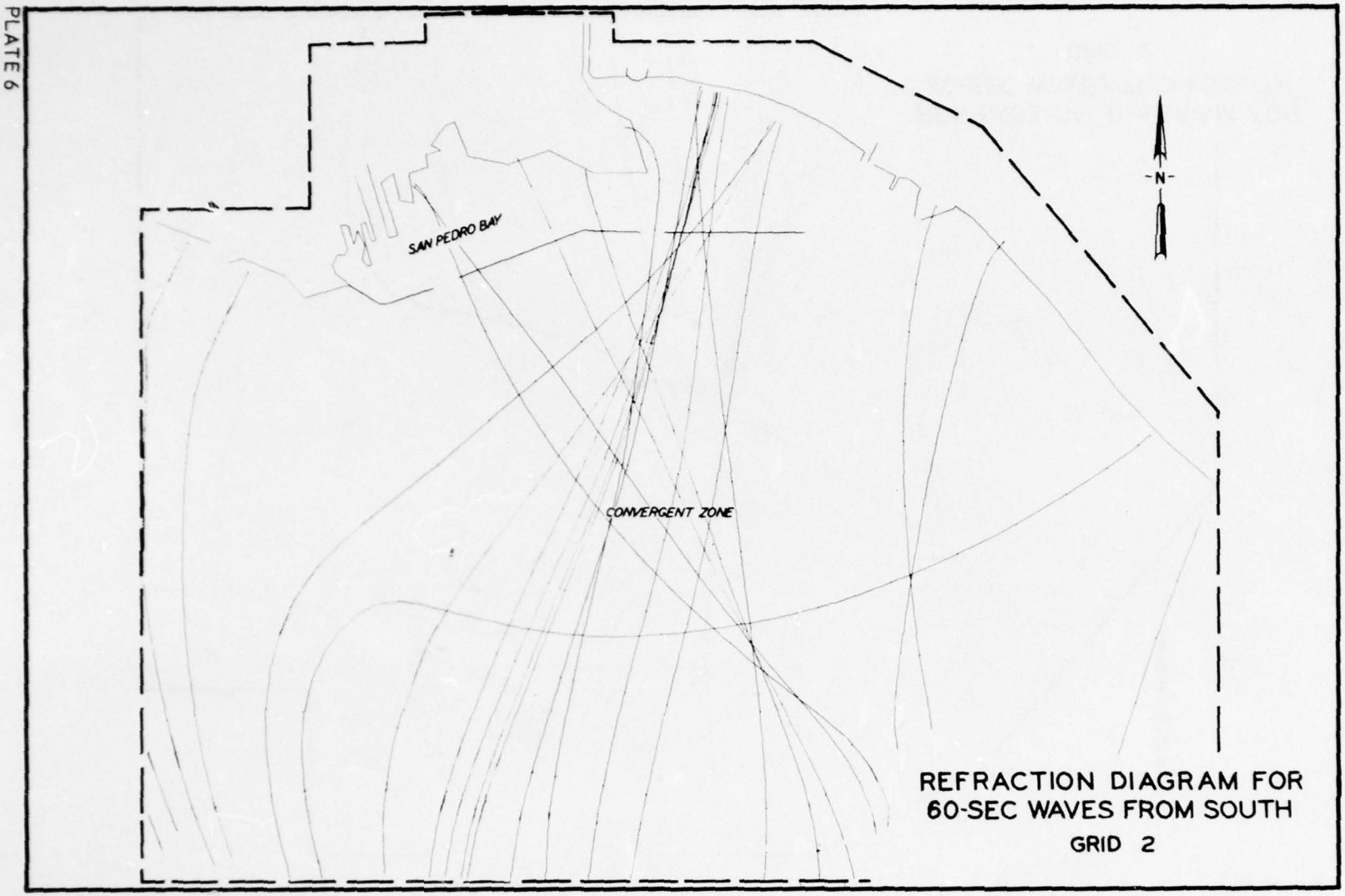

REFRACTION DIAGRAM FOR
60-SEC WAVES FROM SOUTH
GRID 2

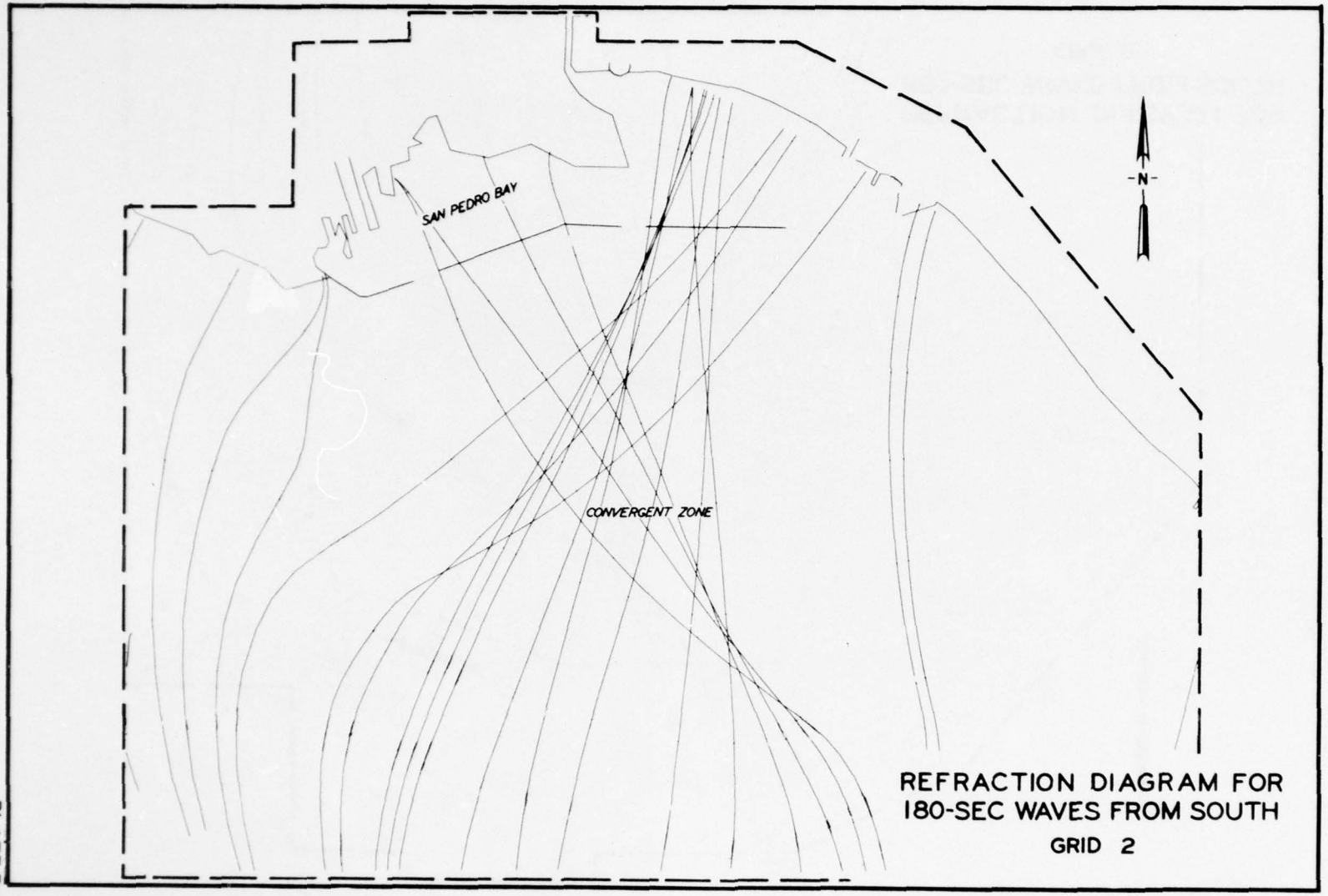

REFRACTION DIAGRAM FOR
180-SEC WAVES FROM SOUTH
GRID 2

PLATE 7

PLATE 8

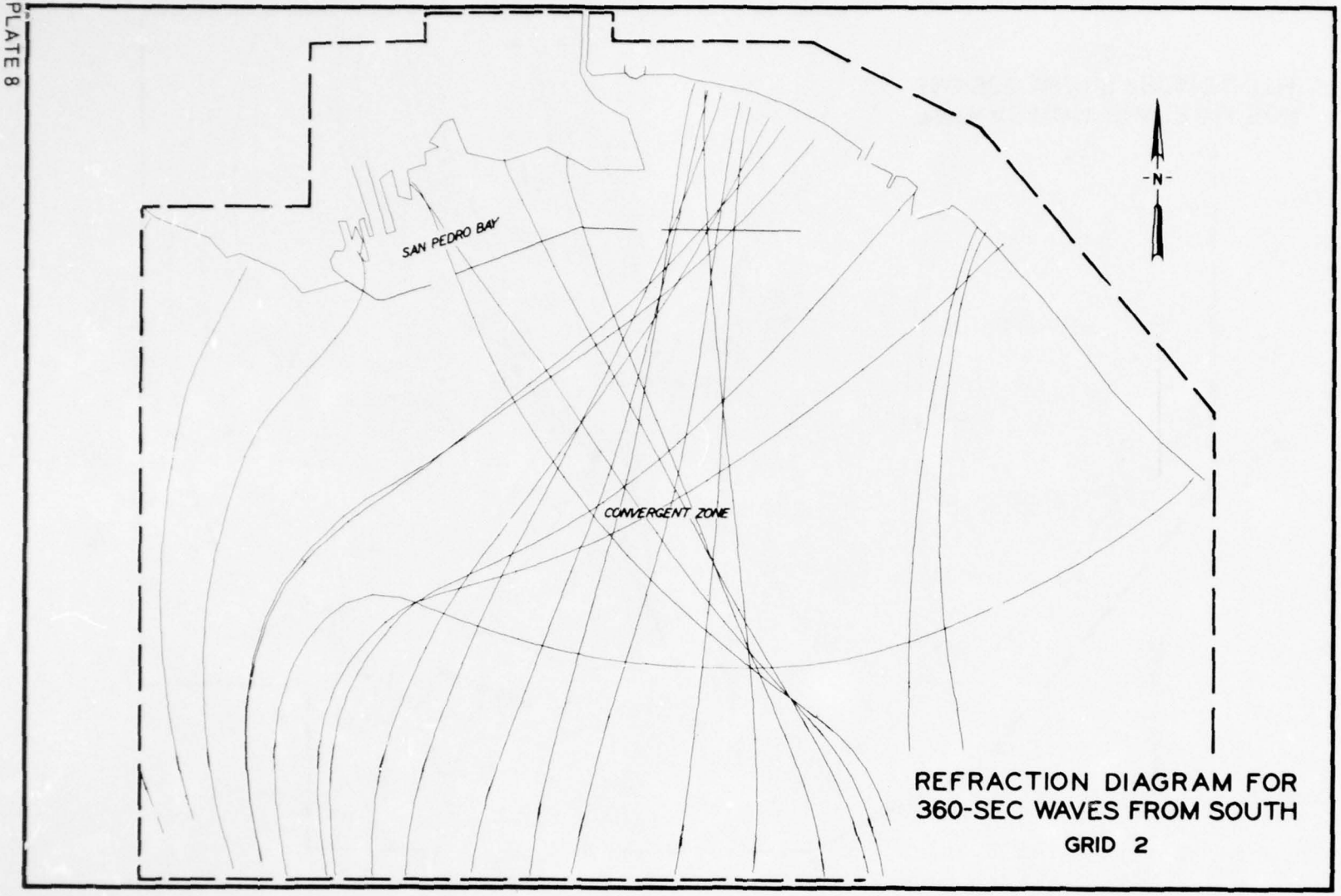

REFRACTION DIAGRAM FOR
360-SEC WAVES FROM SOUTH
GRID 2

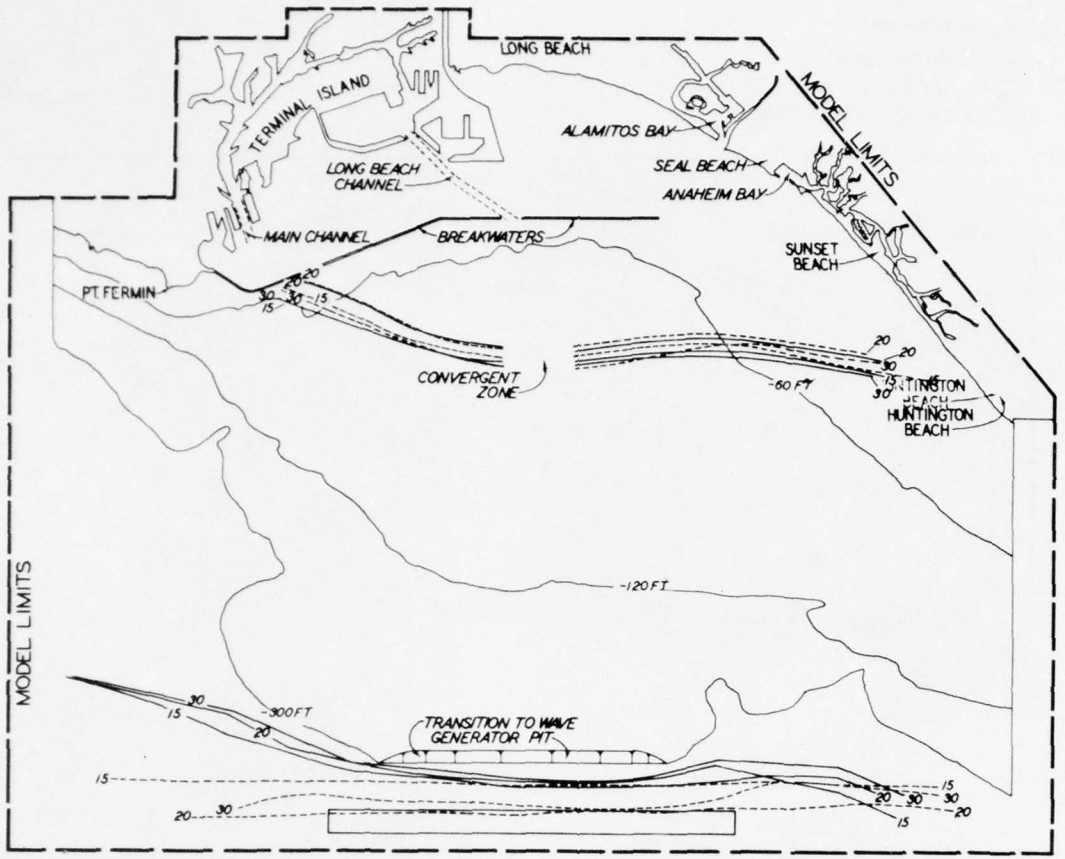

LEGEND

—— MODEL WAVE FRONT ADJUSTED FOR SCALE DISTORTION

– – – PROTOTYPE WAVE FRONT

COMPARISON OF MODEL AND PROTOTYPE WAVE FRONTS NEAR THE -300 FT CONTOUR AND NEAR THE HARBOR

15, 20, AND 30 SECONDS

PLATE 9

PLATE 10

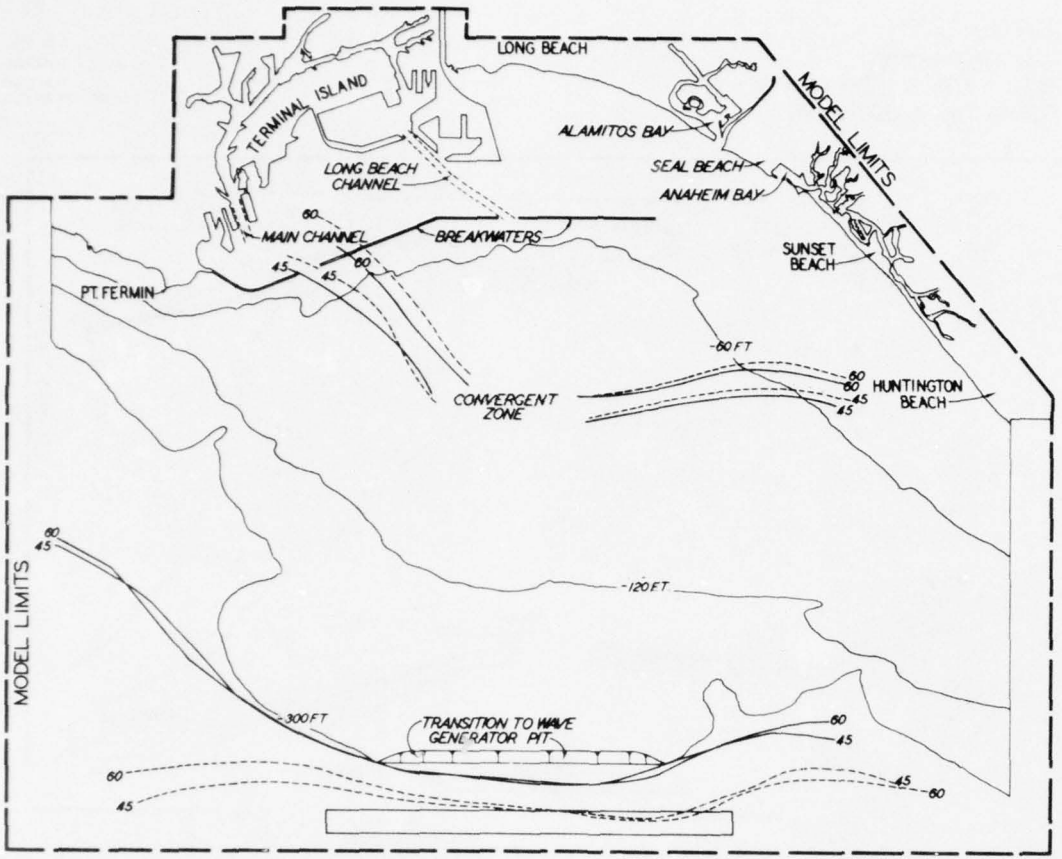

LEGEND

—— MODEL WAVE FRONT ADJUSTED FOR SCALE DISTORTION

– – – PROTOTYPE WAVE FRONT

COMPARISON OF MODEL AND PROTOTYPE WAVE FRONTS NEAR THE -300 FT CONTOUR AND NEAR THE HARBOR

45 AND 60 SECONDS

AD-A037 154 ARMY ENGINEER WATERWAYS EXPERIMENT STATION VICKSBURG MISS F/G 20/4
LOS ANGELES AND LONG BEACH HARBORS MODEL STUDY. REPORT 4. MODEL--ETC(U)
FEB 77 D G OUTLAW, D L DURHAM, C E CHATHAM

UNCLASSIFIED WES-TR-H-75-4-4 NL

2 OF 3
AD
A037154

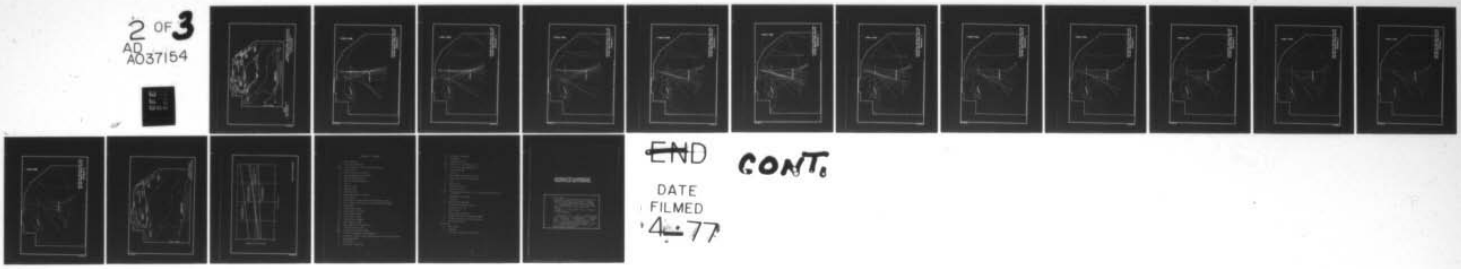

END CONT.

DATE
FILMED
4-77

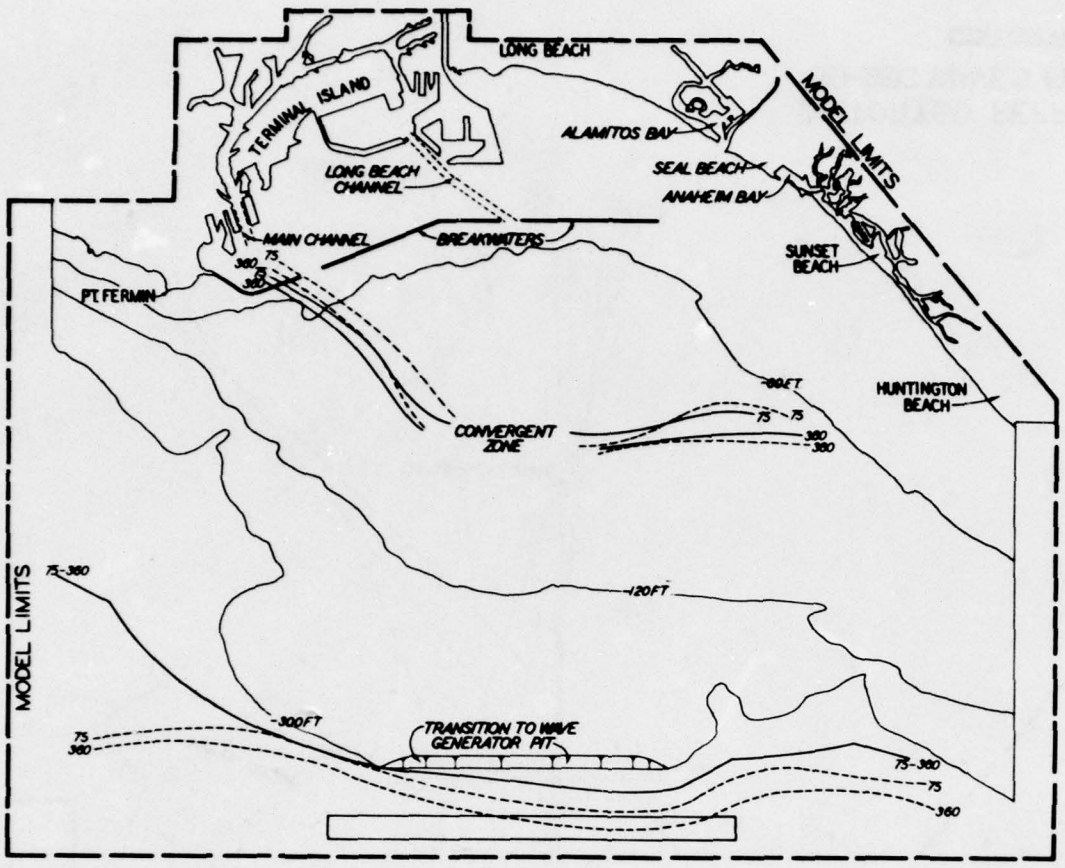

LEGEND

—— MODEL WAVE FRONT ADJUSTED FOR SCALE DISTORTION

--- PROTOTYPE WAVE FRONT

COMPARISON OF MODEL AND PROTOTYPE WAVE FRONTS NEAR THE -300 FT CONTOUR AND NEAR THE HARBOR

75 AND 360 SECONDS

PLATE 11

PLATE 12

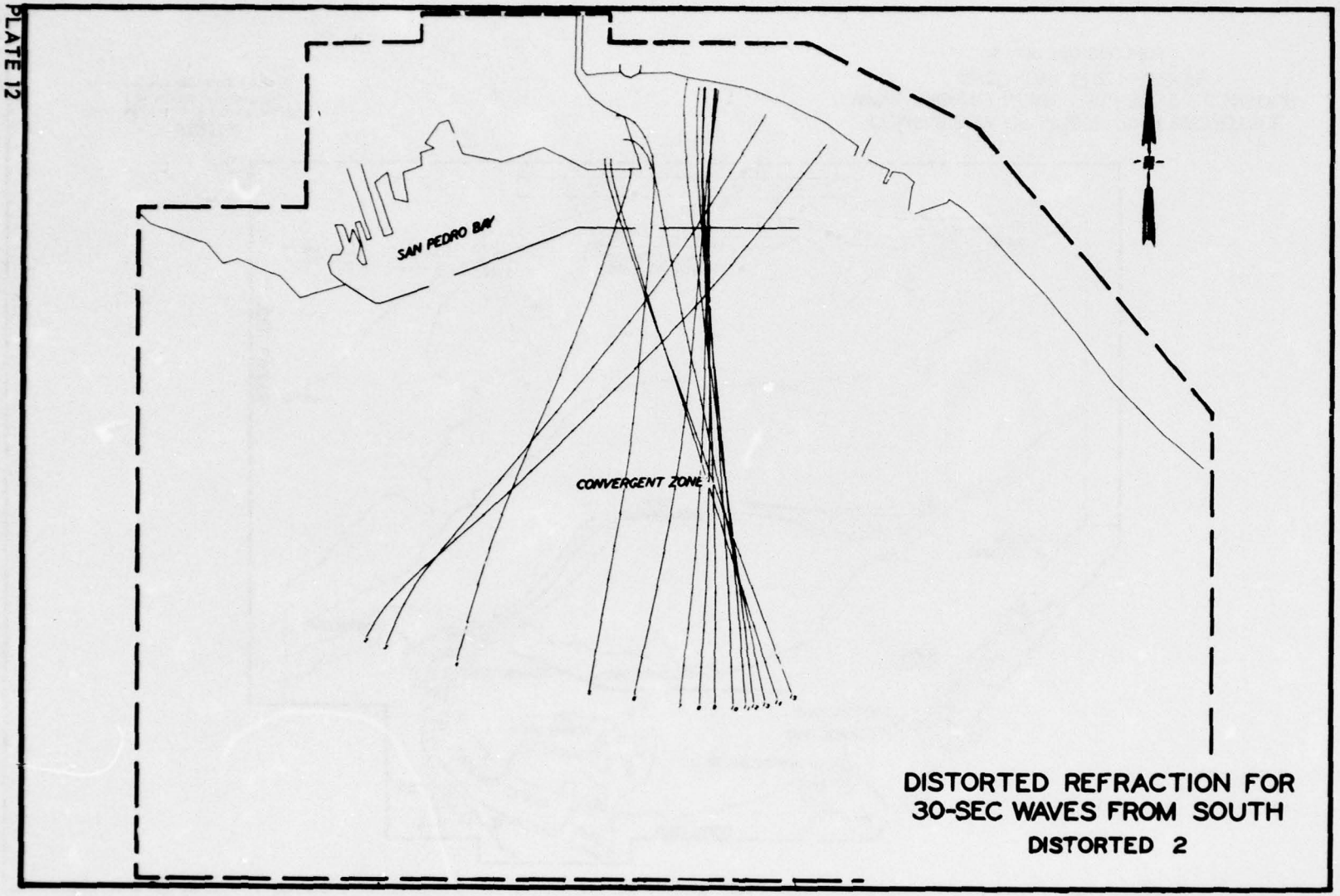

DISTORTED REFRACTION FOR
30-SEC WAVES FROM SOUTH
DISTORTED 2

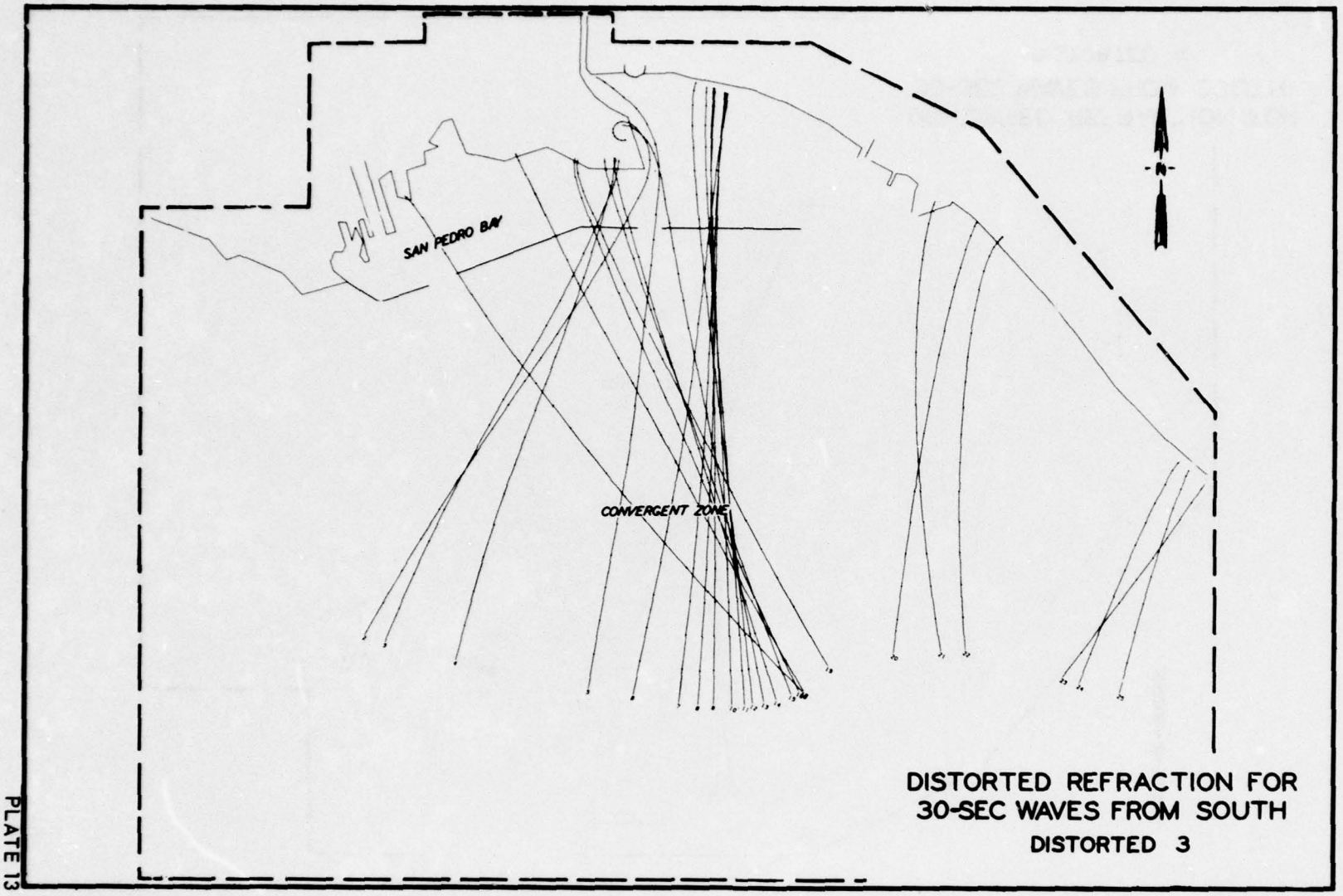

DISTORTED REFRACTION FOR
30-SEC WAVES FROM SOUTH
DISTORTED 3

PLATE 13

PLATE 14

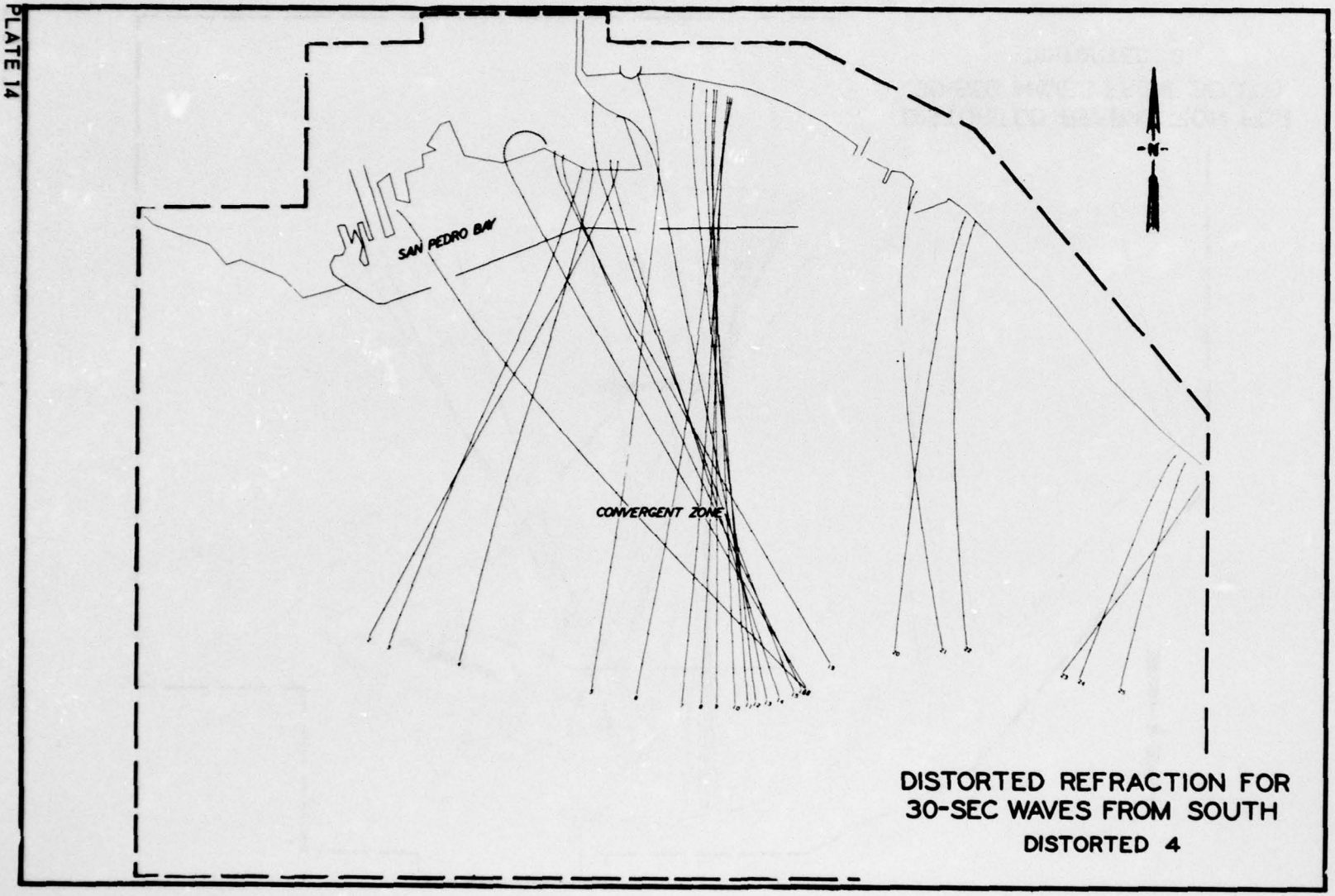

DISTORTED REFRACTION FOR
30-SEC WAVES FROM SOUTH
DISTORTED 4

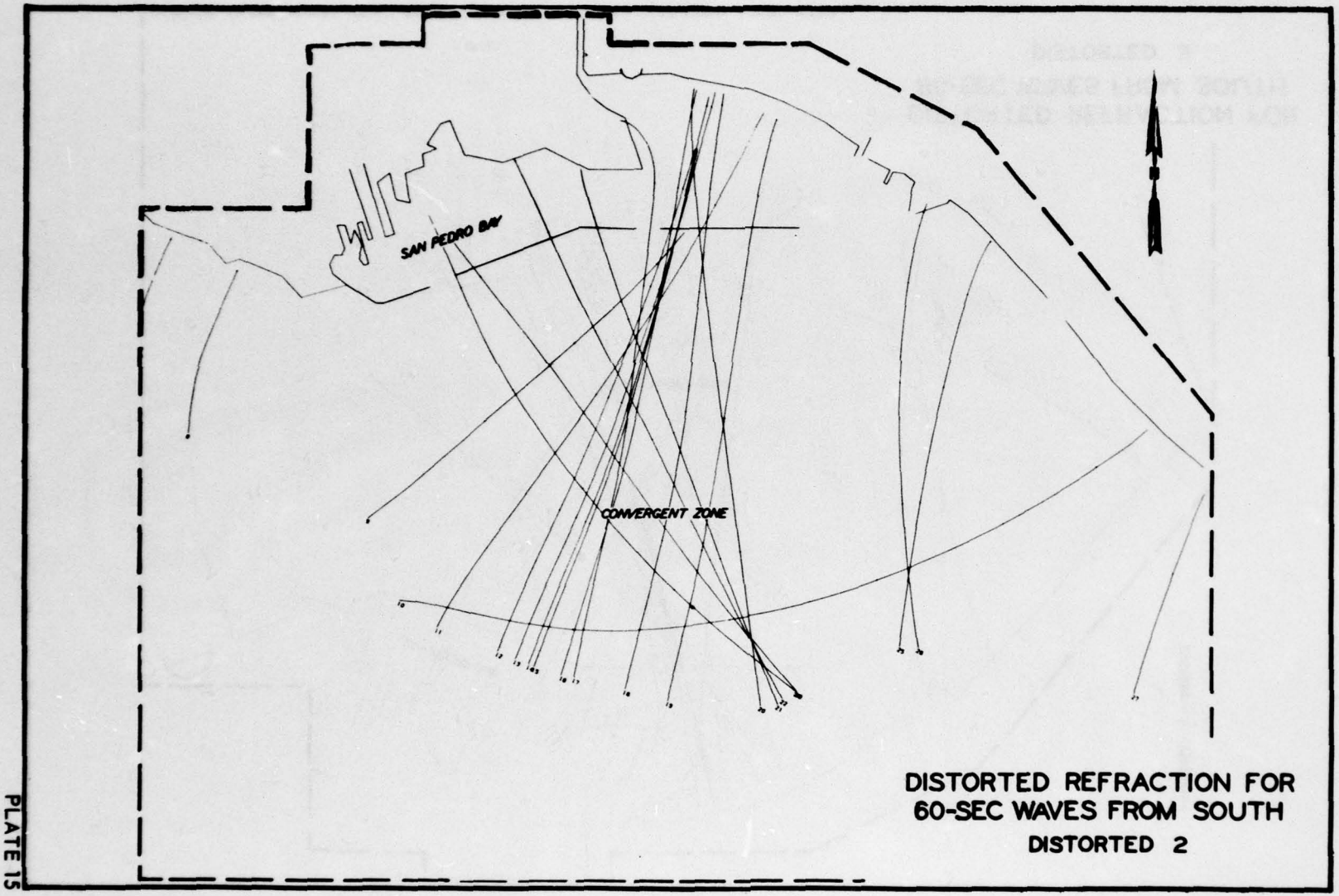

DISTORTED REFRACTION FOR
60-SEC WAVES FROM SOUTH
DISTORTED 2

PLATE 15

PLATE 16

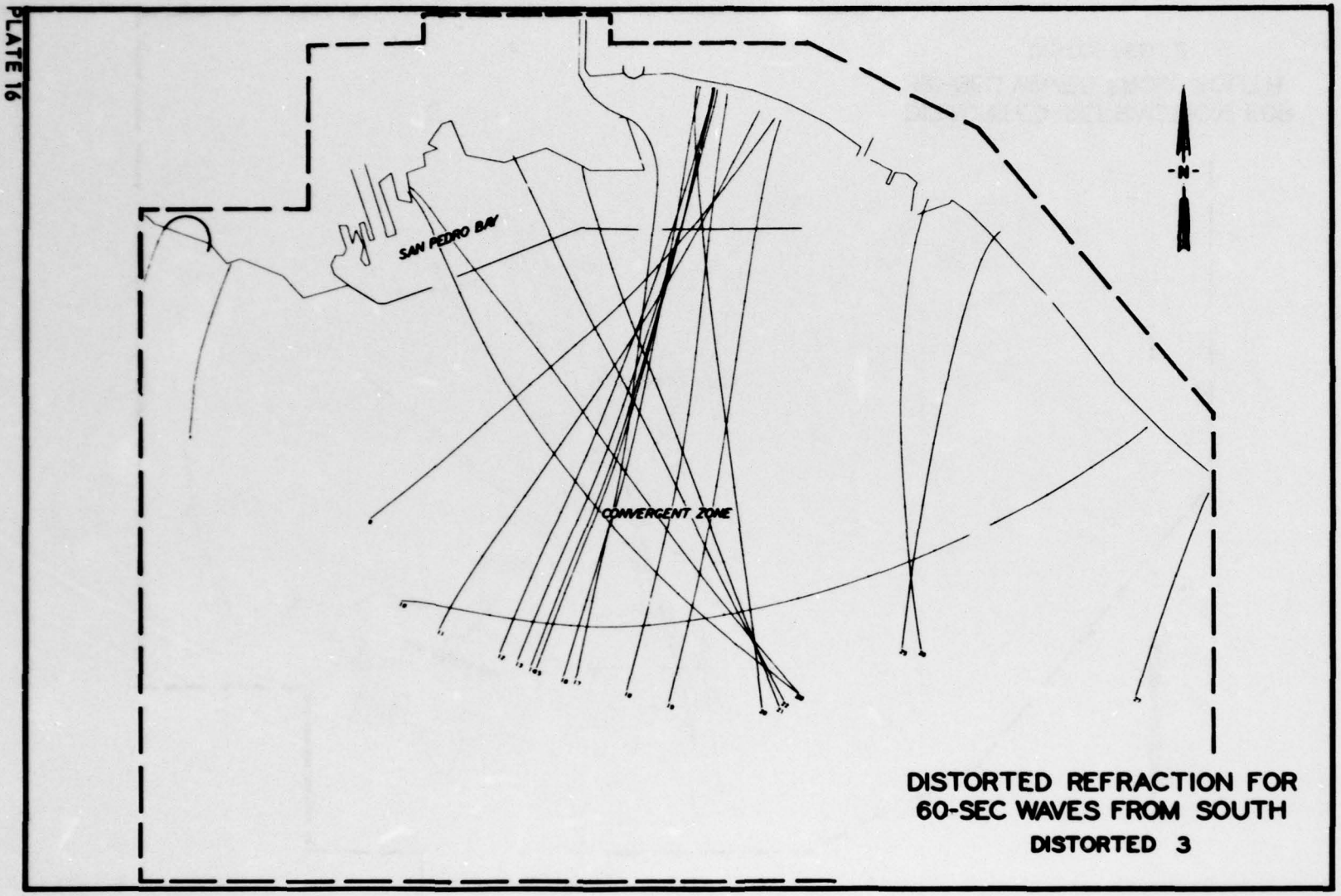

DISTORTED REFRACTION FOR
60-SEC WAVES FROM SOUTH
DISTORTED 3

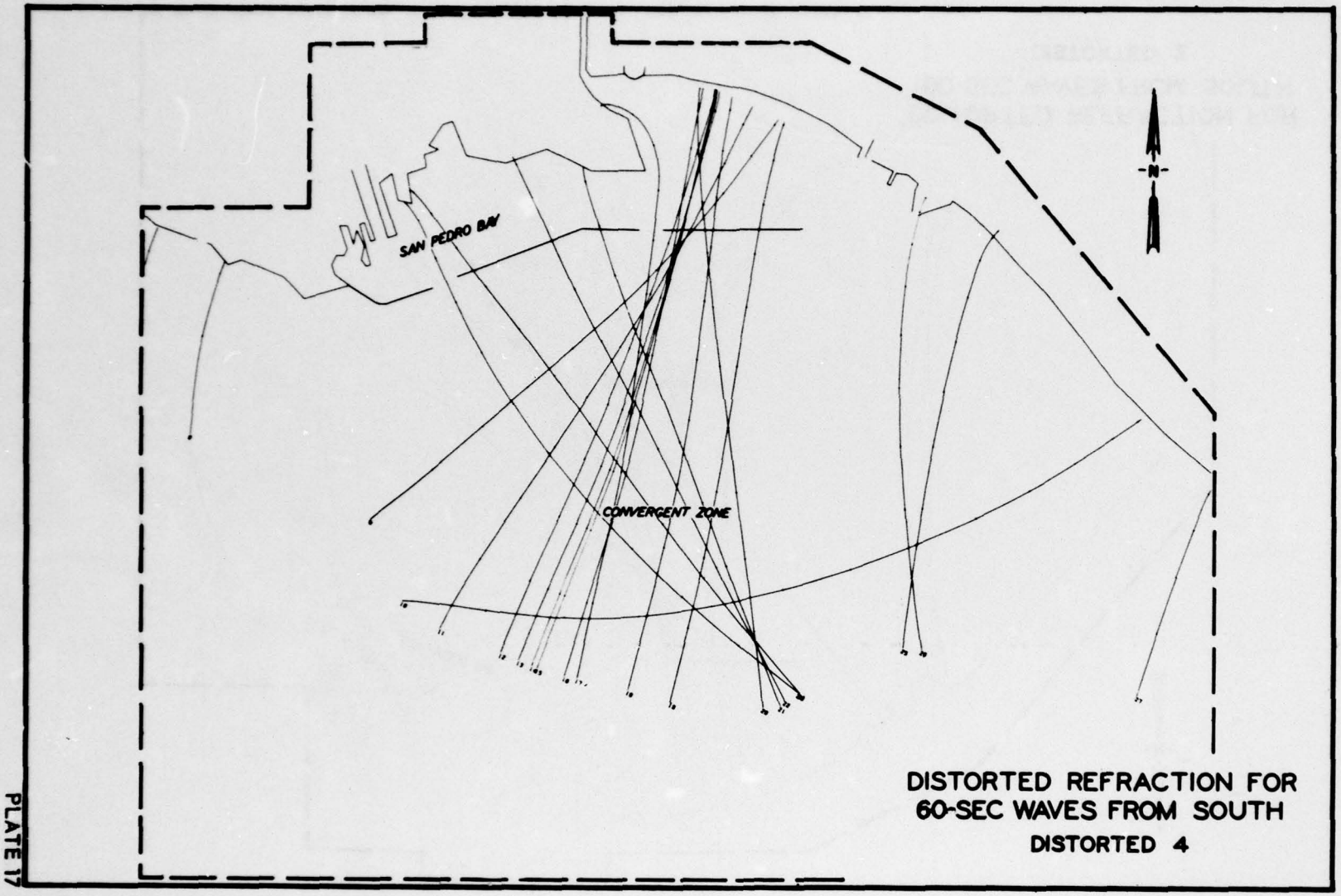

DISTORTED REFRACTION FOR
60-SEC WAVES FROM SOUTH
DISTORTED 4

PLATE 17

PLATE 18

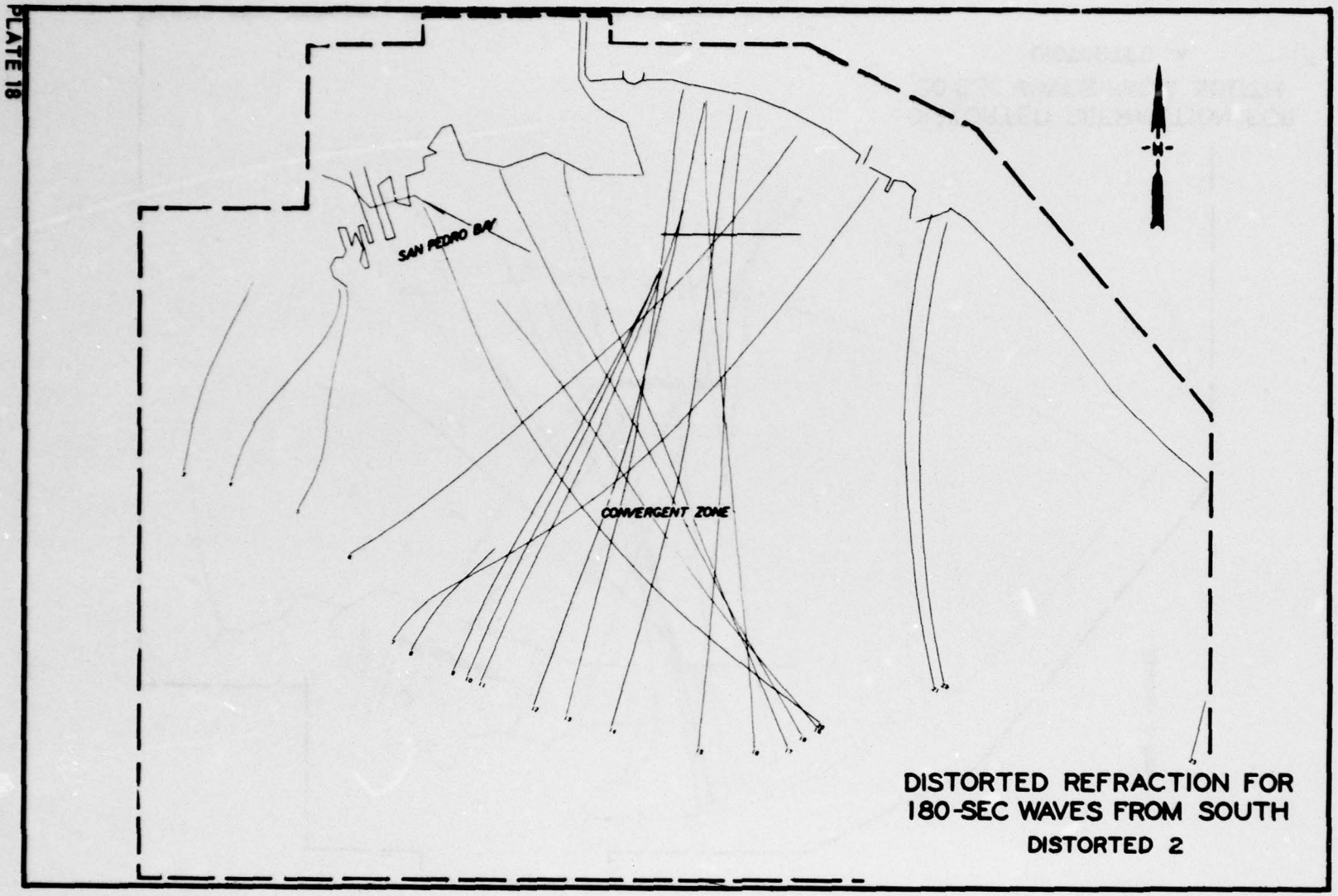

DISTORTED REFRACTION FOR
180-SEC WAVES FROM SOUTH
DISTORTED 2

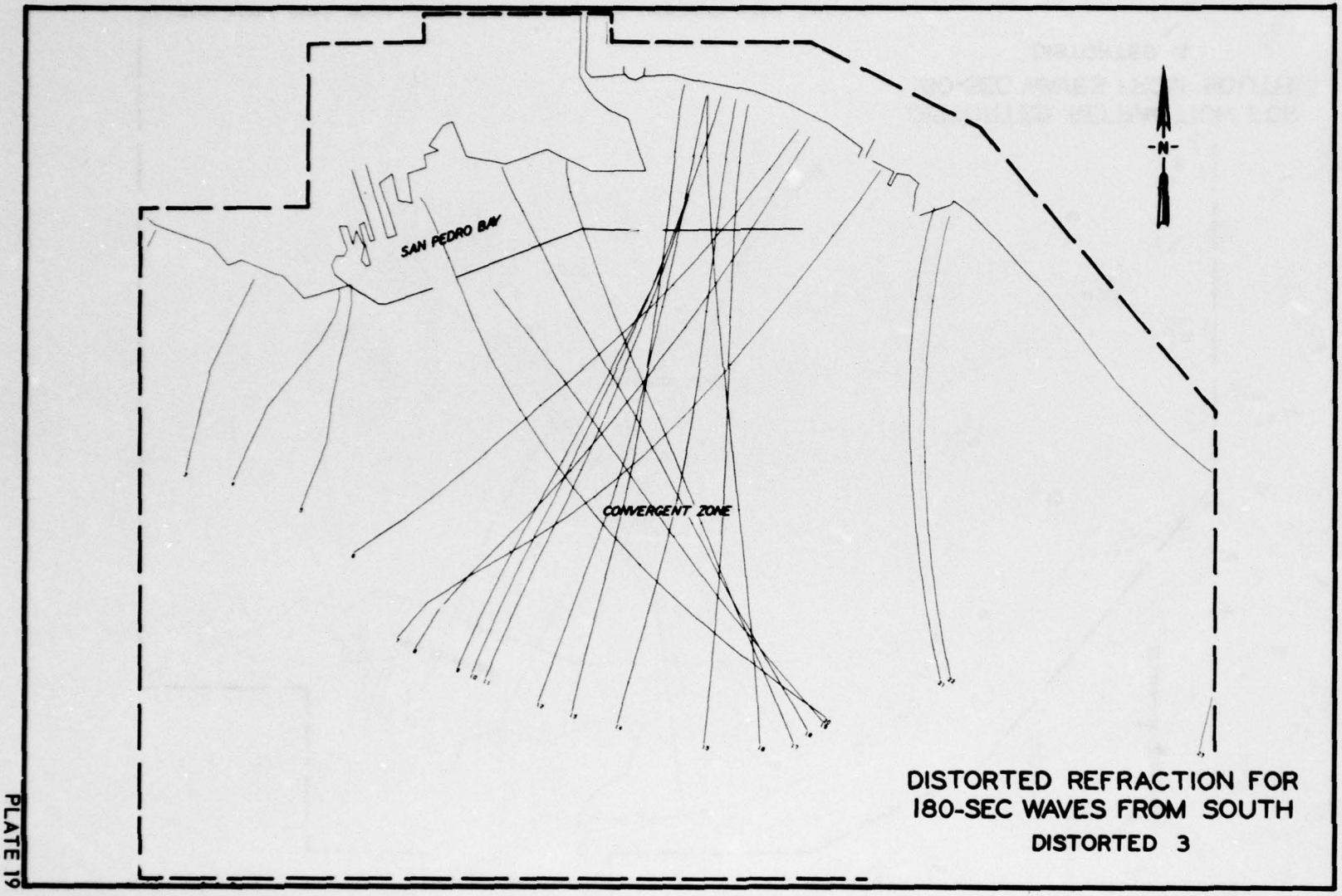

DISTORTED REFRACTION FOR
180-SEC WAVES FROM SOUTH
DISTORTED 3

PLATE 19

PLATE 20

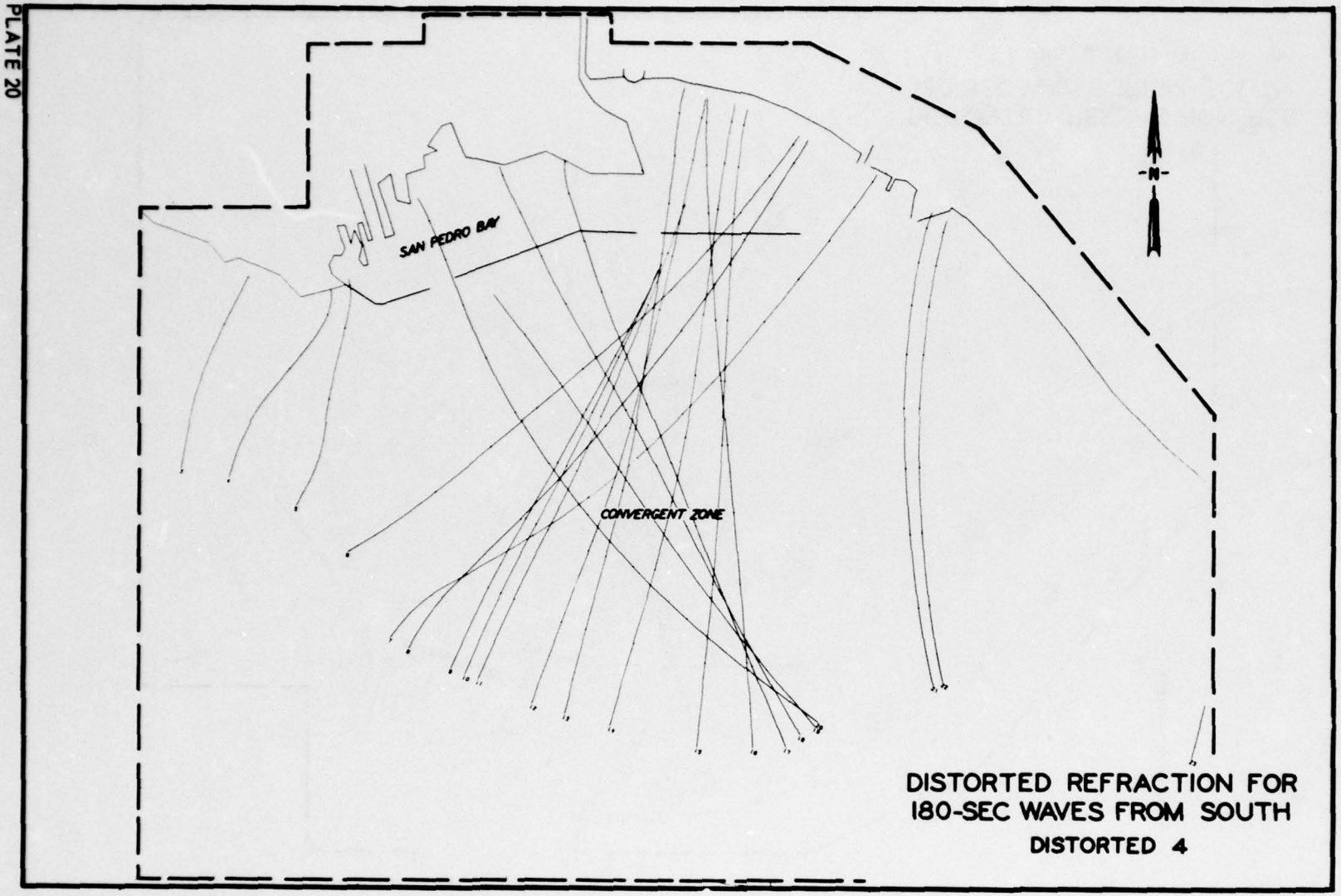

DISTORTED REFRACTION FOR
180-SEC WAVES FROM SOUTH
DISTORTED 4

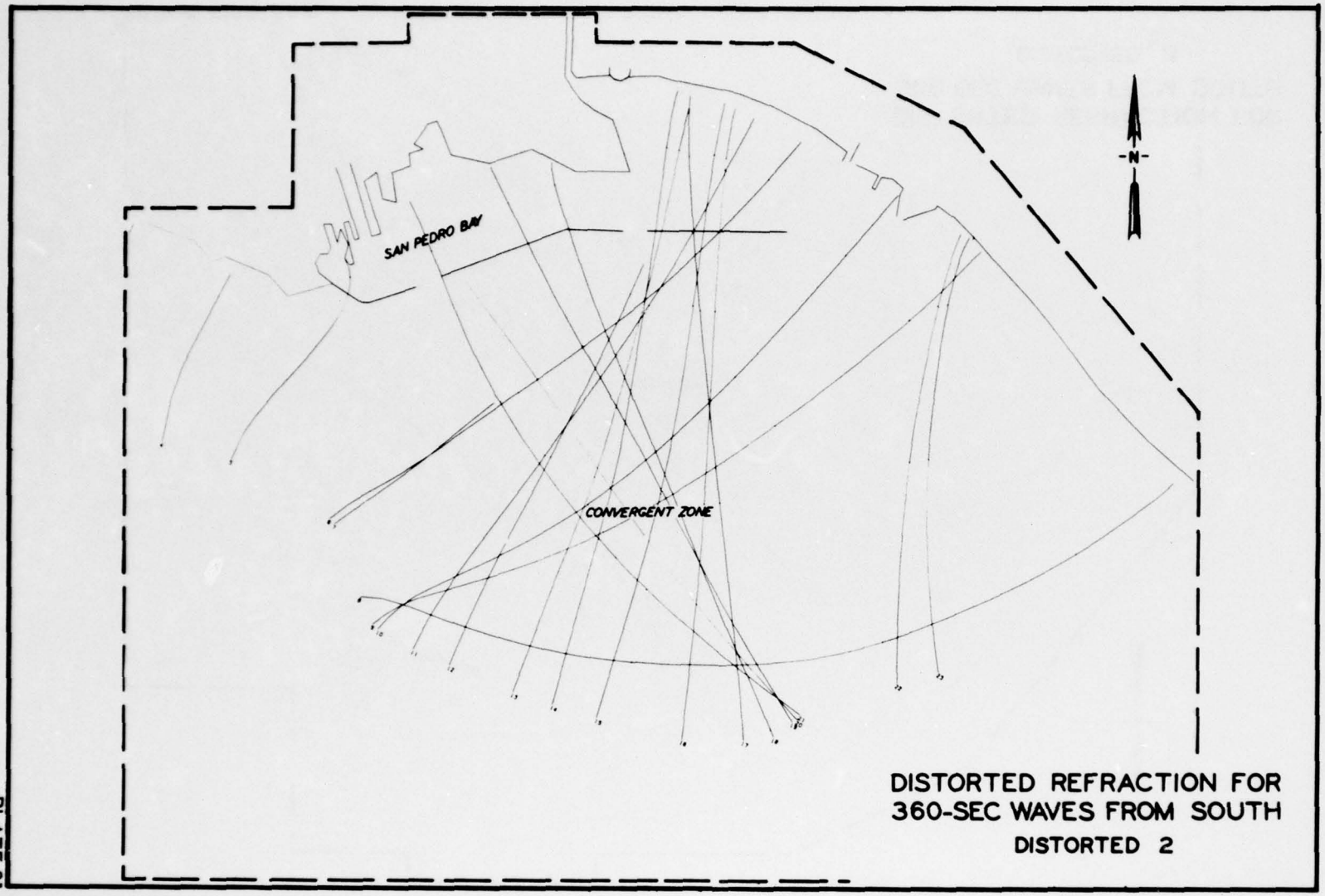

DISTORTED REFRACTION FOR
360-SEC WAVES FROM SOUTH
DISTORTED 2

PLATE 21

PLATE 22

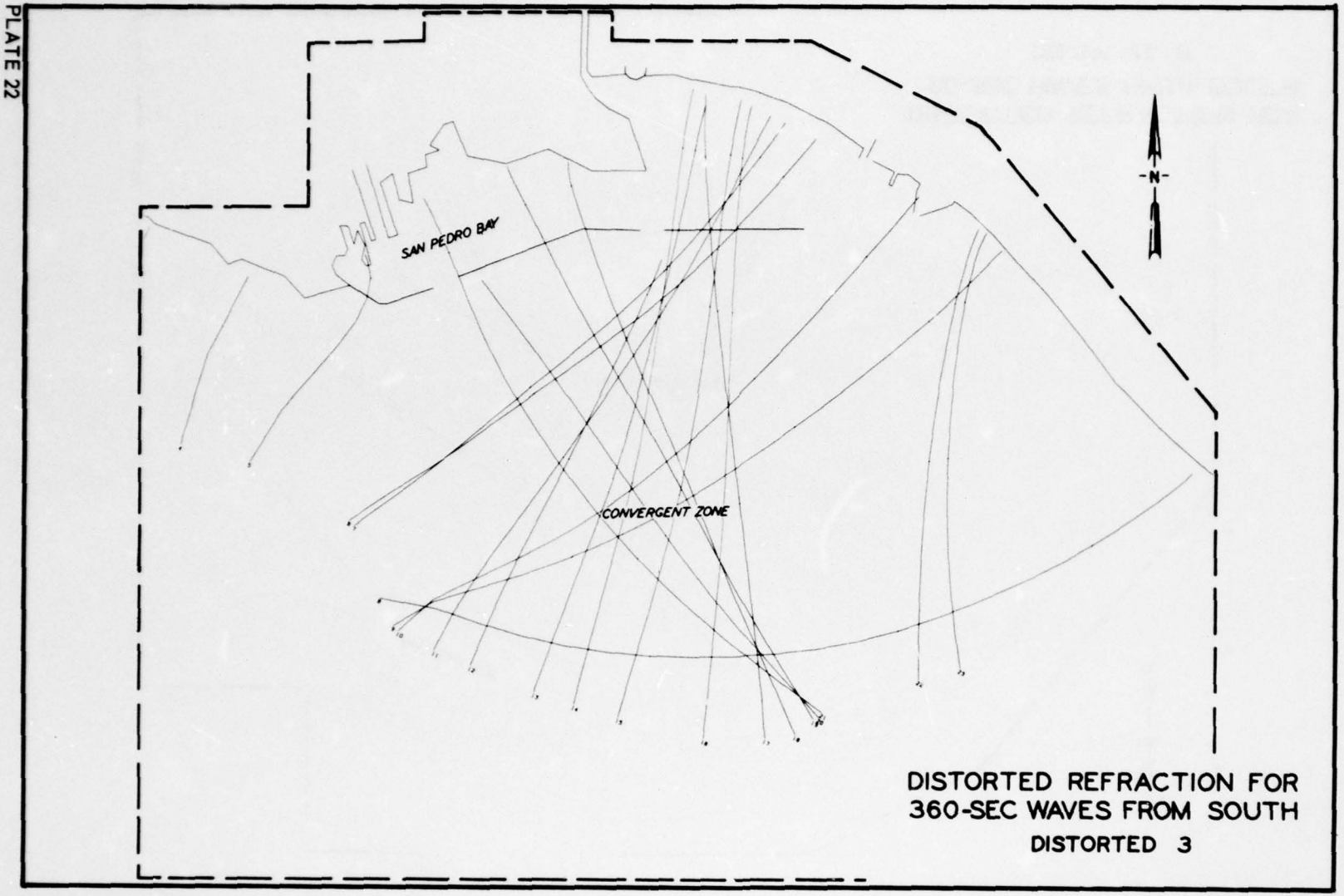

DISTORTED REFRACTION FOR
360-SEC WAVES FROM SOUTH
DISTORTED 3

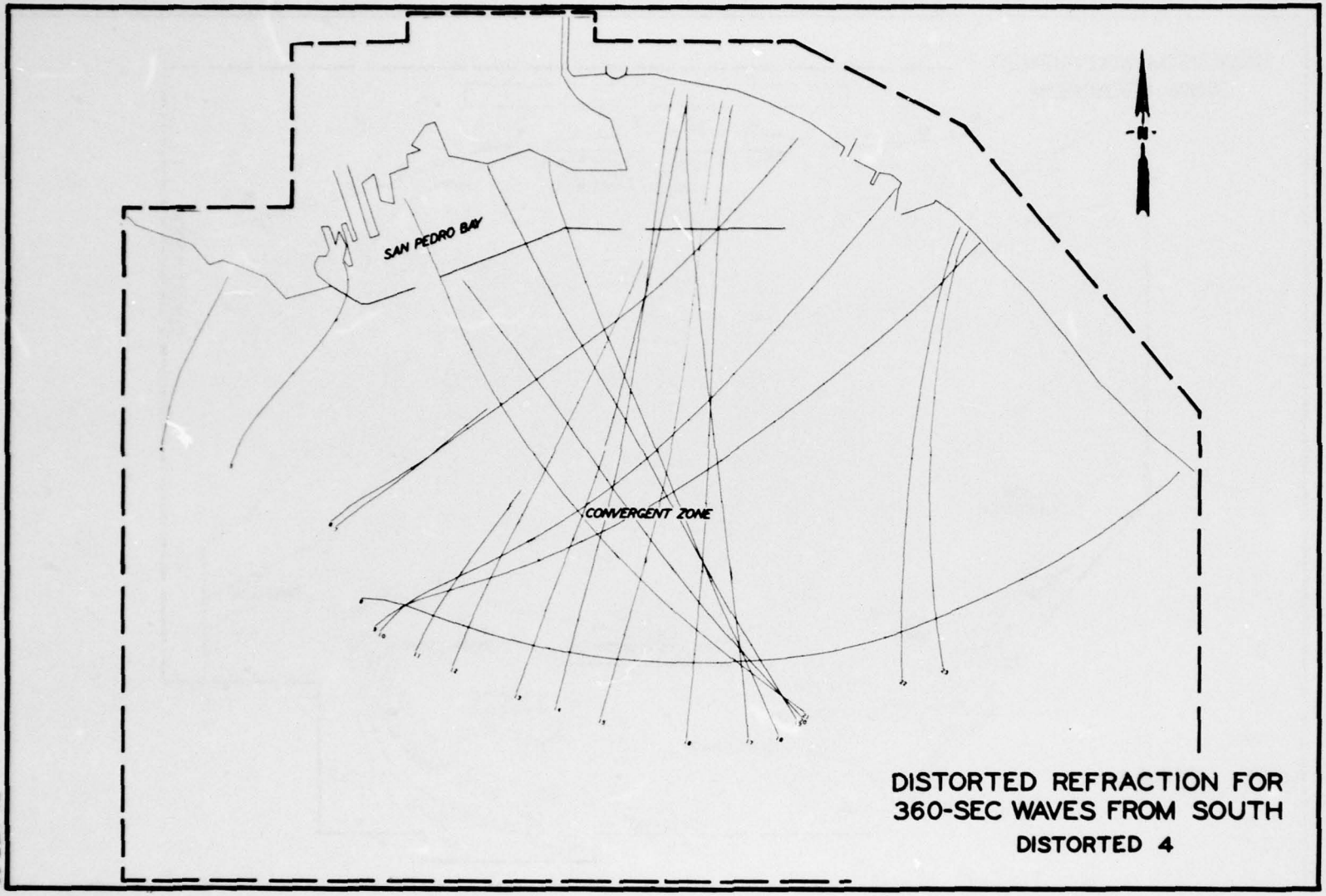

DISTORTED REFRACTION FOR
360-SEC WAVES FROM SOUTH
DISTORTED 4

PLATE 23

PLATE 24

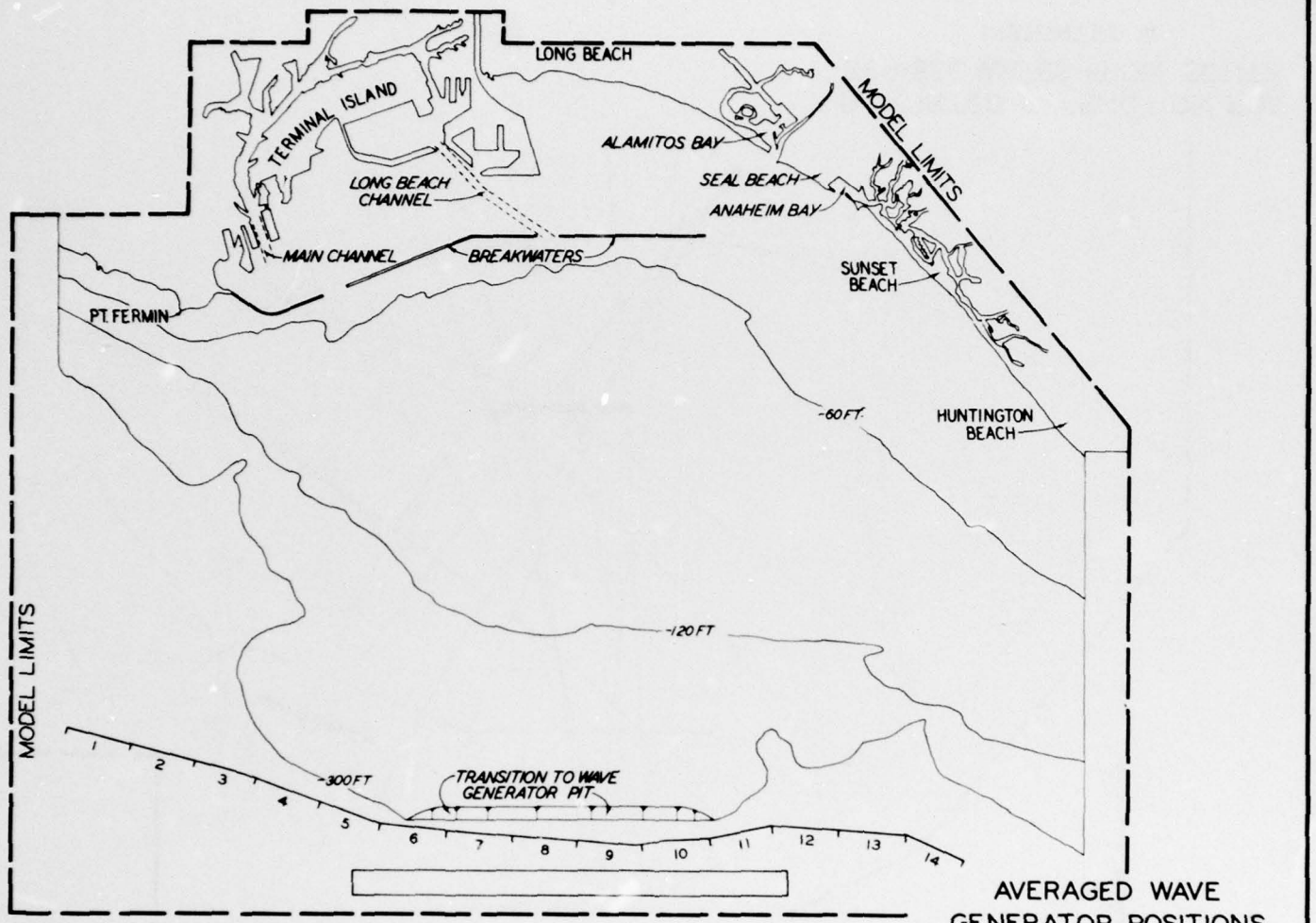

AVERAGED WAVE GENERATOR POSITIONS

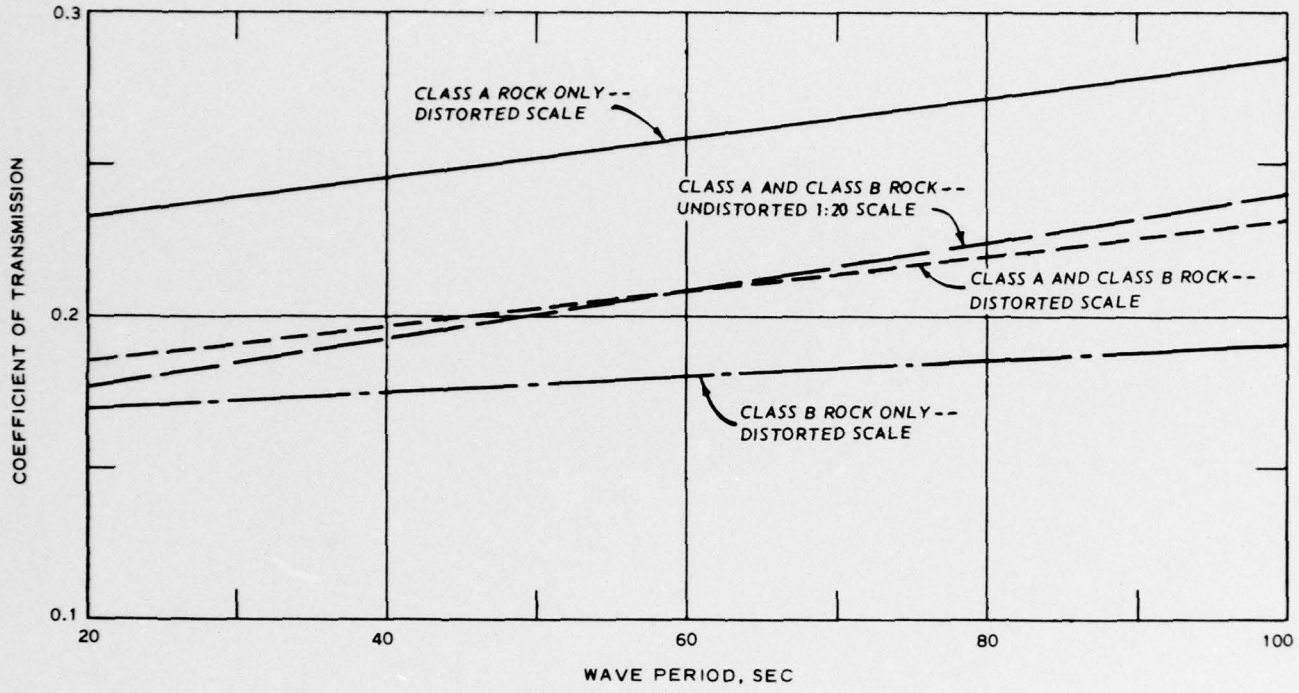

BREAKWATER TRANSMISSION

PLATE 25

APPENDIX A: NOTATION

a	Wave amplitude
a_c	Wave crest amplitude
b_o, b_n	Coefficients in velocity potential function
C	Wave celerity
C_r	Wave reflection coefficient
C_t	Wave transmission coefficient
D	Typical rock dimension
e	Base of natural logarithms
F	Force
F_I	Inertial force
F_m	Maximum force
F_R	Resistive force
g	Acceleration due to gravity
h	Water depth
h_1	Water depth at deep end of bottom elevation change
h_2	Water depth at shallow end of bottom elevation change
H	Wave height
$\overline{H}$	Average wave height
H_a	Wave height at antinode
H_i	Initial wave height
H_n	Wave height at node
H_r	Reflected wave height
H_t	Wave height at time t
H_{CH}	Wave height for closed harbor
H_{tm}	Transmitted wave height
H_{RMS}	Root-mean-square wave height
H_0	Initial wave height in wave absorber
H_1	Final wave height in wave absorber before leaving the absorber
i	Imaginary number
k	Wave number
K_r	Refraction coefficient

K_s	Shoaling coefficient
L	Wavelength
L_r	Length scale ratio
m_o	Solution of $m_o g \tanh m_o h = \sigma^2$
m_n	Solution of $m_n g \tanh m_n h = -\sigma^2$
n	Model distortion
p	Pressure
R	Wave-height amplification factor
s	Wave generator stroke amplitude
t	Time
T	Wave period
$\overline{T}$	Average wave period
T_r	Time scale ratio
x,y,z	Coordinate system with x,y in the horizontal plane and z vertical
α	Dimensionless parameter
β	Variable
ΔL	Width of wave absorber
η	Local water-surface elevation
ν	Kinematic viscosity
ρ	Water density
σ	Angular wave frequency
σ_H	Standard deviation of the wave height
σ_T	Standard deviation of the wave period
ϕ	Velocity potential

Subscripts:

m	Model value
p	Prototype
r	Scale ratio of model to prototype

In accordance with ER 70-2-3, paragraph 6c(1)(b), dated 15 February 1973, a facsimile catalog card in Library of Congress format is reproduced below.

Outlaw, Douglas G

Los Angeles and Long Beach Harbors model study; Report 4: Model design, by Douglas G. Outlaw, Donald L. Durham, Claude E. Chatham, [and] Robert W. Whalin. Vicksburg, U. S. Army Engineer Waterways Experiment Station, 1977.

1 v. (various pagings) illus. 27 cm. (U. S. Waterways Experiment Station. Technical report H-75-4, Report 4)

Prepared for U. S. Army Engineer District, Los Angeles, Los Angeles, Calif.

Includes bibliography.

1. Harbor oscillations. 2. Harbors. 3. Hydraulic models. 4. Long Beach Harbor. 5. Los Angeles Harbor. 6. Prototype data. 7. Water waves. 8. Wave generation. I. Durham, Donald L., joint author. II. Chatham, Claude E., joint author. III. Whalin, Robert Warren, joint author. IV. U. S. Army Engineer District, Los Angeles. (Series: U. S. Waterways Experiment Station, Vicksburg, Miss. Technical report H-75-4, Report 4)

TA7.W34 no.H-75-4 Report 4

AD-A037 154 ARMY ENGINEER WATERWAYS EXPERIMENT STATION VICKSBURG MISS F/G 20/4
LOS ANGELES AND LONG BEACH HARBORS MODEL STUDY. REPORT 4. MODEL--ETC(U)
FEB 77 D G OUTLAW, D L DURHAM, C E CHATHAM

UNCLASSIFIED WES-TR-H-75-4-4 NL

3 OF 3
AD
A037154

END
DATE
FILMED
7-78
DDC

SUPPLEMENTARY

INFORMATION

DEPARTMENT OF THE ARMY
WATERWAYS EXPERIMENT STATION, CORPS OF ENGINEERS
P. O. BOX 631
VICKSBURG, MISSISSIPPI 39180

IN REPLY REFER TO:

10 February 1978

Errata Sheet

No. 1

LOS ANGELES AND LONG BEACH HARBORS MODEL STUDY; Report 4, MODEL DESIGN

Technical Report H-75-4

February 1977

Replace Plate 24 with the inclosed Plate 24.

PLATE 24

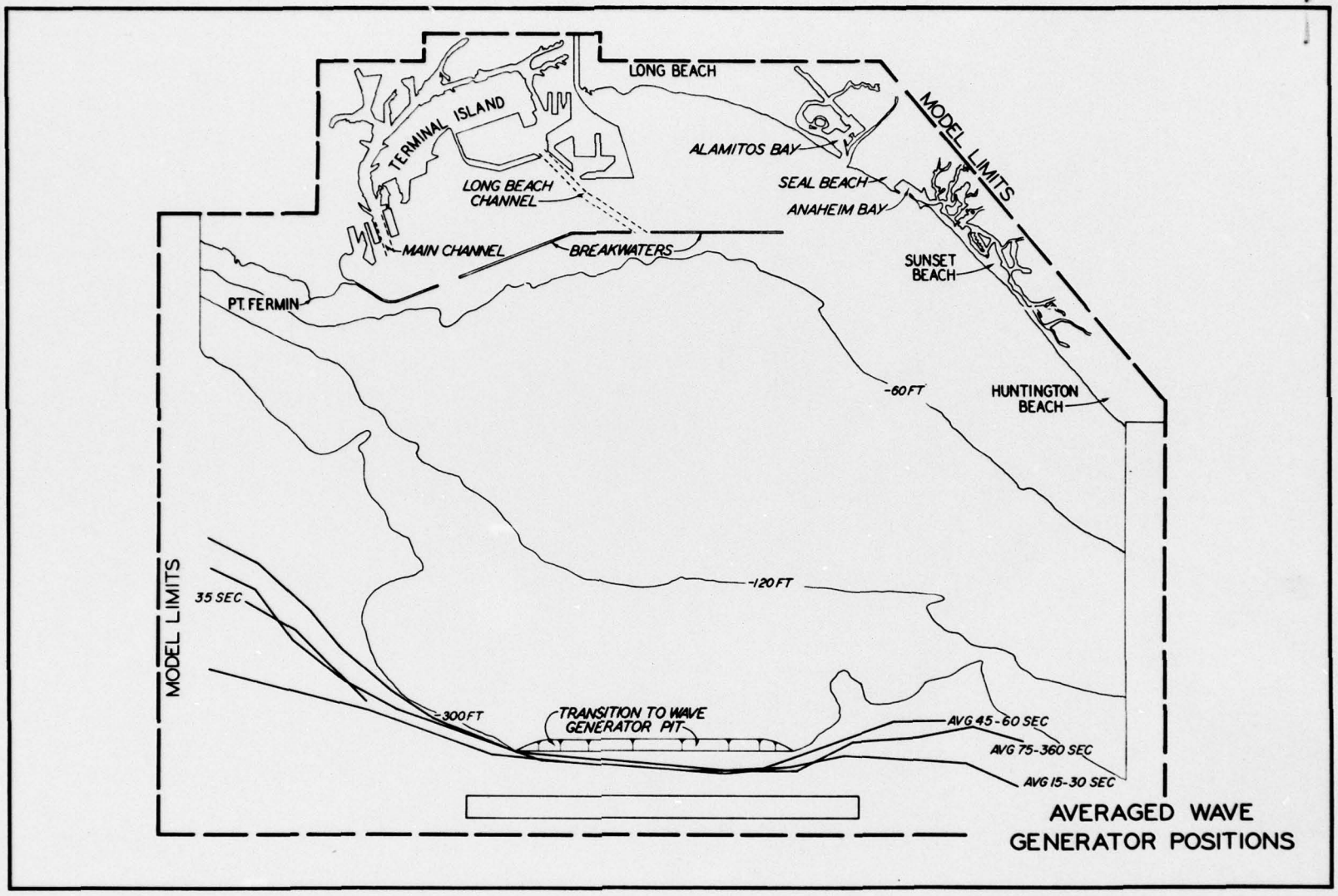

AVERAGED WAVE GENERATOR POSITIONS